UNIVERSITAT DE BARCELONA

Fibroblastic SNAIL1 induces a metastasis-permissive tumor stroma by regulating fibronectin alternative splicing

Héctor Franco Valls

Aquesta tesi doctoral està subjecta a la llicència *Reconeixement- SenseObraDerivada 4.0. Espanya de Creative Commons*.

Esta tesis doctoral está sujeta a la licencia *Reconocimiento - SinObraDerivada 4.0. España de Creative* Commons.

This doctoral thesis is licensed under the *Creative Commons Attribution-NoDerivatives 4.0. Spain License.*

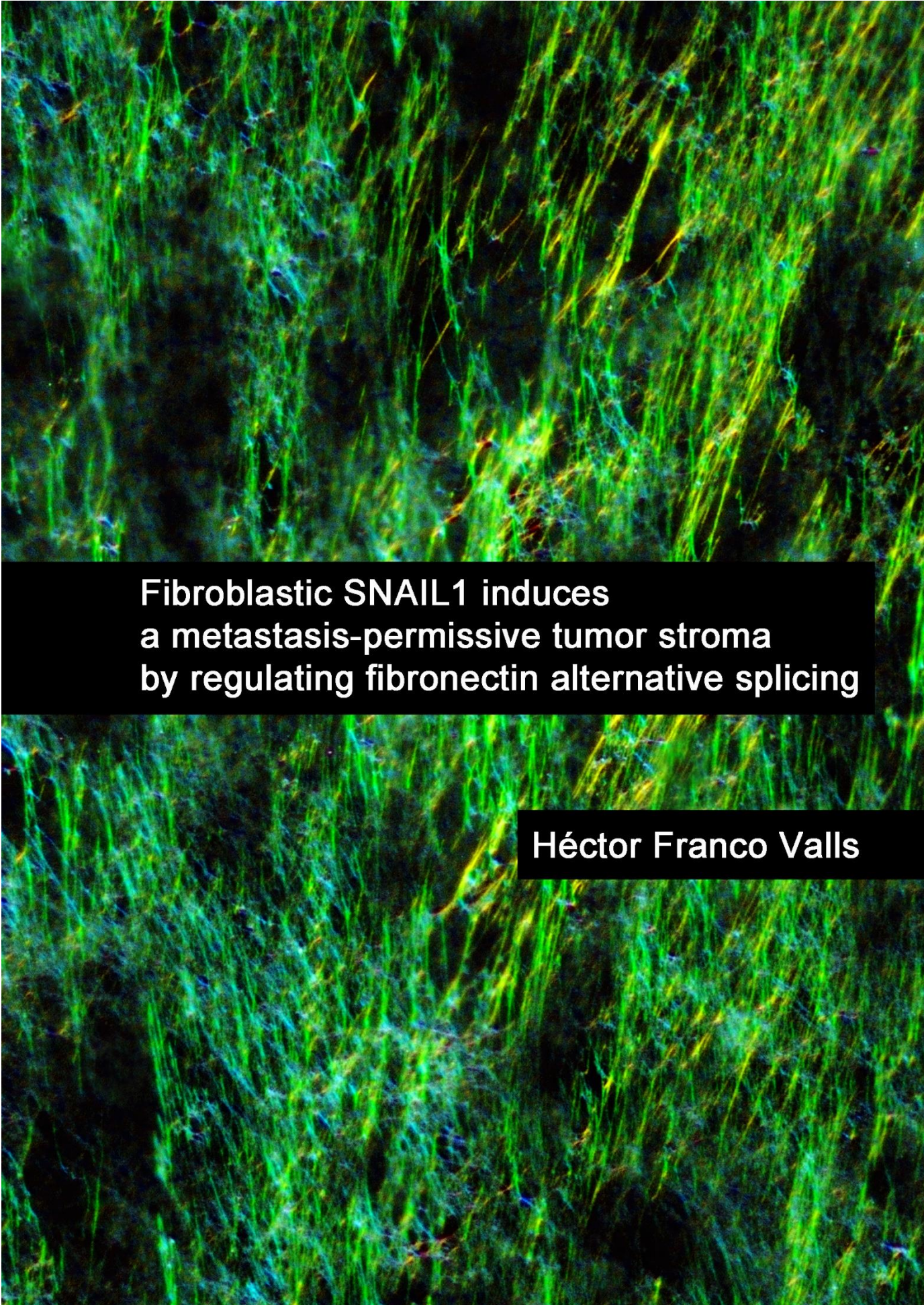

Fibroblastic SNAIL1 induces a metastasis-permissive tumor stroma by regulating fibronectin alternative splicing

Héctor Franco Valls

Tesis Doctoral

Programa de Doctorat Genètica (Universitat de Barcelona)

Grup de Recerca en Càncer (IMIM)

Fibroblastic SNAIL1 induces a metastasis-permissive tumor stroma by regulating fibronectin alternative splicing

Memòria presentada per optar al grau de

Doctor per la Universitat de Barcelona.

Barcelona 2022

Héctor Franco Valls

Directors de la Tesi Doctoral:

Dr. Josep Baulida Estadella

Dr. Antonio García de Herreros Madueño

Tutora de la Tesi Doctoral:

Dra. Susanna Balcells Comas

ACKNOWLEDGEMENTS

Aquesta tesi ha sigut més complicada del que m'esperava al començar. M'ha portat 4 anys i mig on hi ha hagut infinits moments complicats, d'experiments que insisteixen en no sortir, de quedar-nos tots tancats a casa i intentar seguir endavant, de sessions inacabables de cultius i de microscopi... I tot i això, no podria estar més agraït per totes les persones que l'heu convertit en una experiència irrepetible.

Jepi, gràcies per tot. Gràcies per la oportunitat de treballar en aquest projecte, sempre has confiat en mi, m'has deixat fer i triar i això m'ha fet créixer com a persona i investigador. Gràcies per la teva porta oberta en tot moment, per totes les xerrades una mica disperses però sempre interesants i per tota l'ajuda en els anàlisis, sense tu no hagués pogut amb tot.

També vull donar les gràcies a l'Antonio per totes les preguntes i suggeriments que ens han donat tantes idees i ens han fet anar més enllà. Mireia i Víctor, la vostra experiència, suggeriments i ànims han donat forma a aquest projecte.

Snailitos, presents i passats, sou els millors i us trobaré a faltar a tots. En tot moment heu sigut un suport, m'heu ajudat en tot i heu generat un ambient on és un gust treballar. Cap al final ens hem quedat una mica sols però això només ens ha fet fer més pinya. Marina, gràcies per tots els riures, cafès i barbacoes. Ha sigut molt guay compartir tant temps al laboratori amb tu, i ara que ets la sènior saps que no puc evitar recordar-te que ara et toca a tu escriure. Laura, qui ens anava a dir quan vas començar que series tan divertida encara que de vegades ens abandonis per dinar i ens posis música triste. Raúl, gràcies per les mil xerrades, consells i ajuda. No se com s'ho fan la resta de laboratoris sense tu. Bea, gracias por tu paciencia infinita con mis miles de preguntas y dudas y sobre todo por todas las charlas

terapéuticas cuando me da el bajón. Santi, moltes gràcies per totes les vegades que ens has alimentat, et desitjo lo millor amb la teva nova aventura. Anita, best of luck in your career, enjoy your stay in this amazing lab.

Durant aquests anys he tingut la sort de treballar amb els 4 millors minions que podia demanar. Carmen, fuiste mi conejillo de indias en esto de ser el jefe y no me lo podrías haber hecho más fácil. Trabajar contigo fue mazo guay y ser tu amigo aún más. Mariu, se nos hizo corto, pero espero que te quede un buen recuerdo de tu incursión al laboratorio. Elsa, el Snail lab hagués sortit guanyant si t'haguessis quedat amb nosaltres, estic segur que ho petaràs fort. Y Martín, no me olvido de ti. Me has pillado en un momento complicado pero tu buen rollo en el lab ha hecho más soportables los días de escritura. Muchos ánimos con lo que te queda, cuídame bien el proyecto.

I els Snailitos passats, vaig entrar a un laboratori amb un bon rotllo increïble, musicote a totes hores, cafesitos als sofàs i ple de gent de la que aprendre. Rumi, gràcies per tot el que em vas ensenyar i per la paciència amb tots els dubtes inicials just quan ja acabaves. Ara que hi he passat, no se com podies. Rubén, sempre vas ser font de bons moments i alegria, gràcies per tots els somriures. Guillem i Aida, coraleros, m'alegro moltíssim que la vostra aventura americana vagi tan bé. David, fuiste mi mejor apoyo de novato, a pesar de la tortura a base de Rosalía, las tardes de las Bistec lo compensaron. I Willy, de paio silenciós als lab meetings a DJ oficial del lab i bromista nivell padre. Sort que us veu traslladar, aquesta tesi no hagués sigut el mateix sense tu. Durant la tesi he tingut l'ajut de meravellosos tècnics: Jordi, Neus, Raulillo i Pere. Pere, moltíssimes gràcies per totes les hores a l'estabulari, sense el teu ajut hagués explotat en aquest esprint final. I Jordi, des de que vas marxar els dies ja no sonen a Shakira. Vas ser la meva infermera sexy i em vas ensenyar tot dels in

vivos, fent-me riure en moments inapropiats. Y por supuesto, no me puedo dejar a las tres Snails honoríficas, Judith, Marta y Pecha. Judith, em vas rebre amb els braços oberts, tota somriures, i vas ser el meu support system al principi de la tesi. Marta, casi nos hemos sincronizado al irnos y sé que disfrutaras al máximo la jubilación con esa energía que tú tienes. Gracias por los miles de millones de bloques y de cortes, no habría podido sin ti. Y Pecha, teníamos que acabar esta aventura juntos y me adelantaste por la derecha. Tu energía, tus cantos y tus gritos por el pasillo han sido un rayo de alegría ya fuera lunes a primera hora o viernes por la tarde.

A tots els veïns: Bigas, Celiàs i pàncreas team. Gràcies per tota la ajuda, les cèl·lules, els reactius i els flascs però sobretot gràcies pel bon rotllo que hi ha entre labs. Ivan i Cati, gràcies per les classes pràctiques d'operació i d'IVIS quan tornava a ser un novato total. Jordi, sense tu no sé si haguéssim menjat res a les barbacoes. Luís, compañero de tantos sábados en cultivos, muchos ánimos que ya te queda menos y puedes con todo!

Marisol, prima! Sin ti el estabulario sería un sitio muy aburrido, sin todas esas charlas y tus chistes que a veces me cuesta pillar. Gracias por esa calma cuando me estreso y por dejarme tus "herramientas".

Com no tot pot ser feina, al primer dia de la tesi ja em vaig deixar liar i em vaig apuntar a la coral. No ho hagués dit mai però es va convertir en el punt fort de la setmana. Imma, Aleix, Rocco, Oscar, Erika, Marçal i tothom que hi ha passat, especialment als pocs baixos, gràcies per tantes hores de música, per les cervesetes i les pizzes.

Aquesta tesi va començar amb una de les decisions més difícils que he hagut de prendre mai. Susanna, Dani i Roser, moltes gràcies per tot el que em vau ensenyar en els anys treballant amb vosaltres, per les vostres maneres de ser. Sé que fent la tesi amb vosaltres també hauria

sigut molt feliç. Ara, es clar, ja casi no hi queda ningú de la meva època. Per sort, encara us tinc a tots en la meva vida, Neus, Ester, Noe, Guillem. Gràcies pel temps compartit i pel que encara compartirem. Núria, no te me olvido, mi primera jefa y profe de PCRs, me enseñaste más de lo que crees y aún transmito tus manías en el lab a todos a los que enseño. I Edgar i Laura, us estimo molt. Em feu molt feliç i no em puc creure que en breus serem tots doctors, Edgar, a ver si et poses les piles...

Molts altres no heu participat tant directament en aquesta tesi, però heu estat allà quan us he necessitat i m'heu fet arribar fins aquí.

Biotecs. Hem anat fent cadascú pel seu costat però sempre hem trobat moments per trobar-nos, fer una cerveseta, jugar a algun joc o parlar una mica de ciència. Gràcies per la amistat a la facultat i fora d'ella. Y Sara, apareciste en el PRBB y te uniste a la coral, al vóley y ahora a este grupo, que bien tenerte.

Slims: Maiso, Ezke, Edi, Ale, Sebas. Gràcies per les cerveses, tots els riures i les converses. Sou clau en la meva vida, em doneu ànims i hi sou sempre, sobretot en els moments importants. Eloi, tan de bo hi fossis. T'estimem.

I els meus metges preferits: Vani, Nati, Genís, Cris i Manish, que no et puc tenir a Instagram però a la meva tesi hi mano jo. Gràcies per acollir-me en el vostre grupet i fer-me sentir com a casa.

Suegris, que des de ben petit m'heu cuidat i ara més que mai. M'heu fet sentir com a casa i sempre us heu preocupat per si podia amb la tesi o la tesi podia amb mi. Gràcies per tot.

Carol, aquesta tesi sense tu no hagués sortit. Sempre has cregut en mi, has escoltat les meves xapes científiques i m'has muntat festes quan em sortia un experiment. M'has aguantat en tots els moments

complicats, especialment aquests últims mesos d'estrès, i m'has animat com només tu saps. Gràcies per tota la felicitat que em dones. T'estimo.

Per últim, a la meva família. Iaies, us estimo molt. Mama, papa, moltes gràcies per tot el que heu fet i encara feu per mi. Gràcies per intentar preguntar-me com anava la tesi i que hi feia tot i no entendre mai res. Gràcies per ensenyar-me que l'esforç val la pena i gràcies per fer-me feliç.

ABSTRACT

SNAIL1 is a transcription factor with roles in repression of epithelial genes and enhancement of mesenchymal genes. As such, it plays a key role in Epithelial-to-mesenchymal transition and in fibroblast activation into myofibroblast. In this thesis, we characterize a novel role in splicing regulation, focusing on the induction of inclusion of the fibronectin extra domain A. This alternatively spliced domain, expressed in pathological situations such as wound healing and cancer, has various roles in inflammatory response, fibroblast activation and tumor cell migration. We show a correlation between SNAIL1 and EDA inclusion among a breast cancer PDX cohort and samples for 5 solid tumor types in advanced stages. Here, we describe a TGFβ/SNAIL1 dependent recruitment of the splicing factor SRSF1 to the EDA coding RNA, associated to increased inclusion.

We focus on the effects of this increase in EDA inclusion in the context of fibronectin fibers assembled into the extracellular matrix. We use genetically modified fibroblasts, expressing specific isoforms of fibronectin, to derive matrices and demonstrate that, like fibroblastic SNAIL1 expression, the presence of fibronectin EDA is required to organize an aligned and stiffer extracellular matrix. The induced mechanical and topological ECM properties enhance tumor cell oriented individual migration, facilitate coordinated collective movement and induce a more efficient invasion. Depletion of the isoform completely prevents metastasis formation in an orthotopic cancer model. We use specific inhibitors to block EDA signaling reducing fibroblastic activation and leading to a restrictive matrix that

limits tumor cell invasion. Therefore, our results demonstrate the role of the fibronectin EDA isoform in the conversion of a restrictive tumor stroma to a permissive one and its molecular control by the transcription factor SNAIL1.

RESUM

SNAIL1 és un factor de transcripció que regula la repressió de gens epitelials i l'activació de gens mesenquimals. En base a aquests rols, SNAIL1 és clau en la transició Epiteli-mesènquima i en l'activació de fibroblasts. En aquesta tesi, caracteritzem una nova funció com a regulador del "*splicing*", centrant-nos especialment en la capacitat de promoure la inclusió del domini extra A (EDA) de la fibronectina. Aquest domini s'expressa en situacions patològiques com la cicatrització de ferides o el càncer i s'ha associat a la resposta inflamatòria, l'activació de fibroblasts i la migració de cèl·lules tumorals. Presentem l'existència d'una correlació entre els nivells de SNAIL1 i la inclusió d'EDA en una cohort de PDXs derivats de càncer de mama i en mostres de pacients de 5 tipus de tumors sòlids en estadis avançats. En aquest treball descrivim el reclutament del factor de "*splicing"* SRSF1 al RNA codificant per EDA, associat a un augment de la inclusió, de manera dependent de TGFβ i SNAIL1.

El nostre estudi se centra en els efectes associats a aquest augment de la inclusió d'EDA en el context de fibres de fibronectina polimeritzades a la matriu extracel·lular. Usem fibroblasts modificats genèticament, induint l'expressió d'una única isoforma de fibronectina, per generar matrius extracel·lulars i demostrem que la presència de fibronectina EDA es necessària per a l'increment de l'alineament i la rigidesa de les matrius. Les propietats mecàniques i topològiques induïdes per la fibronectina EDA en la matriu extracel·lular augmenten la migració orientada de cèl·lules tumorals individuals, faciliten el moviment coordinat col·lectiu i indueixen una invasió més eficient. L'exclusió

d'aquest domini en un model ortotòpic de càncer de mama porta a la completa eliminació de l'aparició de metàstasis. L'ús d'inhibidors específics per tal de bloquejar la senyalització d'EDA redueix l'activació de fibroblasts i indueix una matriu restrictiva que disminueix la invasió de les cèl·lules tumorals. Per tant, els nostres resultats demostren que el factor de transcripció SNAIL1 promou la inclusió de EDA en l'ARNm de fibronectina i el paper d'aquesta isoforma en la conversió de l'estroma tumoral de restrictiu a permissiu.

TABLE OF CONTENTS

FIGURE INDEX

INTRODUCTION

RESULTS

DISCUSSION

ABBREVIATIONS

IIICS: Fibronectin Type 3 connecting segment

3D-ECM: Three-dimensional extracellular matrix

AFM: Atomic force microscopy

AON: Antisense oligonucleotide

AR: Aspect ratio

BMDM: Bone marrow derived macrophage

BSA: Bovine serum albumin

CAF: Cancer associated fibroblast

cDNA: Complementary deoxyribonucleic acid

cFN: Cellular fibronectin

ChIP: Chromatin immunoprecipitation

ChIP-seq: Chromatin immunoprecipitation sequencing

CTD: C-terminal domain

DAPI: 4',6-diamidino-2-fenilindol

DMEM: Dulbecco's modified Eagle's medium

DNA: Deoxyribonucleic acid

ECM: Extracellular matrix

EDA: Fibronectin extra domain A

EDA-FN1: Fibronectin including the Extra domain A

EDB: Fibronectin extra domain B

EMT: Epithelial-to-mesenchymal transition

ESE: Exonic splicing enhancer

ESS: Exonic splicing silencer

FA: Focal adhesion

FAP: Fibroblast activation protein

FBS: Fetal bovine serum

Fn1: Fibronectin coding gene in mouse

FN1: Fibronectin coding gene in human

FN1: Fibronectin1 protein in mouse and human

HER2: Human epidermal growth factor receptor 2

hnRNP: Heterogeneous nuclear ribonucleoprotein

HRP: Horseradish peroxidase

IF: Immunofluorescence

IL-6: Interleukin-6

ISE: Intronic splicing enhancer

ISS: Intronic splicing silencer

kDa: Kilo Dalton

KHSRP: KH-type splicing regulatory protein

KO: Knock-out

MEF: Mouse embryonic fibroblast

MMP: Matrix Metalloproteinase

mRNA: Messenger ribonucleic acid

MSC: Mesenchymal stem cell

NF-κB: Nuclear factor kappa B

NOD-SCID: Non obese diabetic/severe combined immunodeficiency

OOPS: Orthogonal organic phase separation

PARP1: Poly ADP-ribose polymerase 1

PBS: Phosphate buffered saline

PCR: Polymerase chain reaction

PDGF: Platelet-derived growth factor

PDX: Patient derived xenograft

PFA: Paraformaldehyde

pFN: Plasma fibronectin

Pol II: RNA polymerase II

Pre-mRNA: Precursor messenger ribonucleic acid

PRMT: Protein arginine methyltransferase

PSI: Percent spliced in

qPCR: Quantitative PCR

RBP: RNA binding protein

RIP: RNA immunoprecipitation

RIPA: Radioimmunoprecipitation assay

RNA: Ribonucleic acid

RNase: Ribonuclease

RNA-seq: Ribonucleic acid sequencing

RT-qPCR: Quantitative reverse transcription PCR

RT-sqPCR: Semi-quantitative reverse transcription PCR

SDS: Sodium dodecyl sulfate

SEM: Standard error of the mean

SHG: Second harmonic generation

siRNA: Small interfering ribonucleic acid

***Snai1*:** Snail family transcriptional repressor 1 coding gene in mouse

***SNAI1*:** Snail family transcriptional repressor 1 coding gene in human

SNAIL1: Snail family transcriptional repressor 1 in human and mouse

SNAIL1-HA: Hemagglutinin epitope tagged SNAIL1

snRNP: Small nuclear ribonucleoprotein

SR: Serine/Arginine-rich protein

SRSF: Serine/Arginine-rich splicing factor

STED: Stimulated emission depletion

TBS: Tris buffered saline

TBST: Tris buffered saline supplemented with Tween 20

TGFβ: Transforming growth factor beta

TGS: Tris-glycine-SDS

TLR4: Toll-like receptor 4

TWOMBLI: The workflow of matrix biology informatics

U snRNA: Uridine-rich small nuclear ribonucleic acid

UV: Ultraviolet

WB: Western blot

WT: Wild-type

α-SMA: Alpha-Smooth muscle actin

INTRODUCTION

1. THE ROLE OF STROMA IN CANCER

1.1. Cancer Overview

The World Health Organization defines cancer as a generic term referring to a large group of diseases that can affect any organ. It is characterized by the creation of abnormal cells that proliferate quickly beyond their regular boundaries, invade neighboring tissues and, eventually, spread to other organs in a process called metastasis. Cancer accounts for 10 million deaths in 2020, being the second leading cause of death, only behind cardiovascular diseases.

While the first description of human cancer can be traced back to ancient Egypt (around 3000 BC), its significant understanding and efficient treatment did not initiate until the 20th century. Once considered to be an incurable disease, nowadays, cancer treatments lead to an overall survival rate of approximately 70% taking into consideration all types of cancer. However, this figure still goes as low as 10% survival for pancreas or 21% for lung cancer[1].

In the year 2000, Hanahan and Weinberg published a list of hallmarks or capabilities that regular cells need to acquire in order to allow cancer to survive, grow and disseminate[2]. This list has been updated twice, in the years 2011 and 2022, to include new core hallmarks of cancer as well as prospective hallmarks and enabling characteristics. The current core hallmarks of cancer include self-sufficiency in growth signals, insensitivity to antigrowth signals, capacity to avoid apoptosis, limitless replicative potential, sustained angiogenesis, capability to invade neighboring tissues and produce metastasis, reprogramming of

the energy metabolism and evading immune destruction[2,3]. These traits, together with the two enabling characteristics described in 2011, development of genome instability and a state of tumor promoting inflammation, constitute the current main hallmarks of cancer (Figure1, left). The most recent revision adds 4 new characteristics as emerging hallmarks: unlocking phenotypic plasticity, nonmutational epigenetic reprogramming, senescent cells and polymorphic microbiomes (Figure 1, right).

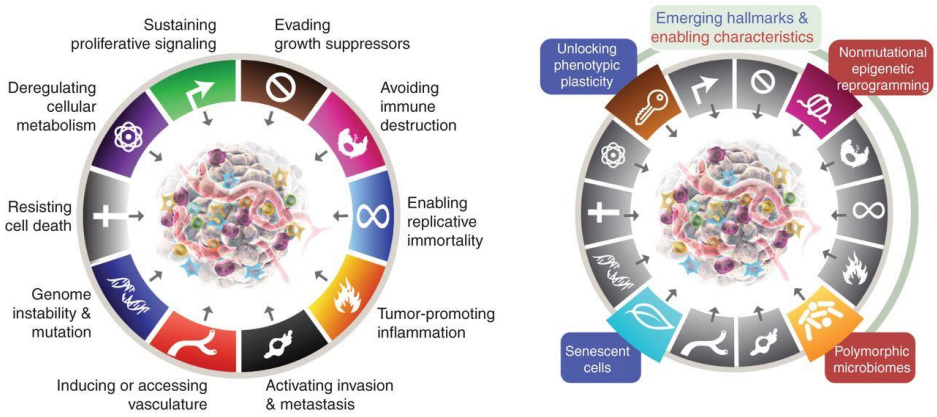

Figure 1: The hallmarks of cancer. *Left*, representation of the core capabilities and enabling characteristics proposed by Hanahan and Weinberg[2,3]. *Right*, proposed emerging hallmarks by Hanahan[4].

Cancer metastatic capability is a key factor in its deadly effects, as it accounts for approximately 90% of cancer related deaths[5]. The metastatic process requires cells to invade the stroma surrounding the tumor, intravasate into blood vessels, survive in circulation, extravasate and invade a new tissue, survive and adapt to the conditions of this secondary site and, finally, regain proliferative

capabilities[6]. Based on their capability to undertake this metastatic process, tumors can be classified as benign or malignant.

Another usual classification method for tumors is according to their histology (the tissue-type in which they originate). Carcinomas, cancers of epithelial origin, account for 80 to 90 percent of total cancer cases. Together with sarcomas, cancers originated in connective or supportive tissue, carcinomas are also called solid tumors. The rest of histological tumor types are the so-called liquid tumors since they derive from blood cells and they do not always form a clearly defined tumor mass. Namely, myelomas arise from plasma cells in the bone marrow, lymphomas are derived from the glands and nodes of the lymphatic system and leukemias are an uncontrolled growth of leukocytes in the bone marrow.

1.2. Tumor stroma

A common misconception about tumors is that they are exclusively composed of the epithelial tumor cells growing out of control. Solid tumors are characterized for having a clearly differentiated parenchyma and stroma. The parenchyma is made of the dysfunctional cancer cells while the stroma includes the non-malignant cells, such as fibroblasts, cells of the immune system, adipocytes and cells of the vascular system; and the surrounding extracellular matrix (ECM), a complex mesh of macromolecules and fibrous proteins (Figure 2). The interaction between these two compartments is key in every step of the process of tumorigenesis, from the initial growth to the eventual escape of invading cells[7]. The

stroma can act as a natural barrier, generating an antitumor microenvironment that keeps potentially tumorigenic cells under control. To overcome this protection, changes must happen in the homeostasis of the tissue. Once the tumor has started developing, the stroma can act as a protective barrier, enhancing the proliferation and helping in the acquisition of the aforementioned hallmarks.

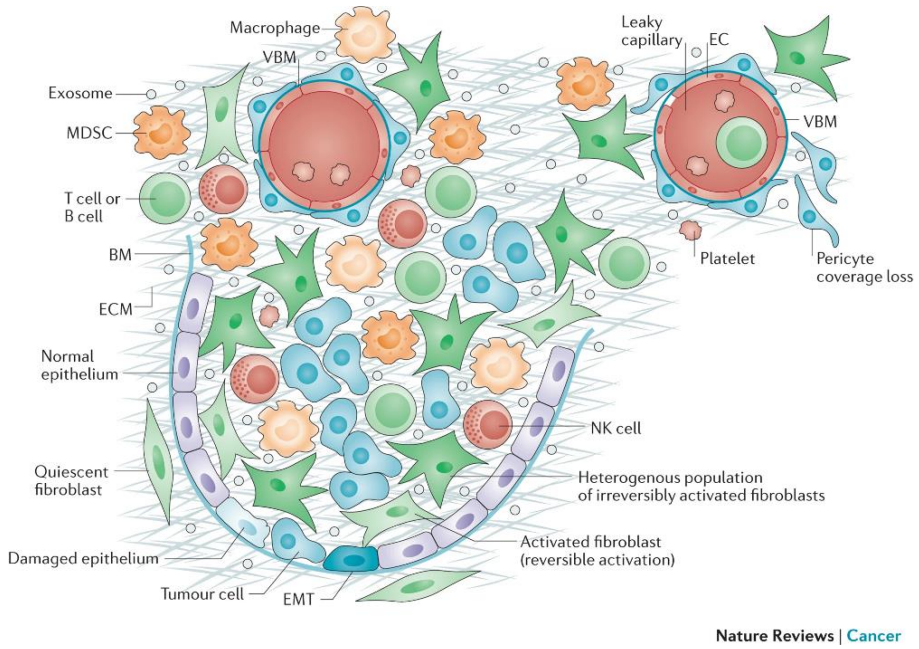

Figure 2: The tumor microenvironment. Schematic diagram representing the various cell types found in a tumor including cancer cells, cancer associated fibroblast, endothelial cells and cells of the immune system together with the ECM. Obtained from Kalluri R[8].

The potential role of stroma in determining the appearance of cancer was already hypothesized by Virchow in 1863, when he claimed that malignant tumors arose at sites of chronic inflammation[9]. Since then, an increasingly complex crosstalk between tumor cells and their

surrounding environment has been reported. Stromal cell behavior is altered by unusual tumor cell signaling generating new environmental conditions. This shift from a restrictive to a permissive stroma can, in turn, provide tumor cells with a malignant behavior. Permissive stroma can provide tumor cells with growth factors, induce angiogenesis, reform the basement membrane that surrounds healthy epithelia, repress immune responses, or alter the ECM to facilitate escape of invasive cells. One of the main effectors in these stroma-derived changes are fibroblasts.

1.2.1. Fibroblast activation

Fibroblasts are the most abundant cell type in connective tissue. They were first described by Virchow[10] and later Duvall[11], who initially characterized them for their ability to synthesize collagen. Fibroblasts present elongated morphology, often described as fusiform or spindle-shaped, and tend to be embedded in the ECM they produce. These cells are usually in a state of quiescence in healthy tissues, having an almost non-existent metabolism or secretory activity[8]. However, they can become activated in response to signals generated in an injury such as a wound or cancer. Fibroblasts activated upon such situations are called myofibroblasts.

This activation process is regulated by factors secreted by other cells, such as transforming growth factor-β (TGFβ), platelet-derived growth factor (PDGF) or interleukin-6 (IL-6), among others[12,13]. Once activated, their functions include synthesizing proteins of the ECM such as collagen and fibronectin (FN1) but also producing matrix degrading

metalloproteinases (MMP). This dual role of synthesis and degradation complemented with the capacity to exert physical forces that rearrange the overall tissue architecture makes fibroblasts the key organizers of the ECM. Also, once activated, they generate abundant cytokines and chemokines that, among other functions, regulate the recruitment of immune cells and the growth of epithelial cells (Figure 3).

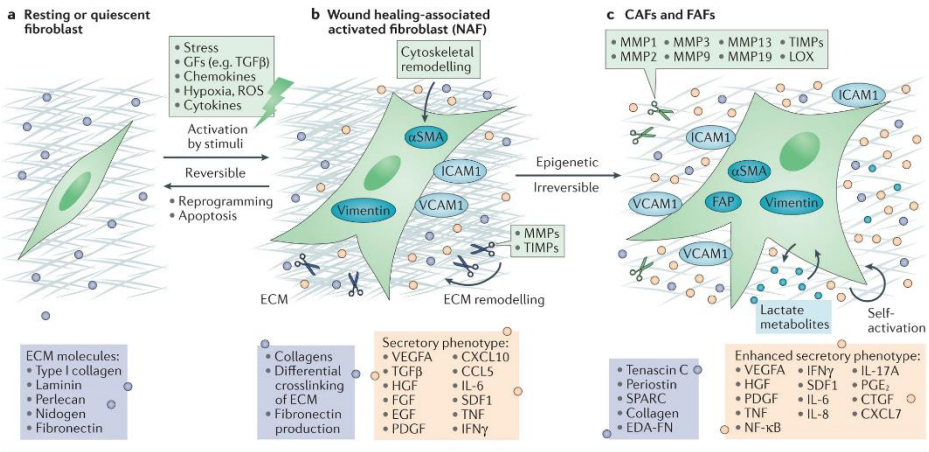

Figure 3: Fibroblast activation process. (A) Resting fibroblast embedded in the ECM of a healthy tissue. (B) Fibroblast activated in response to injury. Increased capacity to regulate the surrounding ECM and high contractile capability. (C) Cancer Associated Fibroblast. Permanently activated with increased secretory function as well as proliferation capability. Modified from Kalluri R[8].

The study of both fibroblasts and myofibroblasts is relatively easy *in vitro* as they can be grown on plastic with ease. Additionally, the activation into myofibroblasts can be reproduced adding TGFβ to the culture medium. This *in vitro* activation mimics the *in vivo* activation as identified by markers such as α-smooth muscle actin (α-SMA)

expression and inclusion into stress fibers, expression of the fibroblast activation protein (FAP), or a marked increase in fibronectin expression. However, not every activated fibroblast will express these markers, as most of the markers used are hardly specific for fibroblasts. This high degree of heterogeneity likely arises from the fact that myofibroblasts have been described as being derived from many cell types such as bone marrow-derived precursors, mesenchymal stem cells (MSCs), endothelial cells, liver and pancreas stellate cells, quiescent fibroblasts and possibly from some types of epithelial cell[14].

Upon activation in a wound healing process, myofibroblasts work in repairing the injured ECM by secreting fibronectin and collagens and help in wound closure by applying physical forces that cause contraction of the skin. While the wound is present, the activation signals remain in place and a series of feedback loops sustain the fibroblastic response. Once the wound is resolved, myofibroblasts undergo senescence in order to stop their activity and avoid pathological scarring[15]. Therefore, the myofibroblastic activation in a wound healing context is reversible and transient.

1.2.2. Wounds that do not heal

Cancers have been called wounds that do not heal[16]. This idea arises from the similarities between the initial response to a wound and the mechanisms cancer uses to obtain a suitable stroma, with the difference that in cancer this response is sustained through time. In this regard, cancer can take advantage of molecular mechanisms that

are already in place in our body to its own benefit[17]. Some of the main steps in wound healing that are mimicked in cancer development are cellular inflammation, angiogenesis, and the generation of mature connective tissue.

Both wounds and cancer share an inflammatory response that attracts immune cells such as neutrophils, macrophages, and lymphocytes. Most of these cells can play radically different roles as protumoral or antitumoral depending on the signals they receive from the tumor microenvironment[18].

The comparison of tumors to wounds that do not heal is especially relevant when looking into the behavior of fibroblasts. While in wound healing myofibroblasts disappear once the injury is gone due to the disappearance of the activation signal, they remain activated in cancer, since the tumor is continuously generating activating signals such as TGFβ secretion. The myofibroblasts activated in a cancer context, a subpopulation of the called cancer associated fibroblasts (CAF), show transcriptional changes similar to those of a wound, with an increased synthesis of fibrillar proteins, mainly collagen and fibronectin. This increased continuous deposition of fibrillar collagen leads to a desmoplastic stroma. This scar-like and highly fibrotic stroma can comprise more than 50% of the total tumor mass[19].

1.2.3. CAFs and cancer progression

An abundance of stroma and high CAF presence has been mostly related to bad prognosis[20]. Also, some genes that had been related to bad prognosis, such as the transcription factor coding *SNAI1*, have

been described as actually being upregulated in CAFs rather than in tumoral cells themselves[21,22].

CAF activity leads to a tumor growth supporting microenvironment. Metastasis is enhanced by CAFs through the release of growth factors and cytokines that directly or indirectly stimulate tumor growth and invasion. Additionally, as has been described for myofibroblasts, CAFs modify the ECM through their elevated synthesis and degradation of fibrillar proteins and their capacity to exert tension on preexisting fibers to rearrange them. Altogether, these lead to changes on the biophysical properties of the ECM, such as increased rigidity and fiber alignment, related to tumor progression and metastasis[23,24].

However, studies have pointed to the possibility that other CAF subpopulations might be playing a tumor suppressor role[25]. This data contributes to the consolidation of CAF as a valid therapeutic target, either aiming to suppress the protumoral activity or turning CAFs into the antitumoral phenotype[26].

1.2.4. ECM remodeling in cancer

The ECM is a complex mesh of fibrous proteins such as fibronectin, collagen, laminin and proteoglycans. Fibroblasts embedded in the matrix have a dual function of synthesizing new ECM proteins while degrading through metalloproteinases in a continual remodeling. The ECM acts as the physical scaffold that supports and arranges the three-dimensional organization of a tissue. In this capability, ECM can act as a barrier isolating a tissue when ECM proteins are arranged in an orderly manner[27]. However, during diseases such as cancer, the

ECM is altered through the tumoral desmoplastic reaction, presenting an increased deposition of fibronectin and fibrillary collagens together with severe remodeling[28]. This remodeled ECM provides guidance to tumoral cells, influencing their migration, invasion and eventual metastasis as ECM fibers act as pathways orienting tumor cell movements[19,29]. Additionally, cancer induced remodeling leads to increased ECM stiffness which, in turn, further activates fibroblasts[30,31].

1.2.5. Fibronectin, the ECM scaffold

Fibronectin initiates and guides ECM assembly acting as a scaffold where other fibrous proteins such as collagen, fibrillin, thrombospondin-1 and tenascin C can bind[32].

Fibronectin is synthesized as monomers composed of repeating units of one of three different domains: type I, II or III. These monomers are grouped into dimers before secretion from the cell. Fibrillogenesis is a cellular dependent process that requires fibronectin dimers binding to integrin clusters in focal adhesions. Folded dimers are linearized by tensional forces generated by the cytosolic stress fibers and transmitted in/out to the integrin clusters. Molecular unfolding exposes internal fibronectin domains allowing multiple interactions between monomers that stabilize fibrils in a first instance and fibers in a second instance when fibrils interact with each other. While the *FN1* gene codes for various isoforms (See 2.1.3. Alternative fibronectin splicing), heterodimers of fibronectin isoforms and incorporation of all isoforms to the extracellular matrix has been described[33]. Along the

assembly process, cryptic domains mediating binding to other ECM molecules are also exposed allowing new intermolecular interactions and the structural coordination of other kinds of fibers (Figure 4).

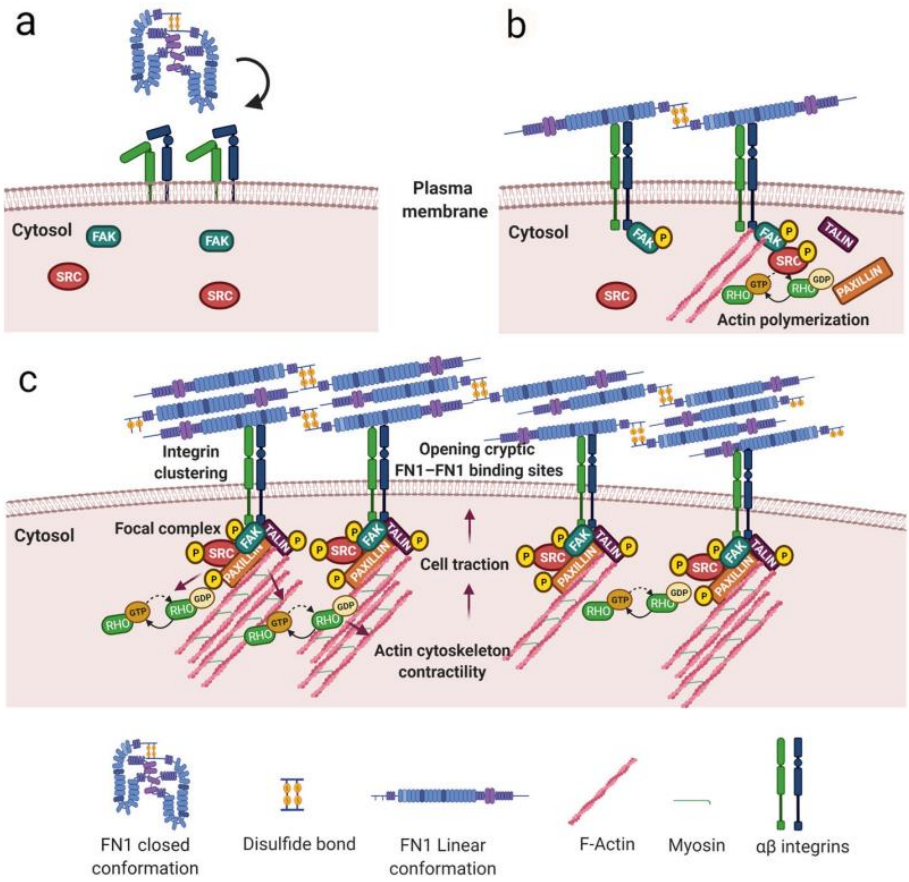

Figure 4: FN1 fibrillogenesis process. (A) Fibronectin dimers are formed and bind to integrins. (B) Binding of dimers to integrins induces conformational changes. Integrins start to form clusters and become activated and recruit focal adhesion components. (C) Actin cytoskeleton associated to mature focal adhesions transmit forces that induce FN1 conformational alterations, exposing new cryptic sites for binding and leading to fibrillogenesis. Obtained from Spada S. et al.[34].

Additionally, the interaction of fibronectin fibers incorporated to the ECM with integrins plays a role in mechanotransduction of the ECM. Mechanical, topographical and motif-directed cues are sensed by out/in fibronectin induced integrin signaling[35,36]. Signals transmitted by focal adhesions are relayed into the cell by actin stress fibers, highly enriched in α-SMA in CAFs[37], greatly increasing the cell capacity to generate mechanical tension. The mechanical forces of the matrix are propagated all the way into the nucleus, leading to alterations of both nucleus and cell shapes[38,39].

In breast cancer, increased ECM fiber remodeling correlates with cancer progression. Presence of aligned collagen fibers has been highlighted as a prognostic signature for poor survival[40,41]. Alignment of the ECM fibrils, studied through fibronectin, has been observed *in vitro* when fibroblasts from tumor samples were used to produce *in vivo* like 3D-ECM[19]. ECM derived from tumor fibroblasts activates the tumorigenic capacity of benign cells. Conversely, ECM derived from normal fibroblasts represses the tumorigenic phenotype in cancer cells[42].

1.3. SNAIL1 transcription factor controls stroma activation

1.3.1. SNAIL1 characteristics

SNAIL1 belongs to the Snail superfamily of zinc-finger transcription repressors together with SNAIL2 (Slug) and SNAIL3 (Smuc). The three members of the Snail superfamily share three common domains: the zinc-finger C-terminal domain, a highly conserved region that contains four to six zinc fingers that mediate sequence specific interaction with

the deoxyribonucleic acid (DNA); the central region which is involved in protein stability and localization; and a more variable N-terminal region[43].

SNAIL1 first described roles take place during development, specifically in the formation of the mesoderm[44]. In vertebrates, SNAIL1 participates in the migration of the neural crest[45]. *Snai1* Knock-out (KO) mouse embryos exhibit defects in gastrulation and an early embryonic mortality[46]. Overall, during development, SNAIL1 mediates the repression of the epithelial phenotype promoting a mesenchymal one, essential for the formation of the third embryonic tissue layer during gastrulation.

SNAIL1 has four zinc-finger motifs that directly bind to E-box DNA sequences located in target promoters. This binding is required for transcriptional repression. Additionally, a SNAG domain located in the N-terminal region recruits co-repressors such as the chromatin remodelers HDAC1 and HDAC2[47], Polycomb-group proteins[48] and the arginine methyltransferase 5 among others[49] (Figure 5). As a transcriptional repressor, SNAIL1 acts on the E-cadherin coding gene (CDH1) and other epithelial genes and triggers epithelial-to-mesenchymal transition (EMT)[50]. EMT provides epithelial cells with migratory capabilities, inducing the loss of adherent junctions and apical-basal polarity as well as inducing a rearrangement of the cytoskeleton[51].

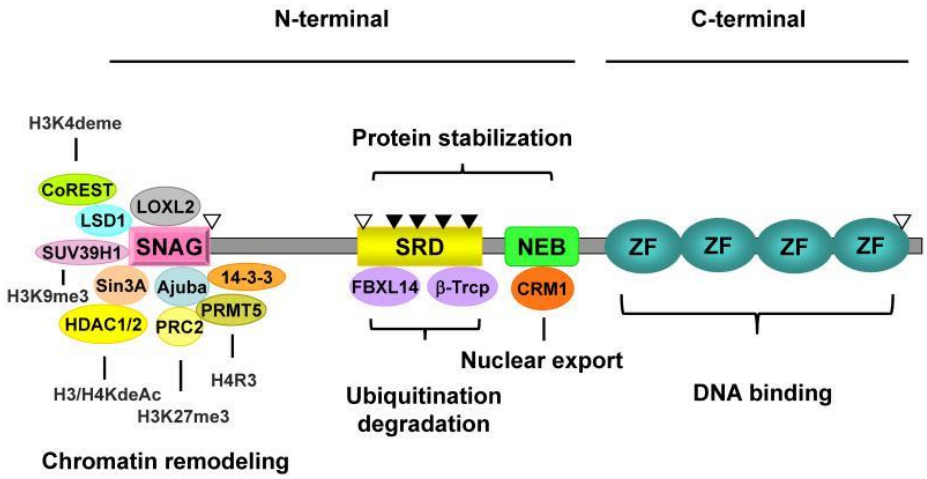

Figure 5: SNAIL1 domain structure. Schematic representation of SNAIL1 showing its described domains, including an N-terminal SNAG domain and the 4 C-terminal zinc-finger domains. The N-terminal SNAG domain interacts with several transcription repressors and epigenetic remodelers. Phosphorylation sites are indicated as triangles. Obtained from Wang Y. et al.[52].

However, SNAIL1 has also been described to act as a transcriptional activator of typically mesenchymal genes, such as fibronectin, in epithelial cells undergoing EMT and fibroblasts. The attachment of SNAIL1 to the *Fn1* promoter requires the interaction with a different set of proteins. p65-NF-κB binds to the *Fn1* promoter and recruits both SNAIL1 and PARP1 to form a complex[53]. Arginine methyltransferase 1 and 4 have also been described to bind to this complex, inducing methylation of the *Fn1* promoter, driving its expression. Other mechanisms of transcription activation by SNAIL1 regulating specific genes have been proposed[54–56]. However, a consensus SNAIL1-activator complex is not as well stablished as the classical repressor one.

1.3.2. SNAIL1 in fibroblasts

Although initially described roles for SNAIL1 relate to promoting EMT during development and tumor progression, current data show that it is preferentially expressed in mesenchymal cells[57,58]. After development, SNAIL1 expression is limited to pathological situations either short termed, such as wound healing, or continuous, such as fibrosis and cancer[22,59,60].

Depletion of SNAIL1 has been shown to delay wound healing, as myofibroblasts do not become activated and the ECM of the granulation tissue does not undergo the necessary rearrangement to close the wound[61].

In fibrosis, SNAIL1 expression has been shown to be necessary for fibroblast activation into myofibroblasts and for maintaining their activated state. Studies have been carried out in various fibrosis types such as cutaneous, cardiac and hepatic[62–64].

In tumors, as previously remarked, SNAIL1 expression is predominantly detected in stromal CAFs. In breast cancer, stromal areas positive for SNAIL1 in CAFs show increased fibronectin and collagen fiber alignment and have been associated to poor patient prognosis[40,61]. Previous work by our group linked SNAIL1 stromal expression in colon to a poor prognosis for patients, especially due to a higher risk of metastasis[22].

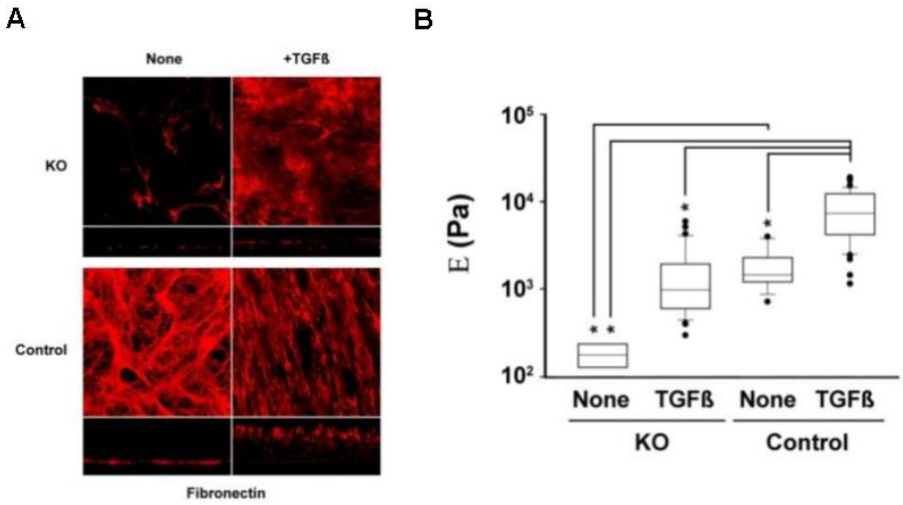

Figure 6: SNAIL1 is essential for the formation of aligned stiff matrices. (A) Fibronectin immunofluorescence of 3D-ECM obtained from MEFs control or KO for *Snai1* untreated and treated with TGFβ. Each image is accompanied by a transversal section of the ECM immunofluorescence at the bottom. (B) Young's modulus, E, obtained on decellularized 3D-ECM showed in A by atomic force microscopy, showing SNAIL1 dependent matrix stiffness. Adapted from Stanisavljevic J. et al.[61].

Fibroblasts knock-out for *Snai1* fail to acquire myofibroblastic traits in response to TGFβ, as studied through *in vivo* like 3D-ECM produced *in vitro*. In this model, SNAIL1 is essential for the formation of aligned stiff matrices (Figure 6), capable of inducing an oriented movement on tumoral cells, such as the MDA-MB-231 tumor cell line, leading to invasive behavior (Figure 7)[61]. In *in vivo* models, induction of breast cancer in mice through the transplantation of cancer cells with SNAIL1 depleted fibroblasts generates a protective stroma, completely repressing the appearance of metastasis[65].

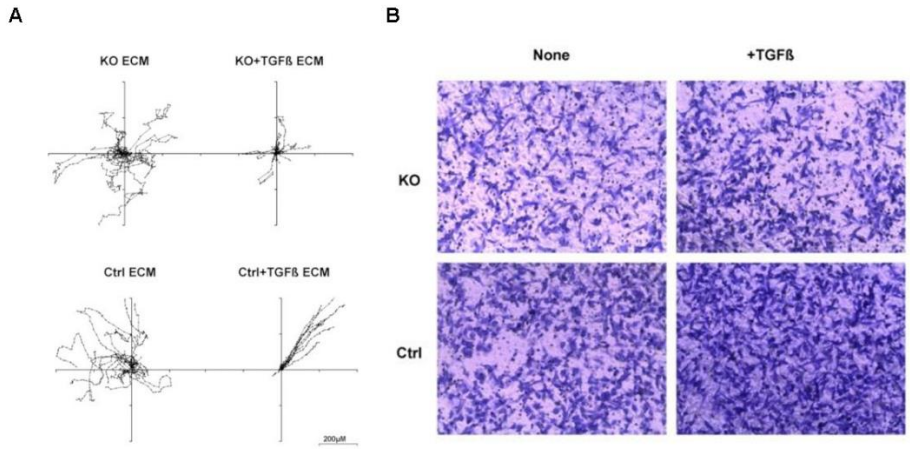

Figure 7: Migration and invasion of MDA-231-MB tumor cells on 3D-ECM from Control and *Snai1* KO MEFs treated or left untreated with TGFβ. (A) Tracking of the movement of MDA-231-MB tumoral cells seeded on top of decellularized 3D-ECM from Control and *Snai1* KO MEFs treated or left untreated with TGFβ. (B) Crystal violet staining of MDA-231-MB tumoral cells that have invaded through decellularized 3D-ECM from Control and *Snai1* KO MEFs treated or left untreated with TGFβ. Adapted from Stanisavljevic J. et al.[61].

2. SPLICING

RNA splicing is a process whereby newly synthesized precursor messenger ribonucleic acids (pre-mRNA) are transformed into mature messenger RNA (mRNA). The process consists of the removal of all introns and the joining of the remaining exons. This process is needed so that the mRNA can be correctly translated into protein and takes place immediately after, even simultaneously, the pre-mRNA synthesis[66].

However, while the splicing of most exons is constitutive and they are always included in the final mRNA, some of the splicing events can be

regulated depending on the cellular context. This regulation leads to more than one transcript arising from one single gene in a process known as alternative splicing. It has been estimated that up to 95% of all multi exon human genes have some form of alternative splicing[67].

2.1. Alternative splicing

Alternative splicing is an essential post-transcriptional regulation mechanism that enables the production of different mRNA transcripts that will result in different protein isoforms being generated from a single gene. This variability can take place in the form of skipped cassette exons, intron retention, mutually exclusive exons and alternative 5' and 3' in exons, being the cassette exon skipping the most common alternative splicing event[68] (Figure 8). This kind of splicing event will lead to the alternative inclusion or skipping of an exon flanked by two other exons that are constitutively included in the mRNA.

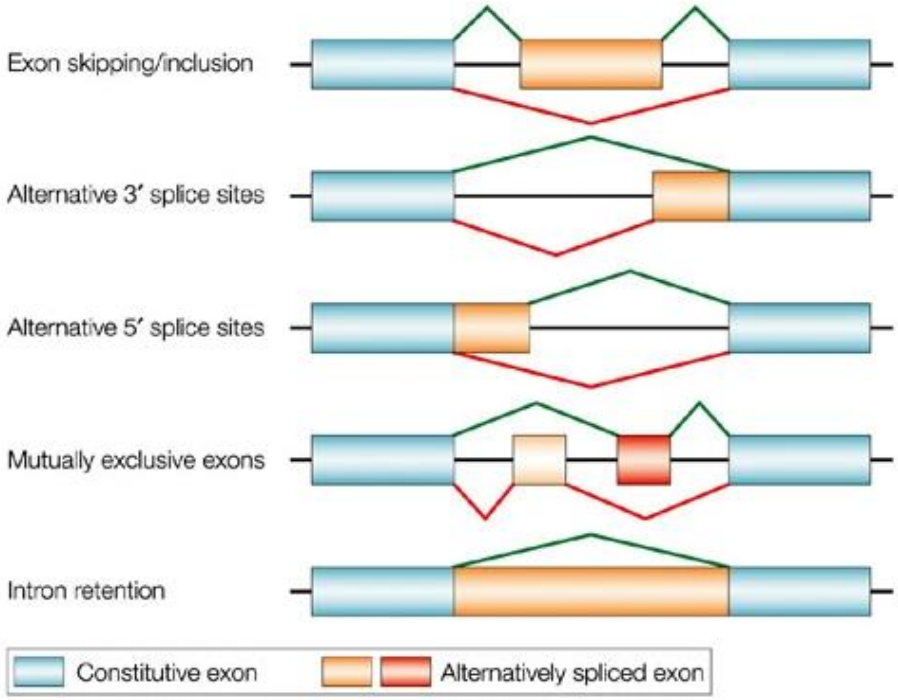

Figure 8: Common patterns of alternative splicing. In each case, one splicing option is indicated in green and the second in red. The exons and introns represented in orange and red are included or excluded on the mRNA depending on the used splicing pattern. Adapted from Cartegne L. et al.[69]

2.1.1. Alternative splicing regulation

Constitutive splicing mechanisms and machinery have been thoroughly studied and are well defined. The process is mainly carried out by the spliceosome, a series of small nuclear ribonucleoprotein complexes (snRNPs) formed by over 300 proteins interacting sequentially with uridine-rich small nuclear RNA molecules (U snRNAs)[70]. This machinery recognizes a series of pre-mRNA motifs such as the 5' and 3' splice sites of an intron, the branchpoint and the polypyrimidine tract. Major spliceosome elements bind to these

regions and interact with them in a predetermined and sequential manner, leading to the removal of an intron and the joining of two consecutive exons in the mature mRNA[71].

However, the splicing process can be regulated by a vast array of circumstances leading to alternative splicing products. The described binding motifs have been shown to be stronger or weaker depending on features such as their conservation relative to the canonical binding motif. Deviations from this cannon lead to weak splicing sites resulting in an exon being skipped in some of the mature mRNAs produced[72,73].

The inclusion and skipping rate is regulated by cis-acting elements and trans-acting factors. Cis-acting elements are genetic sequences that regulate the binding of the trans-acting factors, proteins that will actively regulate the spliceosome. These cis-acting elements have been categorized as splicing enhancers and splicing silencers. Depending on their genomic location this leads to the existence of Exonic Splicing Enhancers (ESE) and Intronic Splicing Enhancers (ISE) or Exonic Splicing Silencers (ESS) and Intronic Splicing Silencers (ISS)[74]. Enhancers are typically bound by positive trans-acting factors, such as proteins belonging to the serine/arginine rich family (SR), while silencers are bound by negative splicing factors such as heterogeneous nuclear ribonucleoproteins (hnRNPs)[75] (Figure 9). ESEs tend to be recognized by, at least, one member of the SR family which will then recruit the rest of the splicing machinery and act at several steps of the splicing reaction[76,77]. However, SR protein binding sites are not exclusive to alternative splicing, as they are also found on exons that are constitutively included in the mature mRNA[78].

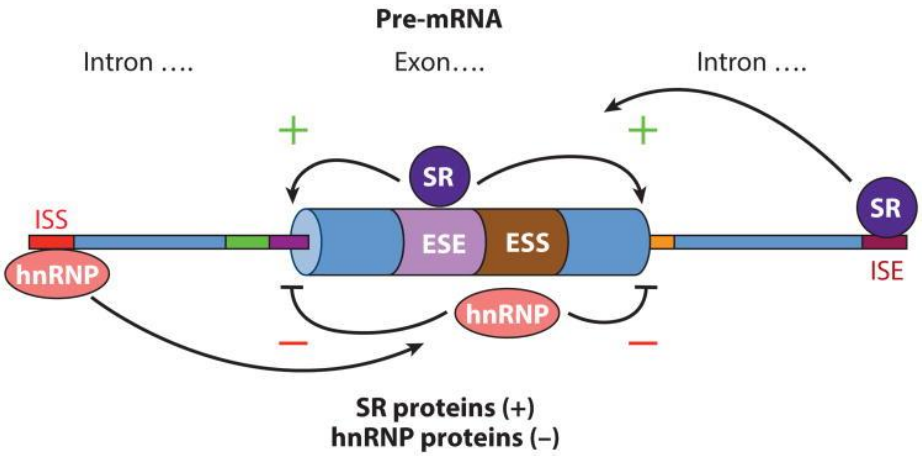

Figure 9: Splicing regulatory elements. Schematic representation of the types of existing cis-acting regulatory elements in a pre-mRNA. Typical trans-acting splicing factors and their effects on splicing are depicted. Obtained from Lee Y. and Rio D. C. [74].

2.1.2. Alternative splicing in cancer

While alternative splicing is necessary for the proper tissue homeostasis, it has also been linked to disease. A study performed on 32 different tumor types across 8705 patients identified thousands of alternative splicing events unique to tumors[79]. These splicing alterations lead to production of functionally distinct protein isoforms advantageous for tumor growth or induce frameshifts leading to nonsense-mediated decay in tumor suppressor genes[80,81]. The effects of this altered splicing patterns are so wide, affecting different aspects of tumor development such as proliferation, vascularization or invasion, that aberrant alternative splicing has been proposed as a new hallmark of cancer[82].

The shift in splicing patterns has been linked to an array of mutations. These mutations can alter elements of the spliceosome, leading to differences in binding motif recognition or hindering their interaction with other components; the cis-acting regulatory elements, leading to a shift in splicing factor recognition; and the splicing factors, altering their affinity for specific binding sites[83]. Additionally, alterations in the expression levels of certain splicing factors can also cause malignant transformation of cells. An example of this behavior is the splicing factor of the SR family SRSF1. This factor, which has been labeled as a proto-oncogene, has upregulated expression levels in many tumor types[84,85]. For instance, the overexpression of SRSF1 leads to an inactive isoform of the tumor suppressor BIN1 and to oncogenic isoforms of kinases MNK2 and S6K1 in rodent fibroblasts. In turn, this results in increased tumor stage, decreased survival and increased resistance to chemotherapy[86]. Similar roles have been proposed for other members of the SR family.

However, increasing knowledge of splicing alterations in cancer has provided new potential therapeutical approaches. These approaches currently consist in either targeting the unique isoforms, taking advantage of the appearance of neoantigens, or reversing the splicing alterations, modulating splicing using antisense oligonucleotides (AONs). AONs are short oligonucleotides, about 15-25 bases long, that correspond to the sequence complementary to a target RNA transcript. They are typically designed to target splice sites or splicing regulatory regions and their objective is to interfere with the binding of trans-acting factors. To increase the stability of the AON and ensure

that the bound transcript is not degraded as would happen using a small interfering RNA (siRNA), AONs are synthesized using modified nucleic acids such as 2'-O-methoxyethyl or 2'-O-methoxy-phosphorothioate, reducing their sensibility to degradation[87]. These AONs have been used and produced on a clinical level as a treatment for other diseases such as Duchenne muscular dystrophy[88] and several cancer treatments based on this therapeutic approach are being tested and developed[89].

2.1.3. Alternative fibronectin splicing

As already mentioned, fibronectin plays a key role in ECM deposition and arrangement. Although there is one single gene coding for fibronectin, up to 20 isoforms of the protein have been described in humans[90]. This variability arises from alternative splicing for three of the 46 exons that form the fibronectin gene: exons 25, 33 and 40. Both exons 25 and 33 code for a complete type III domain, extra domain B (EDB) and extra domain A (EDA) respectively, while exon 40 encodes for a segment of variable length (IIICS) that serves as a connector between two different type III domains. Inclusion of both EDA and EDB is regulated in a cassette exon manner, where they can be either included or skipped from the mature mRNA[91]. Inclusion of IIICS follows a complex pattern of splicing which is species dependent[92].

Fibronectin is found either as dimers soluble in plasma (pFN), secreted by hepatocytes and lacking both EDA and EDB, or forming insoluble fibrils in the ECM of tissues (cellular FN or cFN), secreted mostly by fibroblasts and with variable amounts of the alternatively spliced

domains[90]. As previously discussed, in the context of the ECM, fibronectin interacts with a variety of molecules such as collagen, heparin or fibrin, but also with cellular receptors such as integrins. Some of these binding capabilities require the presence of the extra domains (Figure 10). For instance, while the classical cellular receptor for fibronectin is integrin $\alpha5\beta1$, EDA appears to be interacting with integrins $\alpha4\beta1$, $\alpha4\beta7$ and $\alpha9\beta1$ but also the Toll-like receptor 4 (TLR4)[90].

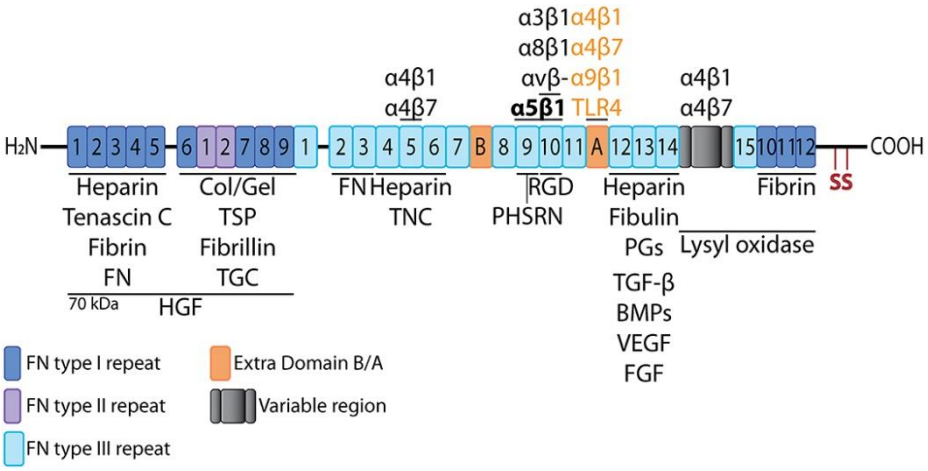

Figure 10: Fibronectin domain structure. Schematic representation of the linear structure of fibronectin, showing the constitutively included domains as well as the alternatively spliced extra domains A and B and the variable region. Interactions for each domain are shown, indicating cellular receptors (up) and other molecules (down). From Efthymiou G. et al.[93].

Under normal conditions, fibronectin EDA expression is restricted to early development and wound healing[94]. It has been shown that while FN1 expression is essential during fetal development, fibronectin EDA KO mice are viable[95]. However, the same studies revealed a decrease in wound healing in an EDA dependent manner, affecting

epithelialization and infiltration of inflammatory cells such as macrophages. Roles for fibronectin EDA in perpetuating the inflammatory response in fibrosis have also been stablished, comparing it to the role of TGFβ[96]. Conflicting roles have also been described, pointing out a protective action against excessive fibrotic tissue formation in a liver fibrosis model[97]. Finally, heightened expression of fibronectin EDA has been reported in cancer[98,99], where many roles have been proposed (See 2.1.5. The role of fibronectin EDA).

2.1.4. Fibronectin EDA splicing regulation

Splicing of EDA into the final transcript of fibronectin undergoes strict regulation leading to its inclusion in early development stages and pathological contexts. Use of a three-exon hybrid *Fn1*-α-globin minigene reveals the existence of exonic sequences regulating splicing[100,101]. In cells of human origin, the minigene reveals an Exonic Splicing Enhancer region consisting of a short polypurine sequence (GAAGAAGA) and an Exonic Splicing Silencer (CAAGG)[102]. The ESE region is also found in the mouse genome with a single nucleotide sequence difference (GAAGACGA)[103]. However, while the mouse sequence homologous to the human ESS also presents a single nucleotide mutation (CAGGG), it radically alters the sequence behavior, turning it into a putative ESE (Figure 11). RNase mapping of the exon shows that, rather than directly acting as an ESE by directly binding positive splicing factors to this region, the mouse ESS plays a role in maintaining RNA secondary structure that ensures spatial

availability for splicing factors to bind to the actual ESE[104]. This shift has been related to changes in the RNA secondary structure that arise from the total of 8 non-conserved nucleotides from human to mouse, as simultaneous directed mutagenesis of these 8 nucleotides confers an ESS behavior back to the homologous sequence.

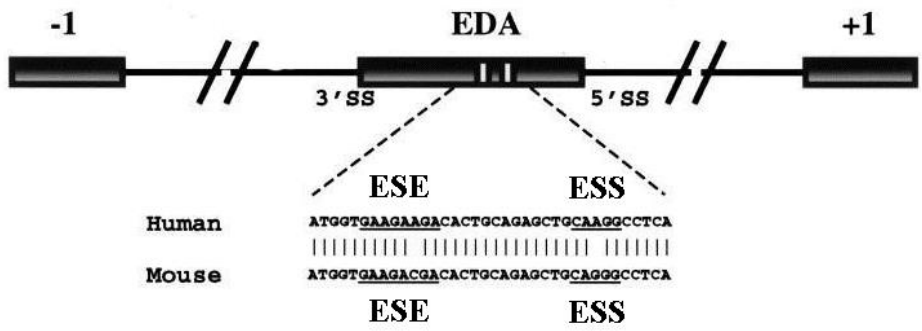

Figure 11: Comparison of EDA splicing regulators. Schematic representation of the EDA region of *FN1* including the two regulatory sequences. Sequence comparison between human and mouse is shown. Adapted from Muro AF. et al.[103]

Initial *in vitro* experiments performed using the aforementioned minigene reveal that many members of the serine-arginine rich splicing factor family bind to EDA coding RNA, including SRSF1[104,105]. Specifically, the ESE region contains the consensus sequence described for SRSF1[106] and its deletion removes the binding[104]. Overall, SRSF1 tightly regulates EDA inclusion rate, as overexpression and loss-of-function experiments for SRSF1 respectively lead to increased and reduced EDA inclusion rates[105,107]. Studies focusing on how SRSF1 is

recruited to the EDA have pointed towards a polymerase II dependent recruitment that takes advantage of the simultaneous nature of transcription and splicing[105,108]. However, a lot remains unclear regarding the regulation of EDA splicing and SRSF1 recruitment to its ESE.

2.1.5. The role of fibronectin EDA

Inclusion of EDA into fibronectin leads to the acquisition of new functions. Some studies propose that the presence of EDA in the protein may be altering either the entire general tertiary structure of the molecule[109] or the availability of the RGD sequence, the main cell binding site[94] (see Figure 9). Besides the potential effects in altering the binding of other fibronectin domains, the presence of EDA generates novel interactions with a different subset of integrins and the TLR4, which can't interact with pFN[110,111].

Up to date, a long list of functions has been proposed for EDA fibronectin including: wound healing, matrix assembly, dimer formation, secretion, cell adhesion, cell differentiation, tissue injury and inflammation and cell cycle progression and mitogenic signal[95].

A body of literature describes the effects of EDA fibronectin interaction with TLR4 in a variety of immune cells, such as monocytes[112] and macrophages[113], and its consequences on inflammatory response in models of lung and liver fibrosis and atherosclerosis[114,115]. Indeed, The EDA is considered a damage-associated molecular pattern inducing innate immune system. This corpus of knowledge indicates that fibronectin EDA may directly affect

the behavior of cells such as fibroblasts[116,117] and epithelial cells[109,118,119]; however, there is also literature describing indirect effects through immune cell activation.

It should be noted that most of the studies that investigate EDA fibronectin function on cells have been performed supplying cells with recombinant monomeric fibronectin or small soluble fragments, ranging from exclusively the EDA peptide to the EDA flanked by a couple of extra exons. Alternatively, a few studies have focused on *in vivo* effects of EDA fibronectin through the use of genetically modified mice[95]. Therefore, the role of EDA fibronectin in its full form and within the whole ECM context remains obscure. It is of particular interest that, upon beginning this project, we found a complete absence of studies regarding EDA the roles of fibronectin in regulating ECM physical and mechanical properties such as matrix stiffness and alignment. Since then, some studies have been published[120], but a detailed characterization is still lacking (Figure 12).

The better characterized role for EDA is its capacity to activate fibroblasts into myofibroblasts[121]. In this regard, the importance of EDA fibronectin has been compared to that of a stiff ECM[122] and to TGFβ[36,90]. Studies focusing on the pathways necessary for fibronectin EDA induced fibroblast activation point towards its interaction with integrins $\alpha4\beta1$ and $\alpha9\beta1$, inducing focal adhesion maturation[117,123]. Recent studies have tested the use of polypeptides to block these interactions, proving their relevance[124].

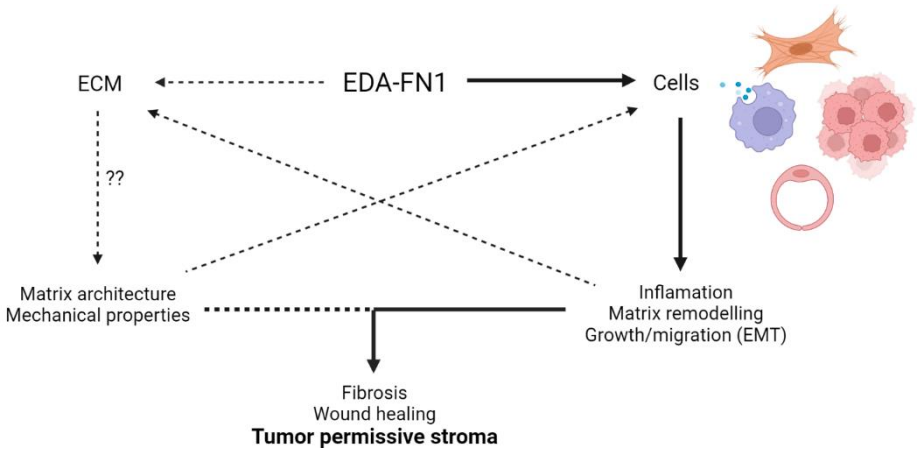

Figure 12: Summary of the roles of fibronectin EDA. Diagram depicting the known roles for fibronectin EDA. It's effects on cells lead to various consequences, including the generation of a permissive stroma in a tumoral context. Fibronectin EDA effects on the ECM, influencing its architecture and mechanical properties, are less studied.

Comparison of fibronectin EDA and TGFβ relevance is especially significant as they both participate in a positive feedback loop[90]. As TGFβ is produced, it is secreted and binds to the ECM in an inactive latent state. Presence of fibronectin EDA in the ECM enhances the binding of the inactive form of TGFβ and its subsequent activation[121]. In turn, TGFβ has been shown to be a positive regulator of EDA inclusion[125]. In particular, TGFβ has been reported to promote EDA inclusion at least partially through activation of the PI3K/AKT/mTOR pathway, leading to mobilization of the splicing factor SRSF1[126]. However, mechanisms behind fibronectin EDA dependent latent TGFβ attachment to the ECM and TGFβ induced EDA splicing remain largely unexplored, and the role SNAIL1 may be playing as a TGFβ target has never been investigated.

EDA fibronectin expression has been used as a marker for tumor development and the use of antibodies targeting the EDA has been tested as a drug-delivery system to treat tumors[99]. Experiments performed *in vitro* on tumoral cell lines using various recombinant fibronectin isoforms suggested roles in cell cycle progression as well as migration induction[109,118]. However, the exact functions of EDA fibronectin in a tumoral context are yet to be elucidated and described in a systematic manner using models closely resembling *in vivo* conditions.

OBJECTIVES

Preliminary experimental data from our group suggests the transcription factor SNAIL1 regulates alternative splicing for the fibronectin extra domain A. The underlying molecular mechanism and the implications this regulation has in the TGFβ/SNAIL1 controlled extracellular matrix architecture, promoting tumor progression, remain unknown.

Thus, the main objectives of this thesis were:

1. To demonstrate that SNAIL1 regulates the alternative inclusion of EDA into fibronectin and to characterize the molecular mechanisms involved.
2. To study the contribution of an increased rate of EDA inclusion to the generation of a metastasis-permissive tumoral microenvironment.
3. To evaluate the potential of EDA-targeting molecules as therapeutic tools for cancer.

RESULTS

1. CHARACTERIZATION OF THE CORRELATION BETWEEN SNAIL1 AND FIBRONECTIN EDA

The first aim of this thesis was to assess the existence of a correlation between the expression of fibroblastic SNAIL1 and the percentage of inclusion of the EDA domain in the final transcript of *Fn1*. Previous differential RNA-seq data from control and *Snai1* KO Mouse embryonic fibroblasts (MEFs), obtained by Dr. Laura Sala and Maria Val in our laboratory during their PhD thesis and Masters thesis respectively, showed that the percentage of EDA including isoforms decreased over 50% in the fibroblasts lacking the transcription factor. Therefore, we focus on confirming this result at RNA and protein levels and extending the observation to other biologically relevant models.

1.1. Inclusion of the EDA into fibronectin is increased in fibroblasts in a SNAIL1 dependent manner

The levels of *Fn1* isoforms including and skipping the EDA coding exon (exon 33) expressed by Control and *Snai1* KO MEFs were assessed through semi-quantitative RT-PCR (RT-sqPCR). In this approach, the isoforms were detected on the cDNA using a PCR primer pair targeting the flanking exons (Figure 13a), leading to amplification of a long (inclusion) or short (skipping) fragment distinguishable by electrophoresis. While the levels of the isoforms including the exon 33 decreased in the *Snai1* KO MEFs, the amount of skipping isoforms increased. A short treatment of the cells with TGFβ did not significantly modify the proportion of isoforms in the MEFs. This effect of SNAIL1 fits nicely with the results obtained previously through RNA-

seq (Figure 13b). As already described, a longer treatment with the cytokine TGFβ, which promotes fibroblast activation and is associated to advanced tumor stages, promotes EDA-FN1 RNA expression. We found that this increase was SNAIL1 dependent (Figure 13c).

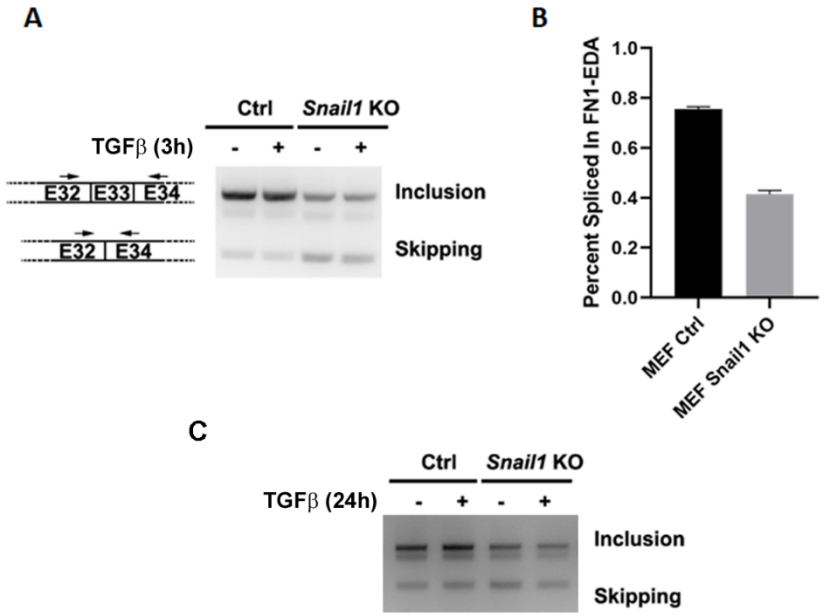

Figure 13: SNAIL1 induces inclusion of the EDA domain into the fibronectin RNA. (A) *Relative RNA amount of EDA fibronectin isoforms.* Left, schematic representation of the annealing location of the PCR primers used and the two possible outcomes corresponding to the alternative splicing of exon 33 in *Fn1*. Right, RNA was obtained from MEFs Ctrl and KO for *Snai1* untreated or treated with 5ng/mL of TGFβ for 3 hours. RNAs were retrotranscribed and amplified using the primers depicted in the left. Resulting DNA was visualized by electrophoresis on a 2% agarose gel. (B) *Quantification of EDA fibronectin inclusion*. RNA sequencing was performed on the samples from indicated MEFs that had been treated with 5ng/mL TGFβ for 3h. Percent spliced in EDA-FN1 was calculated from the exon inclusion and exclusion in RNA-Seq reads. Experiment was performed three times. (C) *Relative RNA amount of EDA fibronectin isoforms.* RNA was obtained from MEFs Ctrl and KO for *Snai1* untreated or treated with 5ng/mL of TGFβ for 24 hours. RNAs were retrotranscribed and amplified as in (A)

Protein samples from two fibroblast cell lines were analyzed to study if changes in EDA RNA levels correlate with changes in protein levels. The expression levels of fibronectin containing the EDA domain (EDA-FN1) were assessed with commercially available antibodies which specifically target the EDA. Protein amounts of EDA-FN1 in MEFs *Snai1* KO were almost undetectable, showing the pivotal role of SNAIL1 in its production (Figure 14a). Treatment of MEFs with TGFβ for 24 hours led to a detectable increase in EDA-FN1 production that was also prevented by the absence of SNAIL1.

Seeking to confirm this result, as well as testing the existence of this correlation in human fibroblasts, we performed the same analysis in human BJ fibroblasts by down-regulating *Snai1* expression levels with a specific siRNA. The siSnai1 treated cells showed not only a reduction in SNAIL1 but in the EDA-FN1 protein levels as well (Figure 14b).

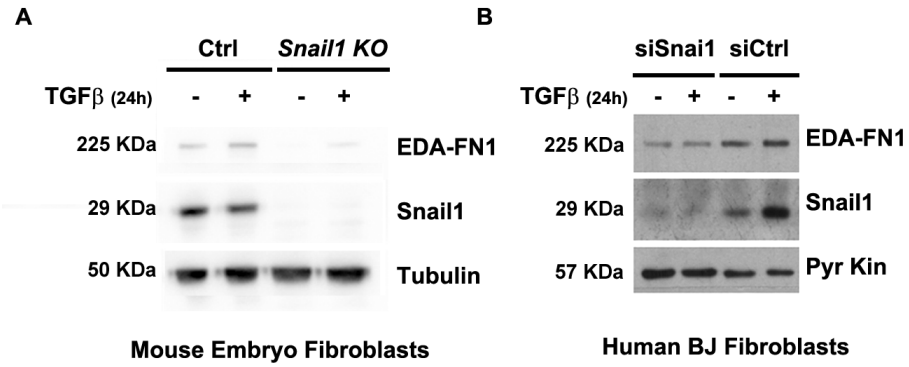

Figure 14: Downregulation of *Snai1* reduces fibronectin EDA protein levels. (A) *Protein amount of EDA fibronectin and SNAIL1 in MEFs.* MEFs Ctrl and KO for *Snai1* were left untreated or treated with 5ng/mL of TGFβ for 24 hours and lysed in SDS buffer. Levels of the indicated proteins were analyzed by Western Blot. (B) *Protein amount of EDA fibronectin and SNAIL1 in BJ*

fibroblasts. Human BJ fibroblasts were transfected with siRNA anti-Snai1 or Control and later treated or not with TGFβ for 24 hours. Cells were lysed in SDS buffer and levels of the indicated proteins were analyzed by Western Blot.

1.2. SNAIL1 induces EDA inclusion in other cellular models

Having confirmed that decreasing SNAIL1 levels in fibroblasts favors EDA skipping, we wondered if an increase in its expression induces inclusion. For this purpose, we analyzed protein and RNA from the human colon adenocarcinoma cancer cell line HT-29 M6, that expresses undetectable endogenous levels of both SNAIL1 and FN1, and its derived cell line established in our lab that overexpresses ectopic SNAIL1 tagged with the Hemagglutinin epitope (SNAIL1-HA)[127]. The increase in SNAIL1 expression was clearly detected through immunoblotting when comparing transfected and parental cells (Figure 15a). The overexpression of SNAIL1 correlated with increased amount of EDA both at protein and RNA levels (Figure 15a and 15b).

Overall, these results in fibroblasts and epithelial cells strongly suggest a role of SNAIL1 in regulating EDA alternative splicing, where an increase in SNAIL1 leads to increased inclusion of EDA in *Fn1* mRNA.

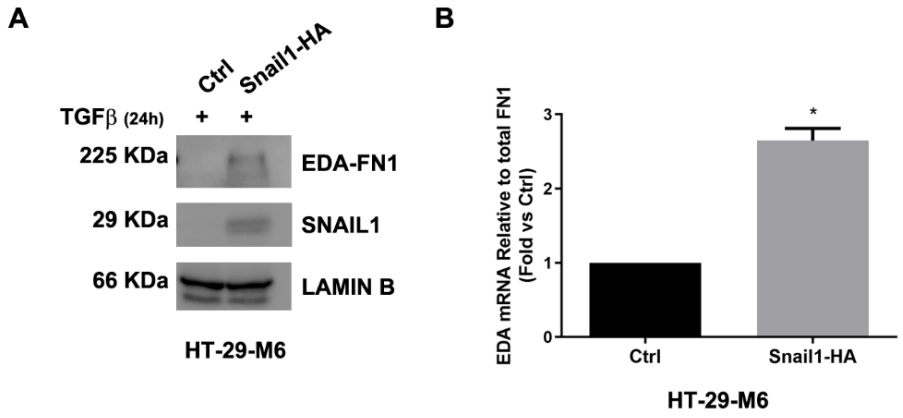

Figure 15: Overexpression of SNAIL1 increases fibronectin EDA levels. (A) *Protein amount of EDA fibronectin and SNAIL1 in HT-29 M6.* HT-29 M6 Ctrl and expressing exogenous SNAIL1-HA were treated with TGFβ for 24 hours. Cells were lysed in SDS buffer and levels of the indicated proteins were analyzed by Western Blot. (B) *Relative RNA amount of EDA fibronectin*. RNA was obtained from HT-29 M6 Control and expressing exogenous SNAIL1-HA that had been treated with TGFβ for 24 hours. RNAs were analyzed by RT-qPCR with oligonucleotides specific for the exon 33 detecting the inclusion of the EDA-*Fn1* or the exons 1 and 2 included in all the isoforms of *Fn1*. EDA-*Fn1* levels were normalized to the amount of total *Fn1*.

1.3. Fibronectin EDA protein levels correlate with SNAIL1 in patient derived xenografts

In order to interrogate the correlation of SNAIL1 and fibronectin EDA expression in a more physiological experimental model, we took advantage of a Patient-derived xenograft (PDX) collection from Dr. J. Arribas' laboratory (Vall Hebron Institute of Oncology – Institut Hospital del Mar d'Investigacions Mèdiques, Barcelona, Spain) previously used in our lab[128]. We analyzed 29 frozen pieces of PDXs stablished from human breast tumors corresponding to $HER2^+$ and triple negative breast neoplasms. Protein samples were extracted and

immunoblots for SNAIL1 and EDA-FN1 were performed (5 representative PDXs are shown in Figure 16a). The specific bands were quantified and a cut-off was set to divide samples in High vs Low levels for each protein.

Fitting with our previous data in cell lines, PDX with high SNAIL1 protein levels showed a 5-fold increased percentage of samples with high EDA-FN1 levels (Figure 16b).

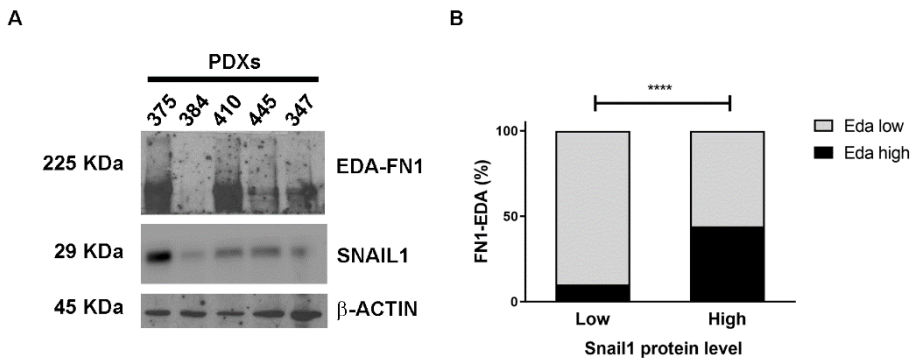

Figure 16: EDA exon inclusion is increased in PDXs with high SNAIL1 levels. (A) *Protein amounts of EDA fibronectin and SNAIL1 in PDX*. Pieces of PDXs were lysed in SDS buffer. Levels of EDA-FN1, SNAIL1 and β-ACTIN were analyzed by Western Blot. 5 representative PDXs are shown out of 29 (B) *Quantification of EDA fibronectin and SNAIL1 protein levels of the 29 PDX*. ImageJ Software was used to quantify EDA-FN1 and SNAIL1 levels relative to β-ACTIN. Three Western Blots were performed for each sample and the average was used for each PDX. EDA-FN1 and SNAIL1 levels were divided into two groups each: Low and High. Significant differences were assessed using Chi-squared test.

1.4. Fibronectin EDA protein levels correlate with SNAIL1 in a variety of tumor types

In addition to the data from PDXs, we wondered how widespread this correlation is *in vivo*. To address this issue, we resorted to information from cBioPortal and TSVdb databases that hold molecular information from patient samples collections of many tumor types.

While most databases collect RNA quantifications, some cBioPortal collections provide data on SNAIL1 protein levels. This was a mandatory requirement for our analysis, as SNAIL1 levels are widely regulated post-transcriptionally. In line with this asseveration, our initial evaluation of available data confirmed that *Snai1* RNA and protein levels in tumors correlated poorly. We also took advantage that TSVdb offers RNA expression data for each splicing isoform of fibronectin. Thus, combining data from TSVdb and cBioPortal databases, we obtained appropriate data from patients to examine the correlation between the two parameters.

Collected tumor data were analyzed as in PDXs. We calculated the proportion of the isoforms that include EDA vs those that don't and classified samples in Low vs High levels. For each studied tumor type (breast adenocarcinoma, lung adenocarcinoma, kidney renal clear cell carcinoma, bladder cancer and skin cutaneous melanoma) we categorized samples in two groups according to their clinical stage. Stages I and II, meaning tumors that are localized or are starting to advance into neighboring tissues; and stages III and IV, meaning

tumors that have started to invade lymph nodes or are already metastatic.

We obtained an equivalent trend in each tumor type: early stages tumors expressing basal fibronectin EDA percentages independently of their SNAIL1 levels (Figure 17) and advanced tumors with high SNAIL1 expression clearly enriched in EDA-FN1.

Altogether, our data indicates a ubiquitous correlation between SNAIL1 and regulation of *Fn1* splicing leading to inclusion of the EDA domain.

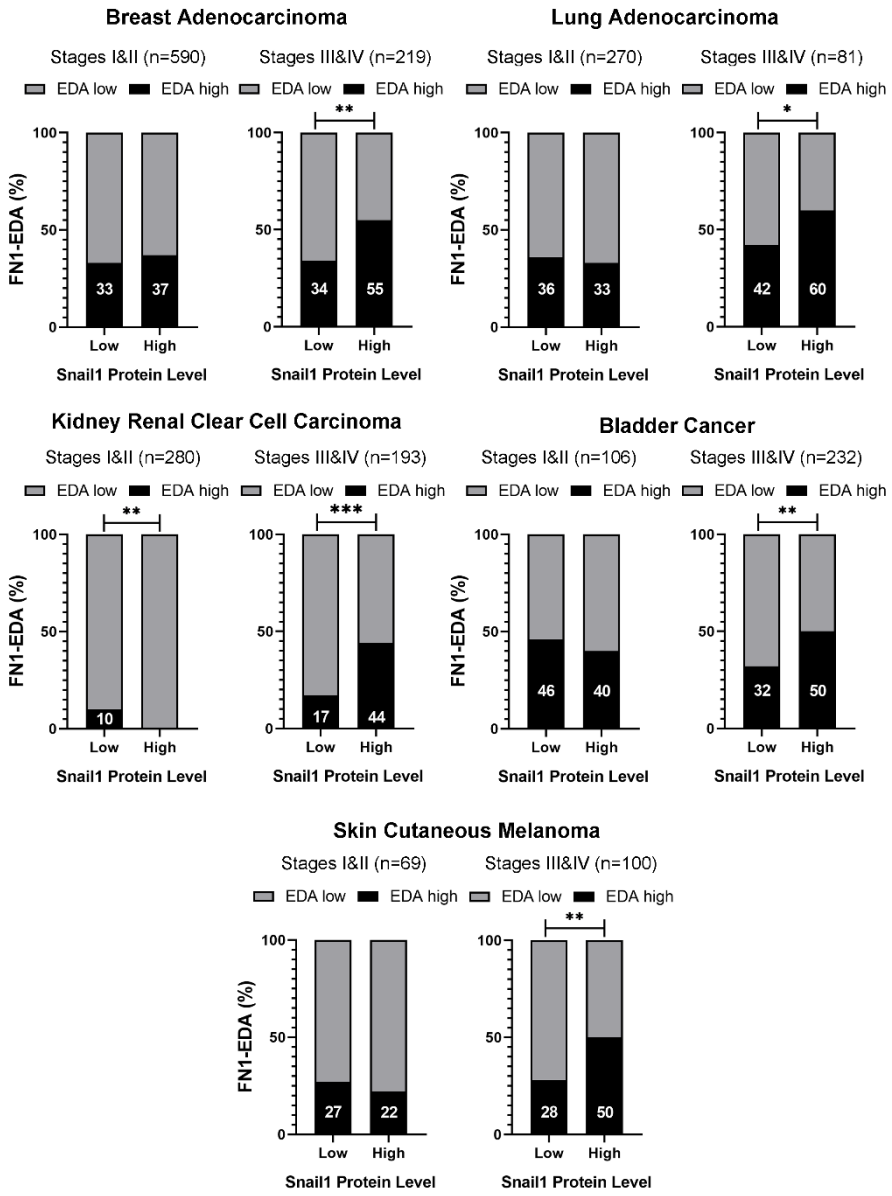

Figure 17: EDA exon inclusion into fibronectin RNA correlates with high SNAIL1 levels in 5 human tumor types. *Fn1* RNA and SNAIL1 protein data of patients of the indicated tumor types were obtained respectively from TSVdb and cBioPortal databases. Percentage of EDA inclusion rate was calculated for each sample. EDA-FN1 percentage and SNAIL1 protein levels were divided into two categories: Low and High. Samples were independently analyzed in two groups: Tumor Stages I and II and Tumor Stages III and IV. The number of tumors per group is indicated as n.

2. ELUCIDATING POSSIBLE MOLECULAR MECHANISMS FOR SNAIL1 SPLICING REGULATION

While SNAIL1 role as an EMT transcription factor repressing epithelial genes and enhancing mesenchymal genes has been reported, a specific role in regulating splicing is yet to be described. It was an objective of this thesis to establish some basic knowledge on the workings of SNAIL1 regulation of alternative splicing.

Among many other splicing events, the splicing factor SRSF1 has already been described as positively regulating the alternative inclusion of fibronectin exon 33 coding for EDA[105]. In contrast, no connection between KHSRP (KH-Type Splicing Regulatory Protein) and EDA splicing regulation has been published up to date. However, using our original RNA-seq data, Dr. Juan Luis Trincado (from Dr. Eyras laboratory, Univesitat Pompeu Fabra) performed bioinformatics analyses to select SNAIL1-dependent splicing events and unveil enrichment of splicing factor motifs in the genomic regulatory sequences around the events. The analysis unveils a small but significant enrichment in KHSRP binding motifs. This finding was deemed of interest, as one of the found binding motifs for KHSRP is located in the splicing regulatory regions of EDA.

2.1. The splicing factors SRSF1 and KHSRP colocalize with SNAIL1

To test if SNAIL1 interacts with either SRSF1 or KHSRP, we first studied their cellular distribution through immunofluorescence. We analyzed MEFs activated with TGFβ as the EDA inclusion is increased in this condition and compared the signal with that from TGFβ activated

Snai1 KO MEFs. Both splicing factors mainly localized in the nuclei of both MEF lines (Figure 18), ruling out a significant role of SNAIL1 in their cellular distribution. Co-localization with SNAIL1 was observed for both splicing factors.

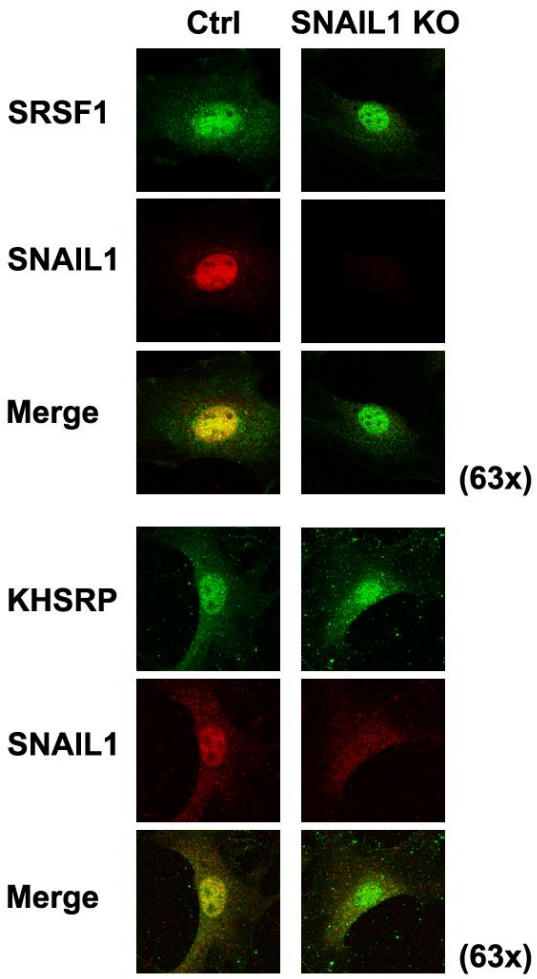

Figure 18: SNAIL1, SRSF1 and KHSRP colocalize in the nucleus of MEFs. Control and *Snai1* KO MEFs were grown on glass coverslips, treated with TGFβ for 24 hours and fixed with 4% PFA. SNAIL1, SRSF1 and KHSRP cellular distribution were analyzed by immunofluorescence with specific antibodies and Alexa 488 and 555 conjugated secondary antibodies. Images were obtained through confocal microscopy. Merge images were produced with ImageJ and show colocalization in yellow.

To confirm that SNAIL1 forms a protein complex with the studied splicing factors we tested if they could be coimmunoprecipitated. Indeed, coimmunoprecipitation of KHSRP with an SNAIL1 antibody was obtained in protein extracts from MEF cells activated with TGFβ for 24 hours (Figure 19a). In equivalent extracts, SNAIL1 was also coimmunoprecipitated with an SRSF1 antibody (Figure 19b).

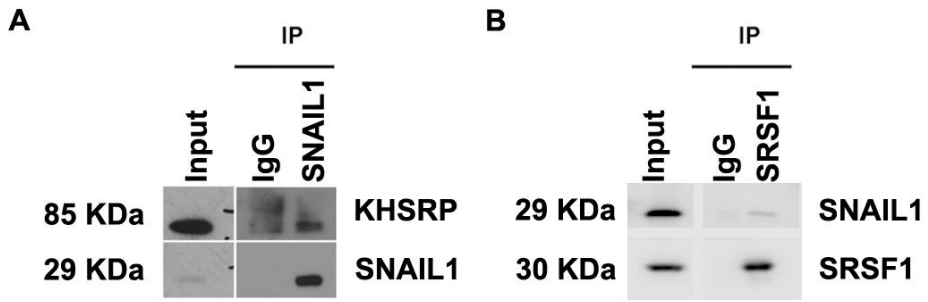

Figure 19: KHSRP and SRSF1 co-immunoprecipitate with SNAIL1. (A) *KHSRP co-immunoprecipitation with SNAIL1*. Extracts of MEFs treated with TGFβ for 24 hours were obtained in RIPA buffer. Immunoprecipitation was performed using an antibody specific for SNAIL1 and agarose beads. Immunoprecipitated proteins were analyzed by western blot. (B) *SNAIL1 co-immunoprecipitation with SRSF1*. Extracts were treated in the same manner as in (A). An antibody specific for SRSF1 was used.

2.2. SNAIL1 is purified into an RNA binding protein fraction

Given the existence of an interaction between SNAIL1 and two RNA binding proteins regulating splicing, we wondered whether SNAIL1 can also behave as an RNA-binding protein (RBP).

To test its RNA-binding potential, we resorted to Orthogonal Organic Phase Separation (OOPS), a recently described technique which uses low doses of UV light to induce RNA to protein cross-linking, while

avoiding cross-linking of both protein to protein and DNA to protein. RNA-protein complexes are obtained from a final interphase fraction of a series of organic phase separations. RNA interacting proteins are visualized by western blot after controlled RNA degradation.

We found SNAIL1 together with other RBP, like SRSF1 and KHSRP, and dislike other proteins (α-tubulin or β-actin) without a role as RBP that were used as negative controls (Figure 20).

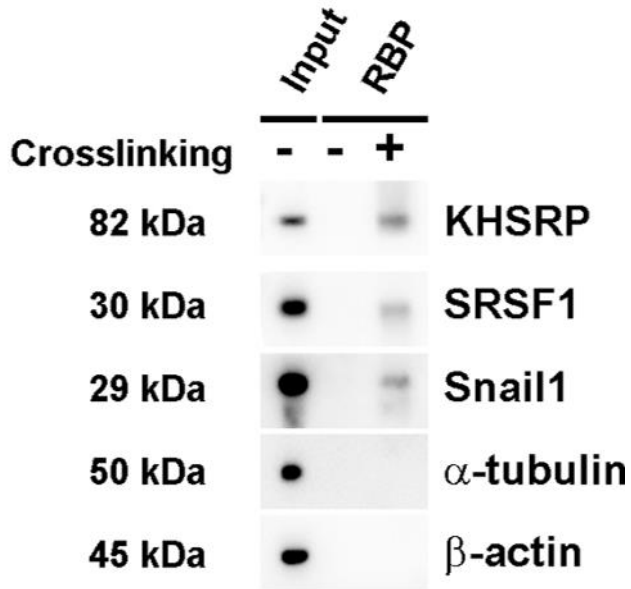

Figure 20: SNAIL1 is an RNA binding protein. MEFs treated with TGFβ for 3 hours were irradiated with a dosage of 300mJ/cm2 UV light to induce protein-RNA crosslinking or left not irradiated. Samples were processed through a series of phase separation steps using TRIzol. The interphase consisting of proteins bound to RNA was then treated with RNase and an additional phase separation was done to isolate the organic phase, consisting of RNA-binding proteins (RBP). Proteins isolated by this process were analyzed by western blot. Samples from the same cells treated with TGFβ for 3 hours were simultaneously obtained using an SDS buffer and used as Inputs for the experiment. α-Tubulin and β-actin were analyzed as negative controls.

2.3. KHSRP down-regulation does not decrease EDA levels

As no evidence of KHSRP role in regulating EDA splicing was previously reported, we performed loss of function experiments using siRNA targeting the gene coding for this protein. We achieved a good efficiency for KHSRP knock-down (Figure 21) in MEFs. However, results obtained showed that depletion of KHSRP does not lead to a decrease in EDA. Since this result rules out KHSRP role in regulating EDA splicing we decided to focus our efforts on the study of SRSF1.

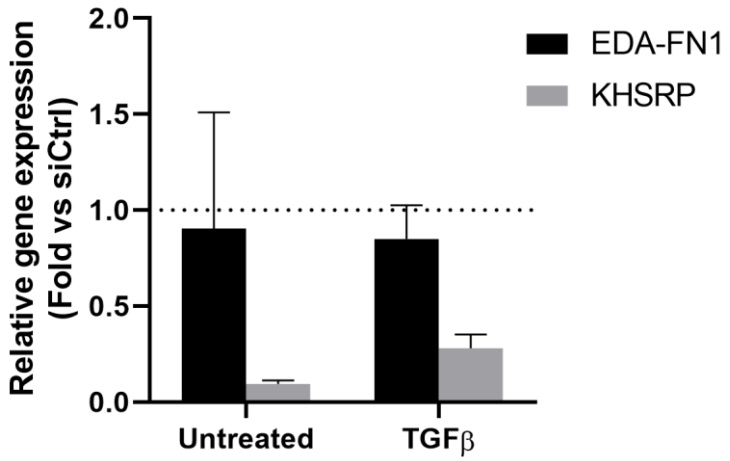

Figure 21: KHSRP knock-down does not down regulate EDA. MEFs were transfected with siRNA anti-KHSRP or Control and later treated or not with TGFβ for 24 hours. RNA was obtained and analyzed through RT-qPCR using primers specific for EDA-FN1, KHSRP and HPRT. EDA-FN1 and KHSRP levels were normalized to HPRT. Each measurement is relative to its own condition transfected with siCtrl.

2.4. SRSF1 interacts with the EDA coding RNA in a SNAIL1 dependent manner

As indicated in the introduction, SRSF1 binds to the exon 33 RNA to regulate its inclusion. Here, we evaluated if SNAIL1 also binds this RNA region by RNA immunoprecipitation (RIP). For that purpose, endogenous SNAIL1 was immunoprecipitated with a specific antibody from extracts of TGFβ-activated MEFs and the EDA coding RNA co-precipitating detected by RT-qPCR with specific oligonucleotide primers. As no EDA RNA was detected we increased the levels of SNAIL1 by transfecting the MEFs with a plasmid coding for SNAIL1 tagged with HA (Figure 22a) and we immunoprecipitated endogenous and ectopic SNAIL1. Again, no significant precipitation of fibronectin RNA was obtained, despite the fact that in this same condition an anti-SRSF1 did precipitate quantifiable EDA RNA (Figure 22b), ruling out potential RNA degradation or technical issues.

Although we did not detect SNAIL1 binding to the RNA coding exon 33 of fibronectin, we evaluate whether it is required for the detected binding of SRSF1. With this purpose, the RIP assay was performed with an anti-SRSF1 in MEFs KO for *Snai1*. We detected no binding of EDA RNA in the immunoprecipitate of SRSF1 in the *Snai1* KO MEFs (Figure 22b). Decreased SRSF1 binding was not a consequence of reduced protein levels in *Snai1* KO MEFs, as they express comparable or even higher protein levels than control MEFs (Figure 22c).

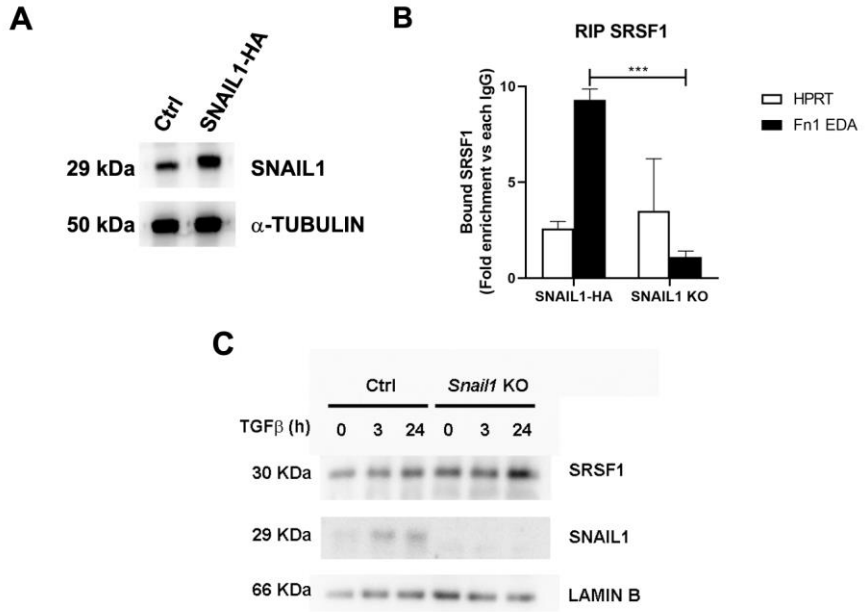

Figure 22: SRSF1 binds to EDA coding RNA in a SNAIL1 dependent manner. (A) *Protein amount of SNAIL1 and α-TUBULIN*. MEF Ctrl and expressing exogenous SNAIL1-HA were lysed in SDS buffer and levels of the indicated proteins were analyzed by Western Blot. (B) *RNA Immunoprecipitation of fibronectin EDA and HPRT RNAs with SRSF1*. RNA Immunoprecipitation (RIP) was performed using an antibody specific for SRSF1 in samples of MEF cells transfected to overexpress SNAIL1-HA and MEF cell KO for *Snai1* treated with TGFβ for 3 hours. Products were analyzed by RT-qPCR using primers targeting the EDA and HPRT as an unspecific control sequence. Bars show binding enrichment compared to immunoprecipitation using unspecific control IgG. At least three replicates were performed for each immunoprecipitation. (C) *Protein amount of SRSF1, SNAIL1 and LAMIN B.* MEF Ctrl and KO for *Snai1* were lysed in SDS buffer after the indicated times of TGFβ treatment and levels of the indicated proteins were analyzed by Western Blot.

2.5. RNA is necessary for SNAIL1 interaction with SRSF1

While OOPS data indicates that SNAIL1 binds to RNA, RIP indicates that it does not bind to EDA RNA. We tested whether RNA is necessary for the interaction of SNAIL1 with SRSF1. Thus, we repeated the coimmunoprecipitation experiment (Figure 19b) after digesting the RNA present in the sample by means of RNase A. Results show that, indeed, SNAIL1 and SRSF1 interaction is dependent on RNA, as coimmunoprecipitation was lost upon RNase A treatment (Figure 23).

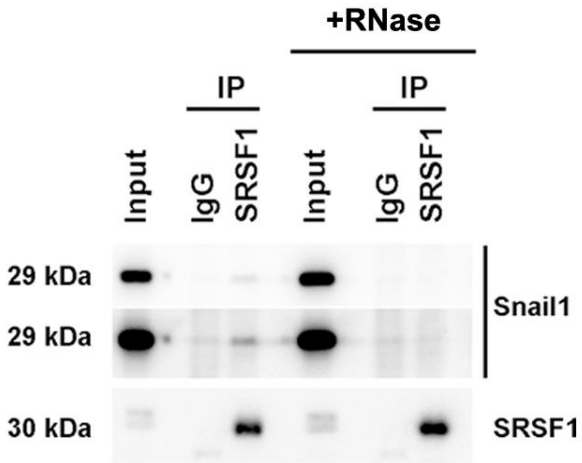

Figure 23: SNAIL1 and SRSF1 interaction is RNA dependent. Extracts of MEFs treated with TGFβ for 3 hours were obtained in RIPA buffer. Half of the sample was treated with 400μg/mL RNase A. RT-qPCR for total fibronectin was performed to confirm the complete elimination of RNA in the samples. Immunoprecipitation was performed using an antibody specific for SRSF1 and agarose beads. Immunoprecipitated proteins were analyzed by western blot.

2.6. Both SNAIL1 and SRSF1 interact with the EDA coding genomic region in a TGFβ dependent manner

Transcription and splicing are connected regulatory mechanism with protein complexes physically linked through nascent RNA[129,130]. In crosslinking conditions, splicing factors have been found interacting with the transcription machinery and precipitating the genomic exons whose alternative splicing they regulate. Thus, we performed ChIP assays with SRSF1 in fibroblasts untreated or treated with TGFβ.

SRSF1 precipitated in a TGFβ independent manner a genomic region at the fibronectin Exon 7 described to be constitutively spliced (Figure 24a). In contrast, we detected TGFβ dependent precipitation of the exon 33 region. Negligible binding was found in a proximal promoter region. These results reinforce the idea that SNAIL1 modulates the ability of SRSF1 to be specifically recruited at the exon 33 region in a complex including DNA and RNA.

To analyze if SNAIL1 interacts with the molecular machinery controlling the exon 33 splicing, we performed ChIP assays with a SNAIL1 antibody. In untreated fibroblasts, none of the studied regions of the *Fn1* gene precipitated with SNAIL1 (Figure 24b). TGFβ treatment not only induced the binding of SNAIL1 to the proximal *Fn1* promoter, as we previously reported[53], but also to exon 33. Negative interaction of SNAIL1 with the exon 7 remarks the specificity of the interaction with the exon 33.

Thus, despite an interaction of SNAIL1 with the exon 33 RNA was not detected by RIP assays, the factor is recruited at the alternative

splicing region, likely as a part of the transcription/splicing DNA-RNA protein complex disrupted by RNase. In this way, SNAIL1 may facilitate the SRSF1-RNA binding and the inclusion event. In contrast, the basal splicing of the exon 33 observed in *Snai1* KO MEFs or the constitutive splicing of exon 7 take place without SNAIL1 recruitment to the exon.

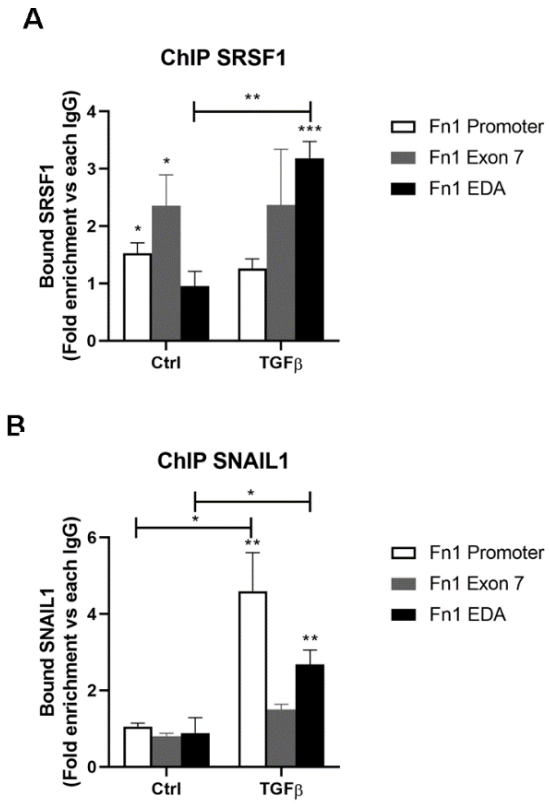

Figure 24: SRSF1 and SNAIL1 bind to the EDA coding region in a TGFβ dependent manner. (A) *Chromatin immunoprecipitation with SRSF1*. Chromatin immunoprecipitation (ChIP) was performed using antibody specific for SRSF1 in samples of MEF cells transfected to overexpress SNAIL-HA untreated or treated with TGFβ for 3 hours. Precipitated DNA was analyzed by qPCR using primers targeting *Fn1* promoter (+116/+265), *Fn1* Exon 7 and *Fn1* Exon 33 (EDA). Bars show binding enrichment compared to Immunoprecipitation using unspecific IgG. At least three replicates were performed for each immunoprecipitation. (B) *Chromatin immunoprecipitation with SNAIL1*. Extracts were treated in the same manner as in (A). An antibody specific for SNAIL1 was used.

3. CHARACTERIZATION OF THE EFFECTS OF EDA IN 3D-ECM PROPERTIES

Given the previously described roles for SNAIL1 in regulating fibroblastic deposition and reorganization of the extracellular matrix (ECM) and its newly described role in inducing inclusion of EDA in fibronectin, we decided to study the effects of EDA enrichment in the ECM context. Since fibronectin is a key element in ECM arrangement, we expect changes in its alternative splicing to lead to changes in matrix alignment and stiffness, parameters closely related to tumor progression.

3.1. Characterization of genetically modified MEFs

In order to study of the effects of the enrichment or the lack of EDA in an *in vivo* like ECM model, we obtained two genetically modified MEF cell lines derived from genetically modified mice as described elsewhere[95]. These cell lines were kindly gifted by Dr. Muro's lab (International Center for Genetic Engineering and Biotechnology, Trieste, Italy). Briefly, the wild-type EDA coding exon was replaced with a "floxed" EDA exon with optimized splice sites. The optimized splice site led to constitutive inclusion of EDA. The "floxing" of the whole exon allowed its removal through crossing with another mice strain expressing the CRE-recombinase. Three cell lines were isolated from homozygous mice: wild-type or wt MEF, with an intact alternative splicing; EDA- MEF, without the capacity of including EDA; and EDA+ MEF, with constitutive inclusion of the EDA. Therefore, both EDA+ and EDA- synthesize homomeric fibronectin fibers, composed by

a single isoform, while wild-type MEF synthesized fibers are heteromeric, fibers composed by a mix of isoforms[33].

The fibronectin production of these cells was tested both at RNA and protein levels (Figure 25). The results obtained show that all three cell lines express the expected isoforms, with only wild-type MEF capable of expressing both.

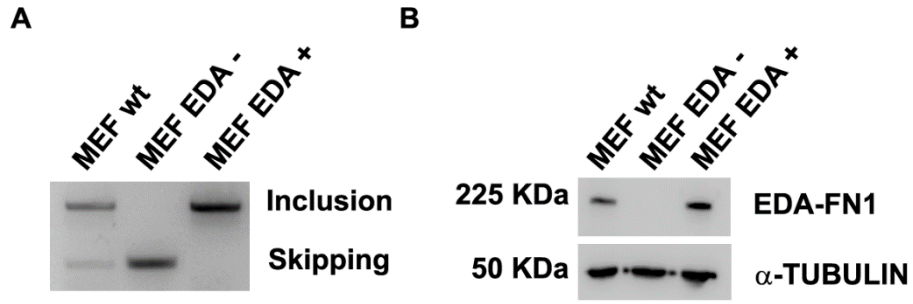

Figure 25: Genetically modified MEFs present altered EDA alternative splicing patterns. (A) *Relative RNA amount of EDA fibronectin isoforms*. RNA was obtained from MEFs wild-type, EDA- and EDA+ treated with 5ng/mL of TGFβ for 3 hours. RNAs were retrotranscribed and amplified using primers flanking exon 33 of *Fn1* as described in Figure 13. Resulting DNAs were visualized by electrophoresis on a 2% agarose gel. (B) *Protein amounts of EDA fibronectin and α-TUBULIN*. Indicated MEFs were lysed in SDS buffer and levels of the indicated proteins were analyzed by Western Blot.

To study the effect of EDA presence in extracellular matrix architecture, we allowed fibroblasts to generate *in vivo* like three-dimensional extracellular matrices (3D-ECM) following a previously described protocol[131] (Figure 26). All cell lines tested were capable of producing 3D-ECM even without TGFβ induction and, as expected, EDA production was absent in EDA- cells. EDA fibronectin staining

matched staining for total fibronectin in wild-type MEF synthesized 3D-ECM, as expected for heteromeric fibers.

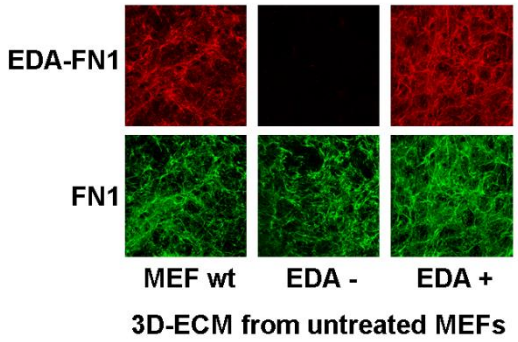

Figure 26: Genetically modified MEFs produce *in vivo* like three-dimensional extracellular matrices with or without fibronectin EDA. MEFs were seeded on coverslips and allowed to produce extracellular matrix for 6 days. Cell cultures were then fixed with 4% PFA and analyzed by IF with anti-EDA fibronectin (red) and anti-fibronectin (green).

3.2. EDA induces increased matrix stiffness

Increased stiffness of the ECM has been described as a key factor in tumor progression, growth and invasive capabilities and has been linked to more advanced tumor stages. As we have shown that tumors in more advanced states have an increased inclusion of EDA, we wonder whether this inclusion plays a role in matrix stiffening.

To test this possibility, we generated 3D-ECM and subsequently decellularized them, so that only the ECM remained to be tested. Rigidity of the samples was tested by Atomic Force Microscopy (AFM) by Álvaro Villarino (from Dr. Jordi Otero's laboratory, Cellular and Respiratory Biomechanics - Institute for Bioengineering of Catalonia, Barcelona, Spain). 3D-ECM obtained from both untreated cells and

cells activated with TGFβ was tested. While no data was obtained from 3D-ECM produced from untreated cells due to technique limitations (sample thickness was insufficient), data from activated matrices shows that matrices rich in fibronectin EDA were almost double as stiff as those without any at all (Figure 27).

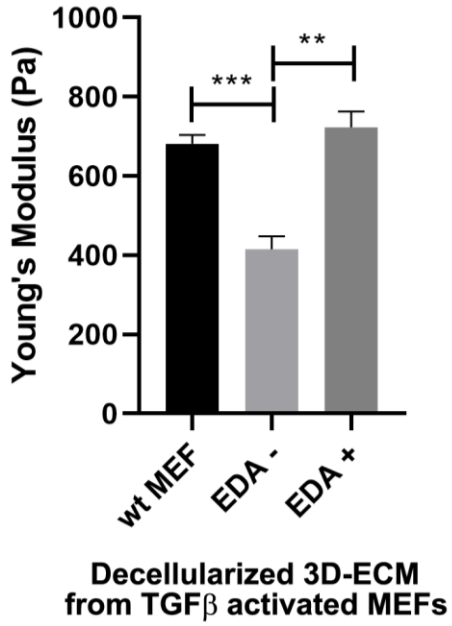

Figure 27: Lack of fibronectin EDA reduces rigidity of *in vivo* like extracellular matrices. MEFs were seeded on coverslips and allowed to produce extracellular matrix for 6 days in the presence of 5ng/mL of TGFβ. Fibroblasts were removed with a decellularization solution and the rigidity of the resulting matrices was analyzed through atomic force microscopy.

3.3. Fibronectin EDA increases matrix alignment

Another physical property of tumor ECM that predicts a worse prognosis is increased matrix fiber alignment, as it leads to the formation of tracks that facilitate tumor cell invasion.

We took advantage that nucleus orientation reflects the orientation of both fibroblasts and fibers deposited by them. Thus, we produced 3D-ECM and stained them with DAPI to calculate their orientation into the 3D-ECM. In parallel, we also stained with an anti-fibronectin (Figure 28a). Use of STED microscopy to visualize fibronectin fibers in detail revealed differential fibronectin fiber organization, with fewer albeit thicker fibers in EDA- matrices.

The relative angle of each nucleus was measured in the imaged areas using ImageJ software. For each condition, nuclei alignment was calculated as the percentage of nuclei oriented within 21 degrees of the orientation mode. As previously described[61], in the presence of TGFβ control fibroblasts adopted an anisotropic orientation into their 3D-ECM while untreated fibroblasts were stochastically distributed (Figure 28b). Nuclei of EDA- and EDA+ fibroblasts in the absence of TGFβ also distributed stochastically but in TGFβ activated conditions nuclei of EDA- fibroblasts barely increased their alignment while those of EDA+ fibroblasts reach over 70% shared orientation (Figure 28b).

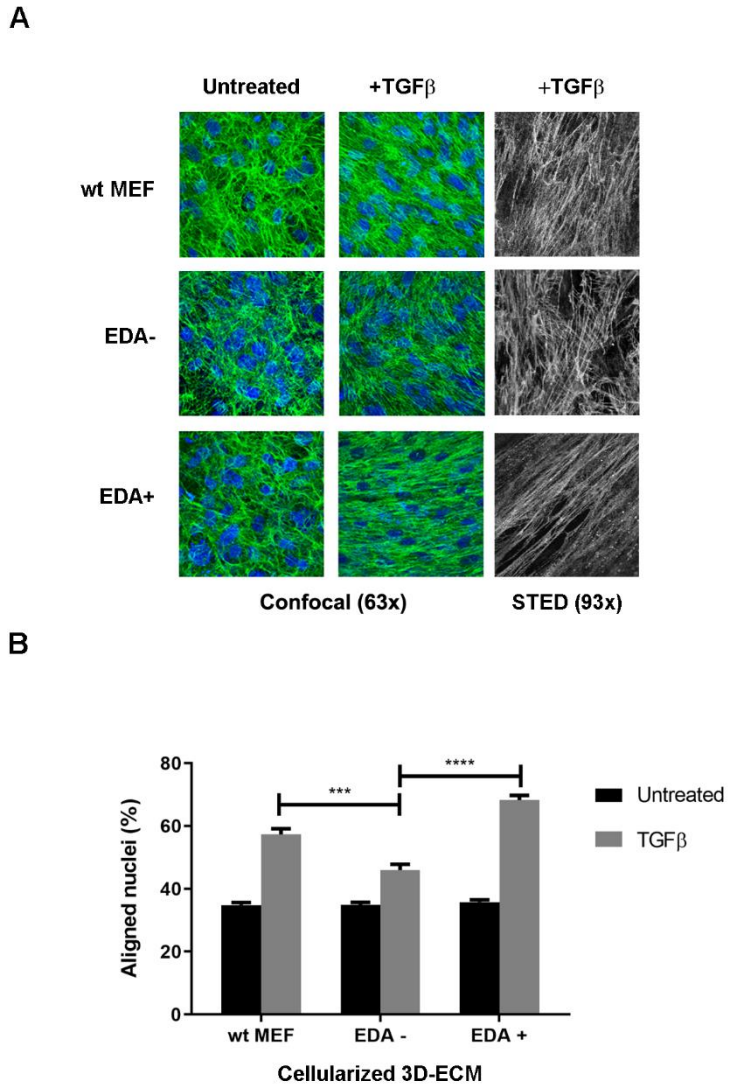

Figure 28: Presence of fibronectin EDA in an *in vivo* like extracellular matrix allows alignment in response to TGFβ. (A) *Fibronectin immunofluorescence of in vivo like 3D-ECM*. MEFs were seeded on coverslips and allowed to produce extracellular matrix for 6 days in the presence or absence of 5ng/mL of TGFβ. Cell cultures were then fixed with 4% PFA and analyzed by IF with anti-fibronectin (green) and DAPI. Confocal and STED microscopy were used to obtain images. (B) *Quantification of nuclei alignment in in vivo like 3D-ECM*. The nuclei orientation angles were calculated using ImageJ from confocal images and plotted as a frequency distribution centered in the most frequent angle. Percentage of cells aligning towards the same direction (up to 21° deviation from the mode) was plotted.

Nuclei orientation was complemented with measurements of the fibronectin fibers orientation obtained from immunofluorescence images of the matrices marked with an anti-fibronectin antibody. The image processing and quantification was performed using two different ImageJ plugins. First, ImageJ OrientationJ plugin yielded fiber alignment histograms that were treated as the nuclei data. Results closely resembled those of nuclei orientation, showing a TGFβ and EDA dependent fiber alignment (Figure 29a). Second, images of matrices generated in the presence of TGFβ were analyzed through TWOMBLI (The Workflow Of Matrix BioLogy Informatics) ImageJ macro[132], which measures additional topological parameters besides alignment. Notably, TWOMBLI outcomes confirmed higher fiber alignment in EDA+ when compared to EDA- matrices (Figure 29b) and decrease of both curvature and appearance of branching points in the EDA+ fibers (Figure 29b).

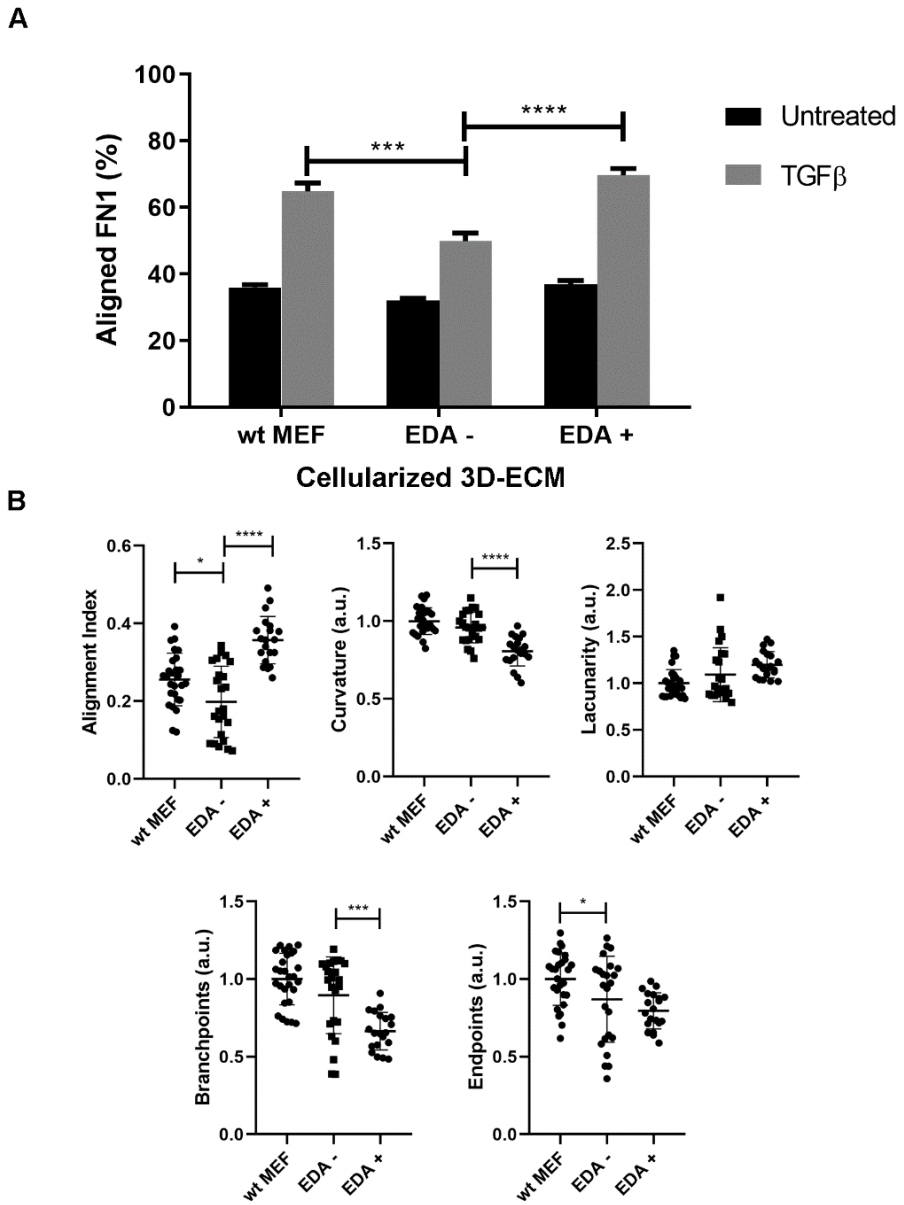

Figure 29: Presence of fibronectin EDA in *in vivo* like extracellular matrices allows fibronectin alignment in response to TGFβ. (A) *Quantification of fibronectin fiber alignment through OrientationJ*. MEFs were seeded on coverslips and allowed to produce extracellular matrix for 6 days in the presence or absence of 5ng/mL of TGFβ. Cell cultures were then fixed with 4% PFA and analyzed by IF with anti-fibronectin (green) and DAPI. Confocal microscopy was used to obtain images. The fibronectin fiber orientation

angles were calculated using the ImageJ plugin OrientationJ and plotted as a frequency distribution centered in the most frequent angle. Percentage of cells aligned towards the same direction (up to 21° deviation from the mode) was plotted. (B) *Quantification of fibronectin fiber parameters through TWOMBLI*. Images from matrices generated by the indicated MEFs treated with TGFβ were analyzed using the ImageJ macro TWOMBLI and data obtained was plotted showing all individual measurements, mean and SD. Arbitrary units are provided by the plugin and are expressed as relative to wild-type MEFs.

3.4. Lack of EDA in *in vivo* like 3D-ECM alters collagen deposition and organization

As fibronectin acts as a template guiding the polymerization of other extracellular fibers, we study if collagen organization depends on EDA presence in the fibronectin matrix. Three-dimensional extracellular matrices were produced and the overall collagen content was visualized through Masson's trichrome staining and individual fibers with Second Harmonic Generation (SHG) (Figure 30). Collagen patterns obtained through both techniques show a closer resemblance between matrices produced by wild-type and EDA+ MEFs than those produced without any EDA at all. Hence, the presence of fibronectin EDA in the fibronectin fibers determines how other extracellular molecules such as collagen organize into the matrix.

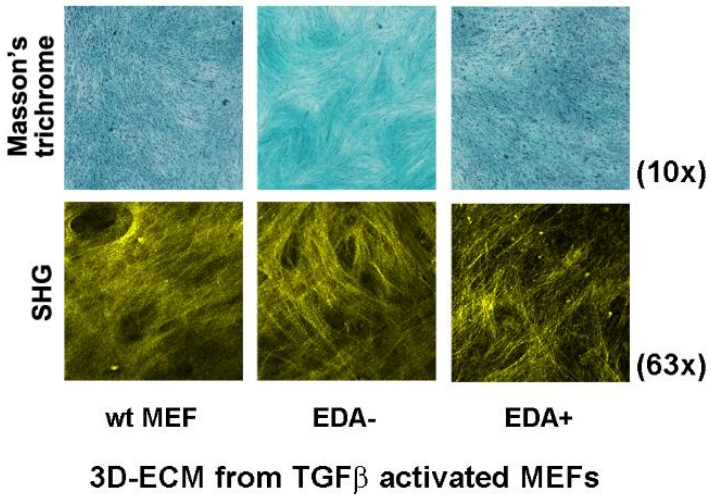

Figure 30: Fibronectin EDA regulates collagen deposition and organization. MEFs were seeded on coverslips and allowed to produce extracellular matrix for 6 days treated with 5ng/mL of TGFβ. Cell cultures were then fixed with 4% PFA and total collagen was visualized by Masson's trichrome staining or Second Harmonic Generation. Images were obtained with a confocal microscope to visualize fibrillar collagen.

3.5. Lack of EDA in the extracellular matrix induces changes in cellular mechanotransduction

The stiffness and topological differences of matrices induced by the presence of fibronectin EDA brought us to study potential differences in focal adhesions (FA) of the fibroblasts embedded in the matrices, as arrangement of these transmembrane structures depends of the cell-matrix interactions. We produced *in vivo* like 3D-ECM from the three EDA MEFs lines and performed IF to visualize a key FA component, Paxillin. The immunofluorescence microscopy images revealed differences in the distribution and conformation of focal adhesions,

being much sparser and longer in cells with an extracellular matrix lacking EDA (Figure 31a).

To follow up these observations of the fibroblast embedded in the matrices, we assess the intracellular fibers anchored to FA. IFs were done to detect the α-SMA positive stress fibers, the subset of fibers in the actin cytoskeleton reinforced to efficiently deal with high tension. Differences were detected even in matrices produced without TGFβ, as EDA- cells failed to form clearly defined stress fibers (Figure 31b). In matrices produced in the presence of TGFβ, all MEF lines presented linear α-SMA positive stress fibers. However, in the presence of fibronectin EDA these fibers tended to be grouped in bundles while in the absence of EDA they were uniformly distributed through the cell. These differences are likely the consequence of the fibroblasts sensing the changes in the matrix topology and stiffness.

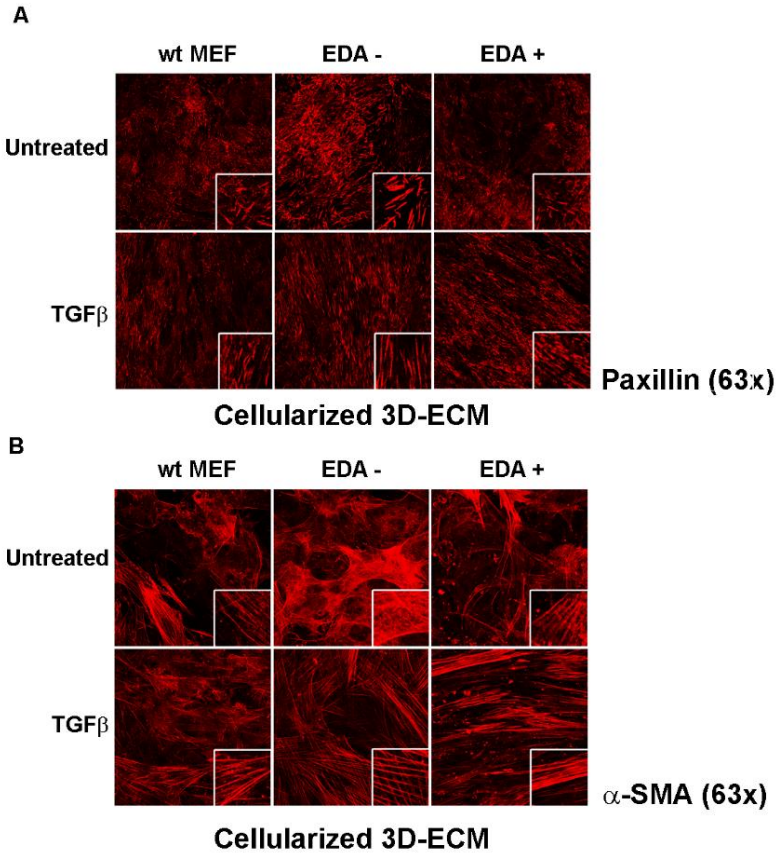

Figure 31: Fibronectin EDA content of the extracellular matrix leads to rearrangement of focal adhesions and the actin cytoskeleton. *Immunofluorescence of (A) Paxillin and (B) α-SMA in in vivo like 3D-ECM.* MEFs were seeded on coverslips and allowed to produce extracellular matrix for 6 days in the presence or absence of 5ng/mL of TGFβ. Cell cultures were then fixed with 4% PFA and analyzed by IF with the indicated antibodies. Confocal microscopy was used to obtain images. Inserts show amplifications of representative areas.

3.6. EDA signaling induces increased cell nuclei elongation

Besides guiding nuclei orientation, TGFβ also modulates nuclei shape, a mechanosensitive parameter controlled by the activity of the actin cytoskeleton. Therefore, we interrogate if fibroblasts embedded into matrices with or without fibronectin EDA alter their response to TGFβ on nuclei shape. The aspect ratio of MEF nuclei (the relation between nuclei length and width) was measured from DAPI images using ImageJ. As previously reported for unmodified fibroblasts, we detect a displacement of nuclei AR towards elevated values (nucleus elongation) when WT fibroblasts were grown in the presence of TGFβ. Similar to nuclei orientation, this phenomenon was absent in MEFs EDA- and potentiated in MEFs EDA+ (Figure 32a). Using these elliptical parameters, we also calculate the average nuclei shape for each MEF line. As showed in Figure 32b, only nucleus elongation of fibroblasts embedded in matrices with fibronectin lacking EDA was unaltered by TGFβ treatment.

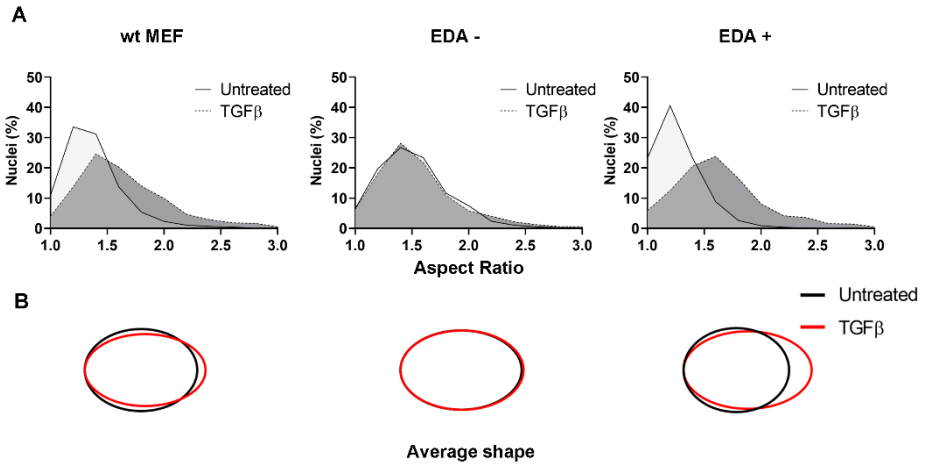

Figure 32: Presence of fibronectin EDA in *in vivo* like extracellular matrices allows nuclei elongation in response to TGFβ. *(A) Nucleus aspect ratio of 3D-ECM embedded MEFs.* MEFs were seeded on coverslips and allowed to produce extracellular matrix for 6 days treated or left untreated with 5ng/mL of TGFβ. Cell cultures were then fixed with 4% PFA and analyzed by IF with DAPI. Confocal microscopy was used to obtain images. Elliptical shape parameters for each nucleus were obtained using ImageJ. Nucleus aspect ratio was plotted as a frequency diagram. (B) *Average nuclear shape*. Representation of the shape and size for the average nucleus of each cell line and condition.

3.7. Presence of fibronectin EDA in *in vivo* like 3D-ECM collaborate with the TGFβ activation

If extracellular fibronectin EDA sustains an activation feedback loop trough mechanical signaling, we anticipated that a pulse of TGFβ would be sufficient to fully sustain TGFβ activation of MEF EDA+. To test this hypothesis, we generated 3D-ECM in the presence of an initial pulse of TGFβ instead of a continuous dose. Analysis of nuclei alignment, carried out as in Figure 28, was performed to evaluate the activation of the fibroblasts and they revealed that while the short

pulse was not enough to produce any significant increase in alignment of wild type MEFs (Figure 33a) it fully activated EDA+. These results point to that, once activation is induced by TGFβ, presence of EDA in the ECM is enough to sustain the response and induce an activated state in fibroblasts.

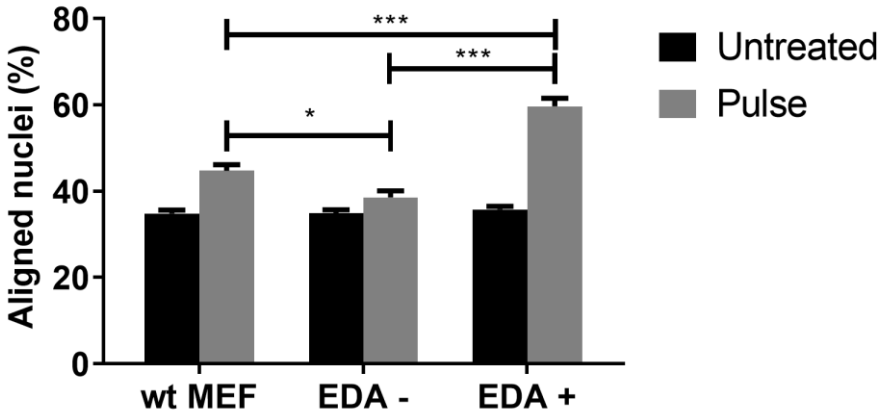

Figure 33: Fibronectin EDA allows complete extracellular remodeling with only an initial pulse of TGFβ. MEFs were seeded on coverslips and allowed to produce extracellular matrix for 6 days. In the pulse condition, MEFs were treated with 5ng/mL of TGFβ for 2 days and kept producing ECM for 4 extra days once treatment was removed. Cell cultures were then fixed with 4% PFA and analyzed by IF with DAPI. Confocal microscopy was used to obtain images. The nuclei orientation angles were calculated as previously described. Percentage of values aligned towards the same direction (up to 21° deviation from the mode) was plotted.

4. DISRUPTING THE GENERATION OF AN ALIGNED ECM BY INTERFERING WITH EDA FIBRONECTIN ACTIVITY

Given the role of fibronectin EDA in generating aligned and rigid ECMs, we investigate different approaches to either suppress the EDA production or to block its activity.

4.1. Antisense oligonucleotides targeting EDA splicing regulatory regions do not achieve sustained splicing repression

The first approach consisted in the design of specific modified Antisense Oligonucleotides to prevent the alternative EDA inclusion. These AONs target the alternative splicing regulatory RNA sequences in exon 33 and the two intron-exon boundaries (Figure 34a) and they should avoid the binding of splicing factors, effectively decreasing exon inclusion.

Control MEFs were separately transfected with five different AONs and the relative amount of the fibronectin isoforms either including or skipping the exon 33 were estimated 3 days post-transfection by RT-sqPCR as described previously. In the control tests both AON 1 (targeting the Exonic Splicing Enhance, ESE) and AON 2 (targeting the Exonic Splicing Silencer, ESS) induced an increased skipping when compared to a control or Scramble AON 3 (Figure 34b). AONs 4 and 5 produced no effect.

Next, we used the transfected cells to obtain *in vivo* like 3D-ECM in the presence of TGFβ to evaluate if the reduction of the EDA inclusion obtained was sufficient to interfere with the long-term (1 week)

acquired matrix properties. Matrix fibronectin visualized a week after initiating the experiment by immunofluorescence revealed no appreciable effects by the AON (Figure 34c). Thus, we discard the use of these AONs for further assays in our experimental model.

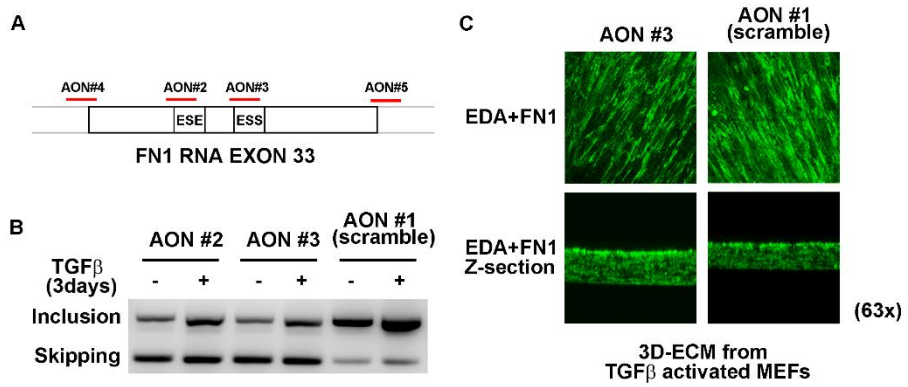

Figure 34: Antisense Oligonucleotides targeting splicing regulatory regions inhibit EDA inclusion. *(A) Schematic representation of fibronectin exon 33.* 4 Antisense Oligonucleotides were designed to prevent exon 33 coding for EDA inclusion into the mature fibronectin mRNA and an additional scramble sequence used as a negative control. Sequences were designed to target the two splicing regulatory sequences (ESE and ESS) and the intron-exon boundaries. (B) *Relative RNA amount of EDA fibronectin isoforms.* Control MEF were transfected with AONs and treated with or without 5ng/mL of TGFβ for 3 days. RNA was obtained, retrotranscribed and amplified using primers flanking fibronectin exon 33. Resulting DNAs were visualized by electrophoresis on a 2% agarose gel. (C) *EDA fibronectin immunofluorescence of in vivo like 3D-ECM.* MEFs were seeded on coverslips 24 after transfection and allowed to produce extracellular matrix for 6 days in the presence of 5ng/mL of TGFβ. Cell cultures were then fixed with 4% PFA and analyzed by IF with anti-EDA+FN1 (green). Confocal microscopy was used to obtain images.

4.2. Inhibitors CLI-095 and Irigenin induce a small reduction in ECM alignment

Another EDA targeting approach we tested was blocking EDA activity with commercially available inhibitors: CLI-095 and Irigenin.

CLI-095 is a cyclohexene derivative that has been shown to strongly inhibit both ligand dependent and independent TLR4 signaling. As such, it has previously been used to target EDA signaling in models such as bone marrow fibrosis or brain injury where TLR4 is activated by EDA[133,134]. Irigenin is a flavonoid with antioxidative activity that directly interacts with EDA. It targets the C-C' loop, which acts as an optimal ligand for integrins $\alpha 9\beta 1$ and $\alpha 4\beta 1$, disrupts the EDA folding and hinds the ability of EDA to interact with partners or receptors[135].

To test the activity of inhibitors, they were added during the generation of the matrices by the EDA+ MEF in the presence or absence of TGFβ (Figure 35). Measurements were carried out as described previously and nuclei analysis show that both CLI-095 and Irigenin reduced the TGFβ-induced nuclei alignment but not enough to mimic the poor alignment of matrices lacking EDA (Figure 35a). The effect of the inhibitors on fibronectin fiber alignment in these matrices reproduced the data of nuclei (Figure 35b).

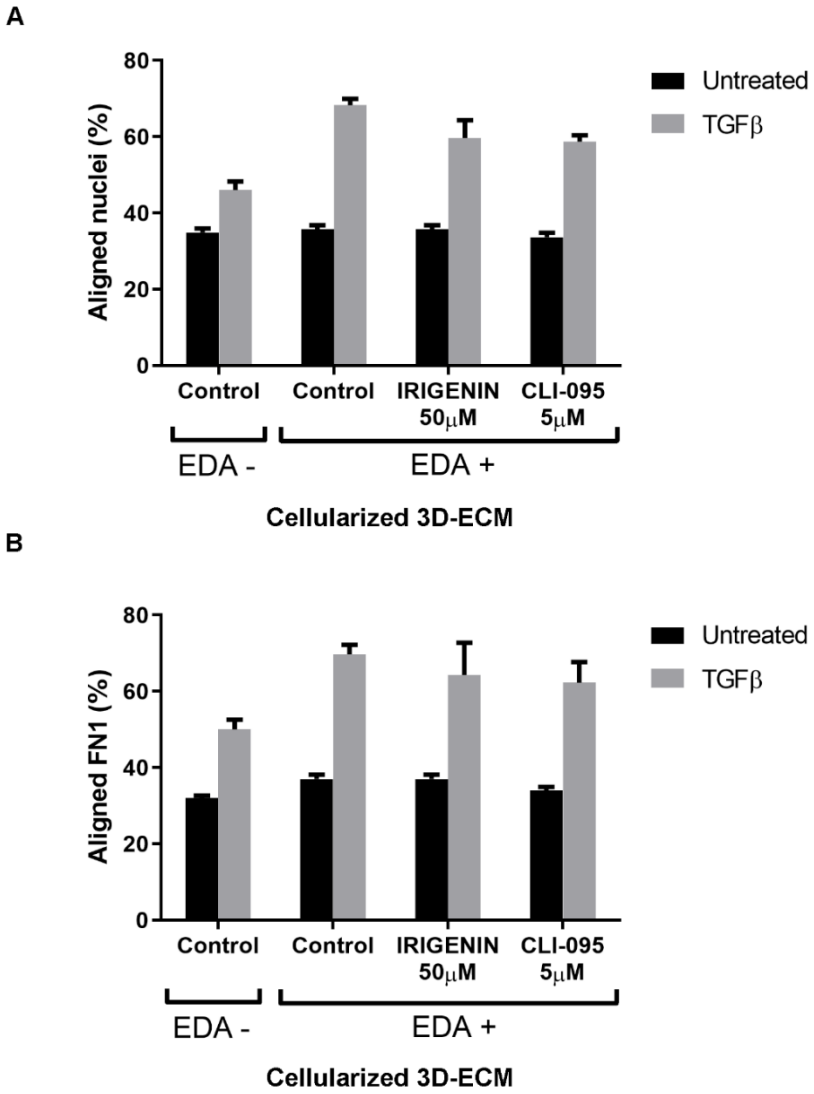

Figure 35: Fibronectin EDA inhibitors slightly interfere with matrix alignment. *Quantification of (A) nuclei and (B) fibronectin fibers alignment in in vivo like 3D-ECM.* MEFs were seeded on coverslips and allowed to produce extracellular matrix for 6 days in the presence or absence of 5ng/mL of TGFβ. When indicated, Irigenin 50μM, CLI-095 5μM or vehicle (control) was also included. Cell cultures were eventually fixed with 4% PFA and analyzed by IF with anti-fibronectin and DAPI. Confocal microscopy was used to obtain images. The respective orientation angles were calculated as previously described. Percentage of values aligned towards the same direction (up to 21° deviation from the mode) was plotted.

We further quantify other fibronectin fiber characteristics with TWOMBLI (Figure 36). Both inhibitors produce a similar increase in the lacunarity parameter (the measure of the gaps between fibers). As observed when quantifying untreated matrices, TWOMBLI better discriminates smaller differences in fiber alignment than orientation J plugin. Thus, only in TWOMBLI analyses matrices treated with Irigenin but not CLI-095 presented a significant reduction in alignment relative to their corresponding controls. Conversely, CLI treated matrices presented a significant decrease in the number of fiber endpoints while Irigenin only induced a tendency. Despite these changes, none of the inhibitors fully reproduced the reduction induced by lack of EDA.

Overall, our results with AONs and inhibitors indicate that they are inefficient molecular tools for preventing the alignment of the extracellular matrices in the presence of exogenous TGFβ. Only Irigenin has a partial interfering capacity.

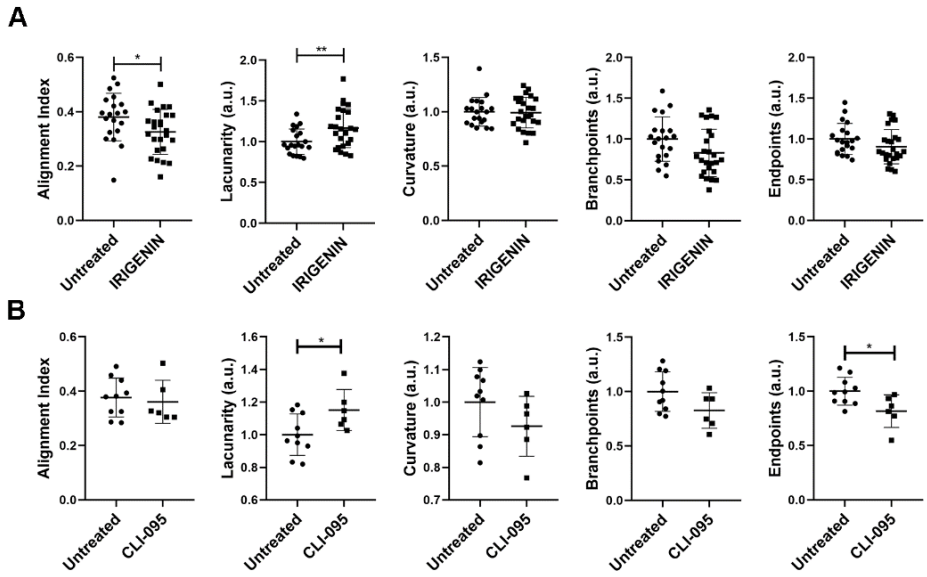

Figure 36: Irigenin decreases the fibronectin alignment induced by TGFβ. *Quantification of fibronectin fiber parameters of in vivo like 3D-ECM treated with (A) Irigenin and (B) CLI-095 through TWOMBLI*. EDA+ MEFs were seeded on coverslips and allowed to produce extracellular matrix for 6 days. Cells were treated with 5ng/mL of TGFβ and Irigenin 50µM or CLI-095 5µM. Cell cultures were then fixed with 4% PFA and analyzed by IF with anti-fibronectin. Confocal microscopy was used to obtain images. Images were analyzed with the ImageJ Macro TWOMBLI. Arbitrary units are provided by the plugin and are expressed as relative to untreated MEFs.

5. STUDY OF THE EFFECTS OF AN EDA RICH ECM ON CELLS OF THE TUMOR MICROENVIRONMENT

So far, we have shown that the presence of fibronectin EDA modifies topological and mechanical properties of the ECM, such as rigidity and alignment that are related with cancer progression and worse prognosis. In order to better understand how an EDA rich ECM impulses cancer progression, we took advantage of the fibronectin EDA including or excluding *in vivo* like 3D-ECM to compare their action on cells present in a tumor microenvironment, such as fibroblasts, macrophages and tumor cells.

5.1. Fibroblasts become activated in EDA rich 3D-ECM

As already mentioned, α-SMA is considered a key marker for activated fibroblasts. The incorporation of this actin isoform into stress fibers is a marker of their activation as it enables ECM remodeling activities. We have compared the activation of the EDA+ or EDA- fibroblasts embedded into the matrices they generate in the presence of TGFβ. Next, we studied the activation of naïve fibroblasts seeded on synthetized and decellularized ECMs so that exogenous TGFβ used to generate the matrix is removed during decellularization and washing steps and does not interact with naïve fibroblasts.

5.1.1. Mesenchymal Stem cells and the NIH-3T3 fibroblast line become activated in response to EDA

We chose two different fibroblastic lines, Mesenchymal Stem cells and NIH-3T3 cell lines. Mouse MSCs previously isolated and described in

the laboratory were tested as an example of fibroblastic cells recruited by tumors. NIH-3T3 were used as a standard and available immortalized line that easily grows in culture.

In the initial experiment, these fibroblasts were seeded on decellularized matrices generated in the absence of TGFβ and the percentage of fibroblasts incorporating α-SMA in fibers 24 hours later was calculated from immunofluorescence images with an anti-α-SMA (Figure 37a). For both cell lines, we detected double the percentage of activated fibroblasts on EDA+ relative to EDA- matrices (Figure 37b). This finding indicates that polymerized fibronectin EDA but not fibronectin lacking the EDA can organize an ECM with the capacity to activate fibroblasts. Basal activation on EDA- matrices was higher in NIH-3T3. However, based on the similarity in the response of both cell lines, we performed subsequent experiments with NIH-3T3.

5.1.2. TGFβ activation depends on EDA splicing regulation

NIH-3T3 activation was further studied on matrices generated in the presence or absence of TGFβ. As described in the previous experiment (Figure 37), EDA+ matrices in the absence of TGFβ stimulated NIH-3T3 much more than EDA- matrices (Figure 38). Additionally, NIH-3T3 activation in each of these matrices was reproduced when they were generated in the presence of TGFβ. Therefore, the ECM with homomeric polymerized fibronectin EDA activates fibroblasts independently of the alignment and rigidity imposed by TGFβ.

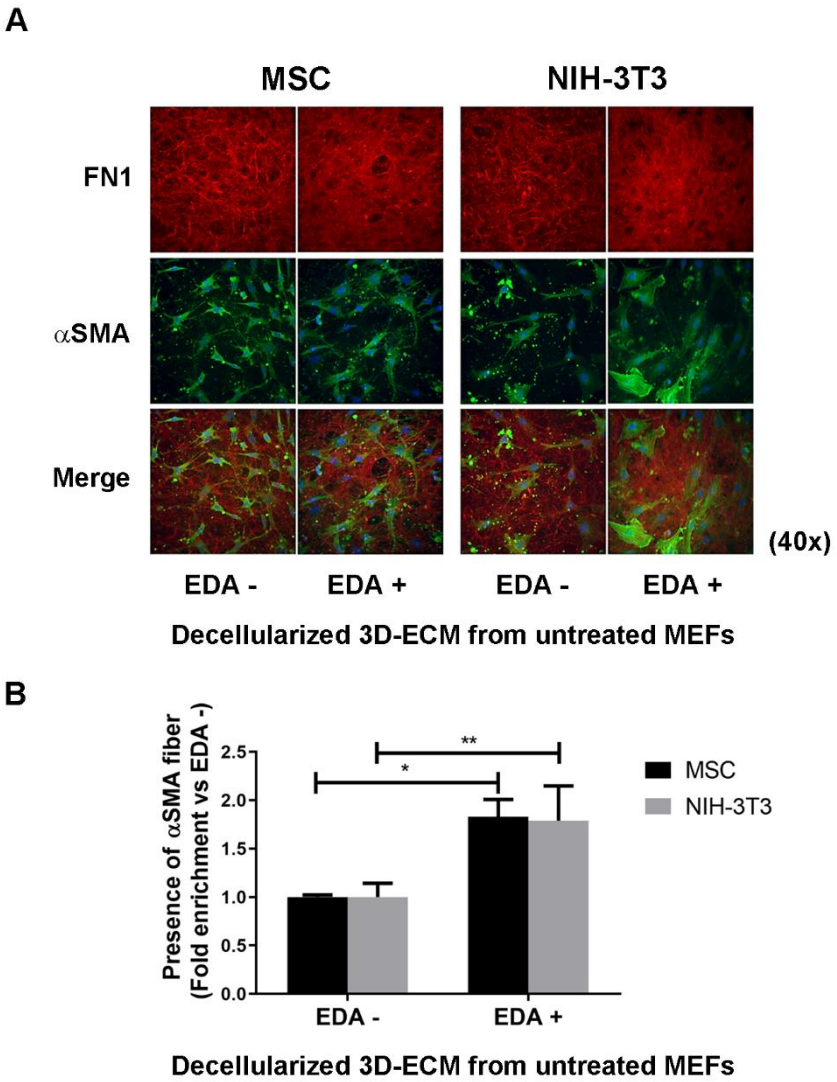

Figure 37: Naive mesenchymal stem cells and NIH-3T3 fibroblasts become activated on matrices with fibronectin EDA. *(A) Fibronectin and α-SMA immunofluorescence of recellularized 3D-ECMs.* 3D-ECMs from MEF EDA- and EDA+ were produced and decellularized. MSC and NIH-3T3 fibroblasts were seeded on top, fixed with 4% PFA 24h later and analyzed by IF with anti-fibronectin (red), anti-α-SMA (green) and DAPI. Images were obtained using fluorescence microscopy. *(B) Quantification of activated fibroblasts.* Images obtained through fluorescence microscopy were used to obtain the percentage of cells presenting α-SMA positive stress fibers. Plotted bars indicate the fold increase relative to average percentage on EDA- matrices.

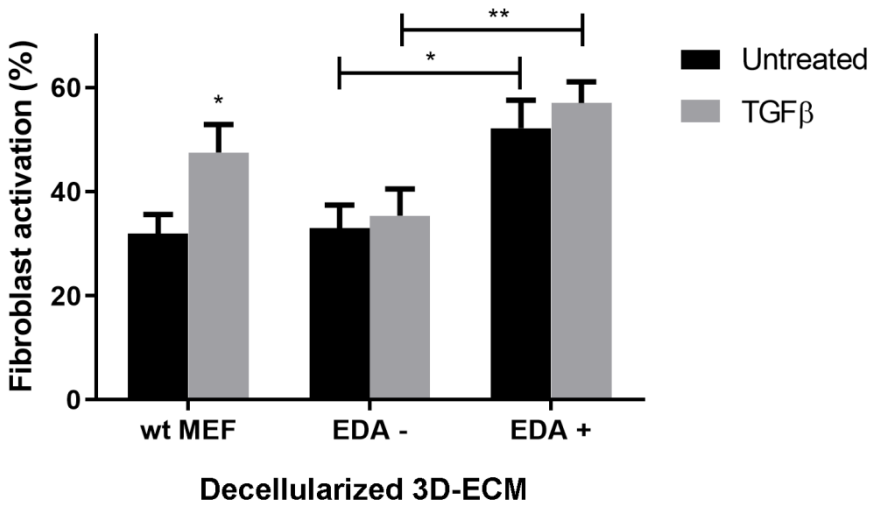

Figure 38: NIH-3T3 fibroblasts become activated on 3D-ECMs with fibronectin EDA. 3D-matrices were obtained from the indicated MEF lines treated with 5ng/mL TGFβ and subsequently decellularized. NIH-3T3 fibroblasts were seeded on top, fixed with 4% PFA 24h later and activation was analyzed as in Figure 37. Images were obtained using fluorescence microscopy and percentage of cells presenting α-SMA positive stress fibers was quantified.

In contrast, on matrices produced by wild-type MEFs containing both EDA- and EDA+ fibronectin isoforms, basal fibroblast activation in the absence of TGFβ, equivalent to activation on EDA- matrices, was increased by the presence of TGFβ to levels similar to EDA+ matrices. Thus, unaligned heteromeric fibers of fibronectin generated by wild-type MEFs in the absence of TGFβ did not increase fibroblast activation. However, aligned heteromeric fibers with a higher inclusion of EDA generated by wild-type MEFs in the presence of TGFβ did sustain further fibroblast activation.

5.1.3. Irigenin and CLI-095 block fibroblast activation

To further analyze the effects of the two inhibitors previously introduced, we tested if they were able to block the acquisition of an activated phenotype by directly administering them to naïve fibroblasts seeded on matrices.

In contrast with its low ability to block matrix alignment (Figure 35), Irigenin administration was successful in significantly inhibiting the activation of fibroblasts in all the conditions shown to induce an increase (Figure 39a). Administration of CLI-095 produced similar results, significantly reducing fibroblast activation supported by both wild-type activated with TGFβ and EDA+ untreated matrices, while inducing a clear tendency towards a reduction in matrices EDA + TGFβ (Figure 39b).

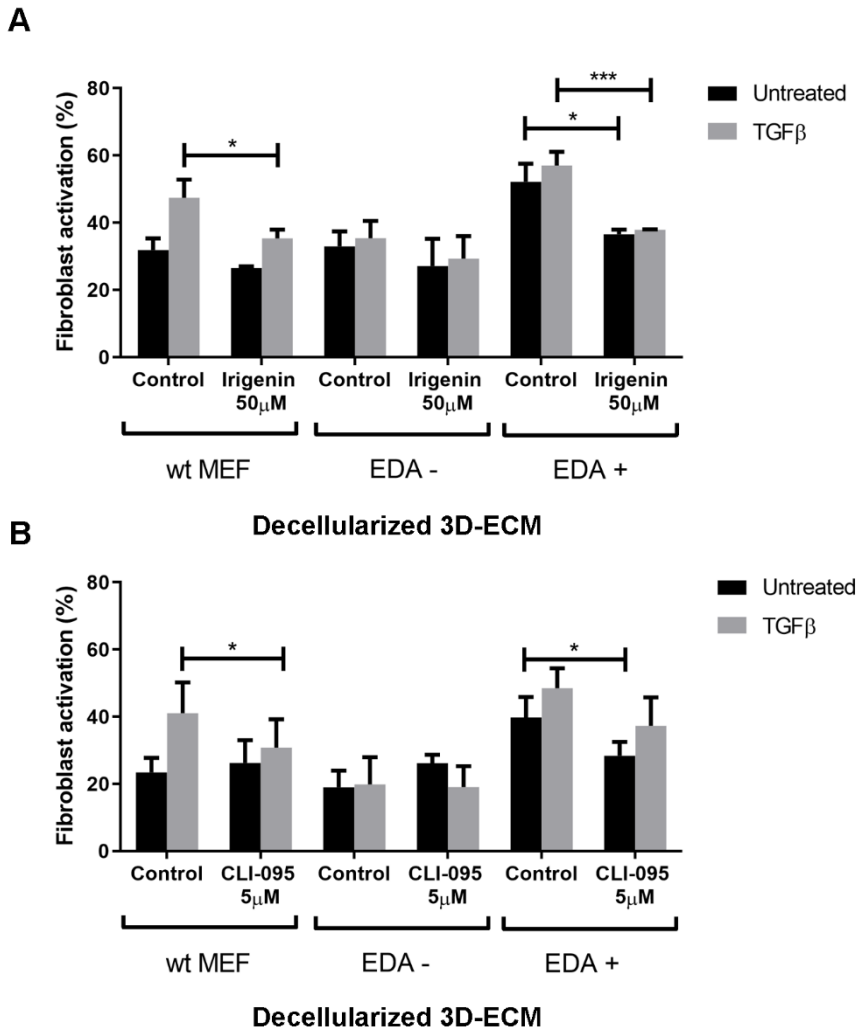

Figure 39: NIH-3T3 activation on 3D-ECM with fibronectin EDA is inhibited with CLI-095 and Irigenin. *Quantification of activated fibroblasts with (A) Irigenin or (B) CLI-095 treatments.* 3D-ECMs were obtained from the indicated cell lines treated with or without 5ng/mL TGFβ and subsequently decellularized. NIH-3T3 fibroblasts were seeded on top and left untreated (Control) or treated with either (A) 50μM Irigenin or (B) 5μm CLI-095. After 24h, cells were fixed with 4% PFA and activation was analyzed as in Figure 37. Images were obtained using fluorescence microscopy and percentage of NIH-3T3 presenting α-SMA positive stress fibers was quantified.

Additionally, we assessed whether there were any improvements upon a combined treatment, but fibroblast activation rates closely resembled those of fibroblasts treated with only Irigenin (Figure 40), discarding the combined treatment for the following experiments.

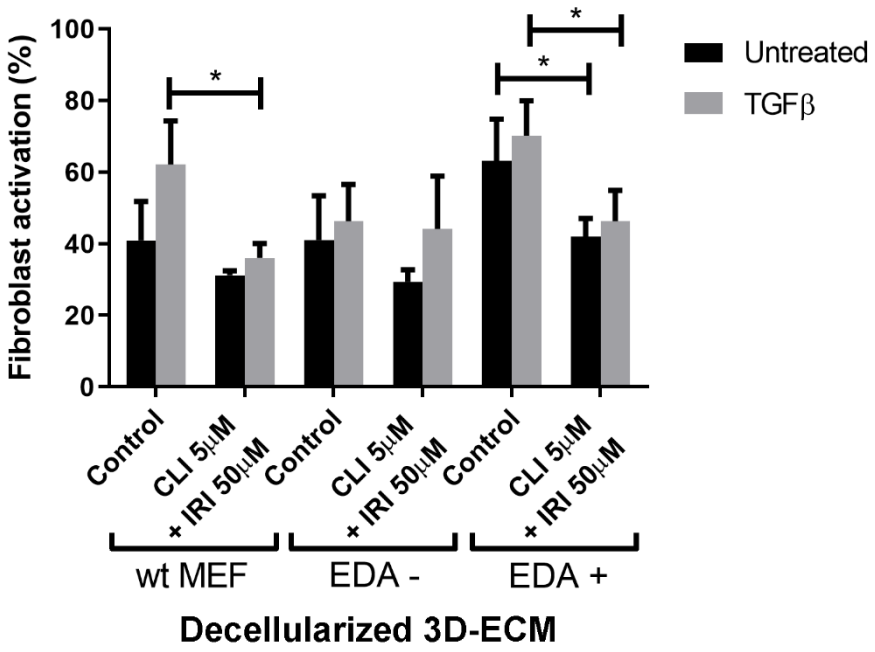

Figure 40: NIH-3T3 activation on 3D-ECM with fibronectin EDA is inhibited by a combined treatment with CLI-095 and Irigenin. 3D-ECMS were obtained from the indicated cell lines treated with or without 5ng/mL TGFβ and subsequently decellularized. NIH-3T3 fibroblasts were seeded on top and left untreated (Control) or treated with 5μm CLI-095+50μM Irigenin. After 24h, cells were fixed with 4% PFA and activation was analyzed as in Figure 37. Images were obtained using fluorescence microscopy and percentage of NIH-3T3 presenting α-SMA positive stress fibers was quantified.

5.1.4. Irigenin treatment reduces the stromal compartment of tumors

Given that Irigenin was effective in blocking fibroblast activation and we had also described a moderate effect in disrupting ECM alignment, we decided to evaluate its potential to regulate the stroma in a mouse *in vivo* model.

We injected AT-3 tumor cells and MSCs in a 1:1 ratio into the inguinal mammary fat pads of NOD-SCID (Non Obese Diabetic/Severe Combined Immunodeficiency) gamma mice. Mice were administrated Irigenin or vehicle daily for 14 days until tumors started reaching 0.4cm length. At this point, primary tumors were surgically resected and measured. No irigenin-induced differences in tumor volume were observed (Figure 41a). Fibronectin immunohistochemistry of paraffin embedded tumor sections revealed a reduction in fibronectin deposition in the tumors from the inhibitor condition (Figure 41b). The percentage of tumor tissue consisting of stroma was quantified based on fibronectin staining, showing a significant reduction (Figure 41c).

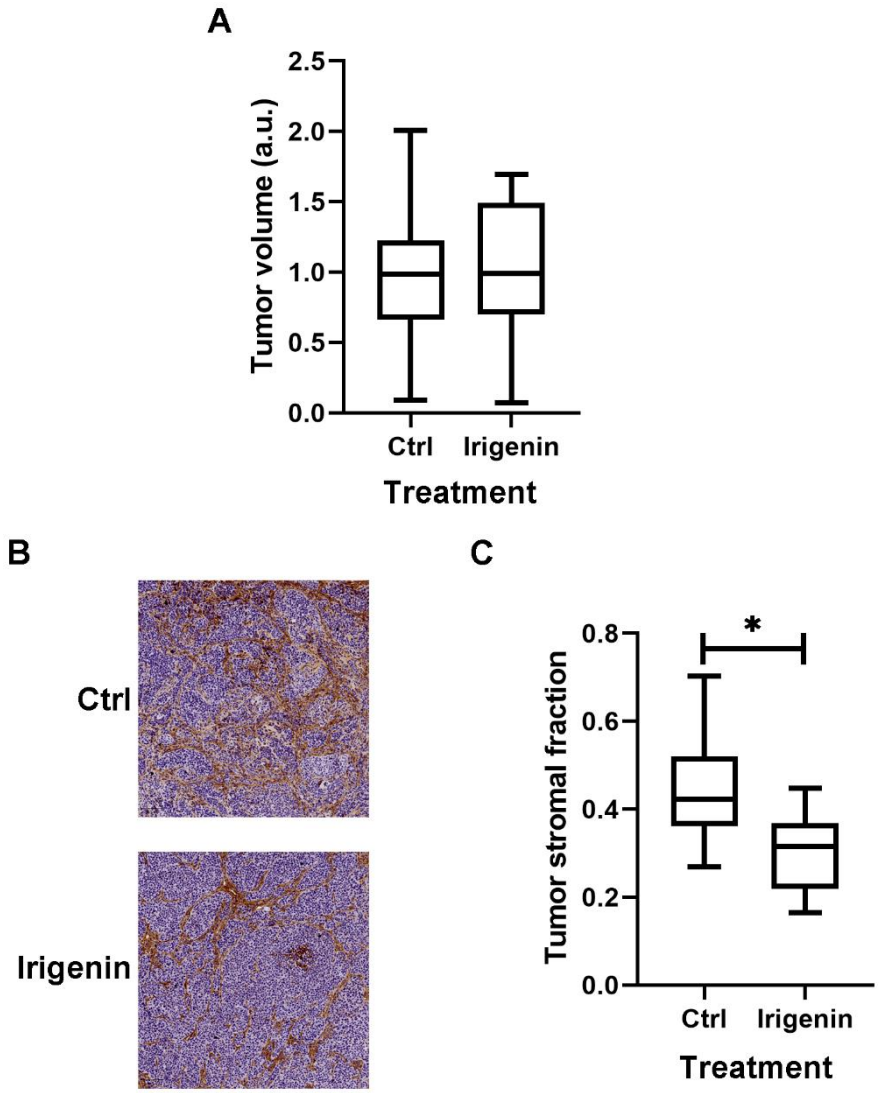

Figure 41: Irigenin treatment reduces primary tumor stromal fraction in mice. *(A) Primary tumor volume quantification.* $5x10^4$ AT-3 and $5x10^4$ MSC were co-injected orthotopically into the mammary fat pad of NOD-SCID gamma mice. Mice were administered either 50mg/kg Irigenin or vehicle intraperitoneally daily for 16 days. Tumors were all resected at the same time once they started reaching 0.5cm approximately. The three main dimensions of resected primary tumors were measured. Tumor volume was calculated and all data obtained is represented as box plots relative to average tumor volume of Control tumor. *(B) Fibronectin immunohistochemistry of primary tumor sections.* Resected tumors were

fixed in 4% PFA and embedded in paraffin. Paraffin sections were cut and immunohistochemistry for fibronectin was performed. *(C) Quantification of primary tumor stromal fraction.* QuPath software was used to quantify the percentage of each primary tumor stained for fibronectin. Data obtained for the stromal fraction for all resected tumors is represented as box plots.

5.2. ECM can regulate macrophagic activity

As mentioned in the introduction, macrophages are one of the main components in the tumor microenvironment. These cells are involved in the immune regulation either enhancing antitumor or protumoral responses. Not much is known of how mechanical signaling from the ECM influence the regulation of these antagonistic responses.

5.2.1. SNAIL1 induces production of ECM that suppresses macrophage activity

To assess the activity of the ECM on macrophage antitumor cytotoxicity, we set up a macrophage cytotoxic assay on 3D-ECMs. The initial experiments were carried on decellularized 3D-ECM produced by control and SNAIL1 deficient MEFs.

Undifferentiated macrophages isolated from mouse tibia and femur bone marrow and tumor MCF7 cells were seeded 1:1 on decellularized matrices and cocultured for 48 h. The amount of MCF7 cells at the end of the assay was quantified in immunofluorescence images by counting cells with intact nuclei (DAPI) and negative for the macrophage marker F4/80. A control condition was performed on each ECM in the absence of macrophages, so cytotoxicity was estimated as the ratio between the remaining MCF7 in presence versus absence of

macrophages. Results showed a much lower survival of MCF7 cells seeded on ECM produced by *Snai1* KO compared to Ctrl MEFs (Figure 42). Although at lower extension, survival was also reduced on ECMs generated by *Snai1* KO versus control MEFs in the presence of TGFβ (Figure 42).

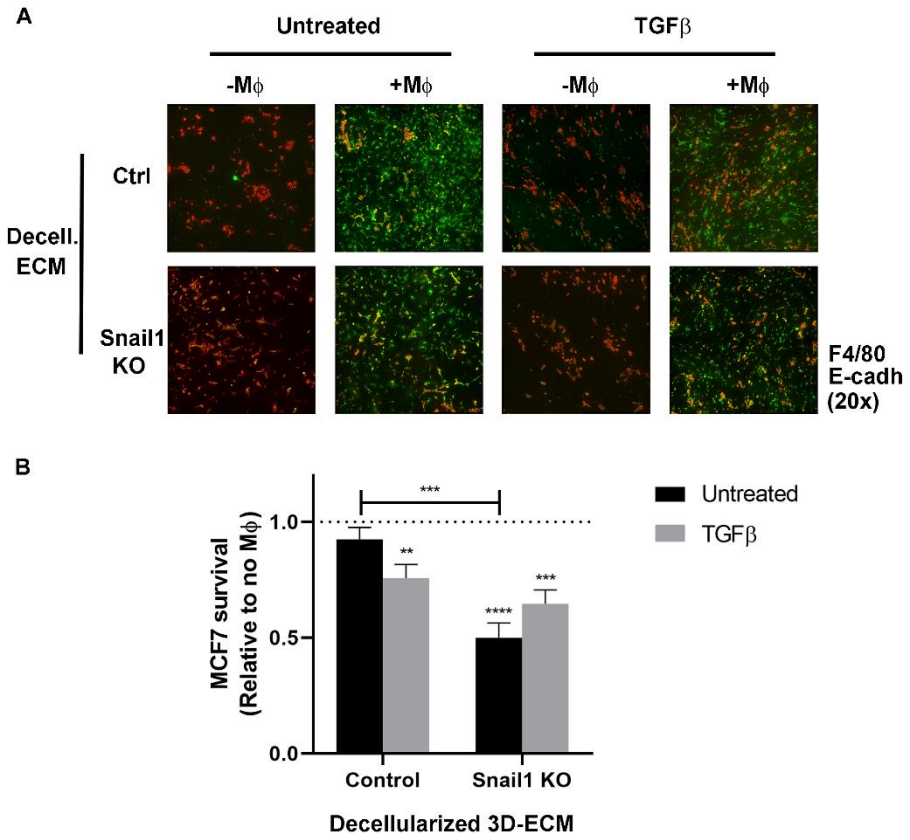

Figure 42: Macrophage activity is increased when seeded on 3D-ECMs generated by *Snai1* KO relative to Control MEFs. *(A) F4/80 and phalloidin immunofluorescence of macrophages and tumor cells.* MEF Ctrl and *Snai1* KO untreated or treated with 5ng/mL TGFβ were allowed to produce 3D-ECMs. Matrices were decellularized and macrophages were seeded on top of half of the matrices. 24 hours later, MCF7 cancer cells were seeded on all matrices. Cultures were fixed with 4% PFA after 48 hours and analyzed by IF with anti-F4/80 (green) and DAPI (red). Images were obtained using fluorescence microscopy. *(B) Quantification of surviving tumoral cells.* The number of

surviving MCF7 cells was quantified as intact nuclei with cytoplasm negative for F4/80. Plotted bars indicate the ratio of MCF7 surviving in the presence of macrophages relative to the absence.

5.2.2. Fibronectin EDA content of the ECM preserves macrophage activity

In order to study whether the detected *Snai1* KO matrix induced macrophage activity differences are consequence of differences in EDA content of the ECM, we analyzed the cytotoxic activity of macrophages using the EDA+, EDA- and wild-type MEFs to produce the decellularized ECM. Based on the current data, macrophage cytotoxicity is not dependent on matrix EDA content as MCF7 survival is unaffected (Figure 43).

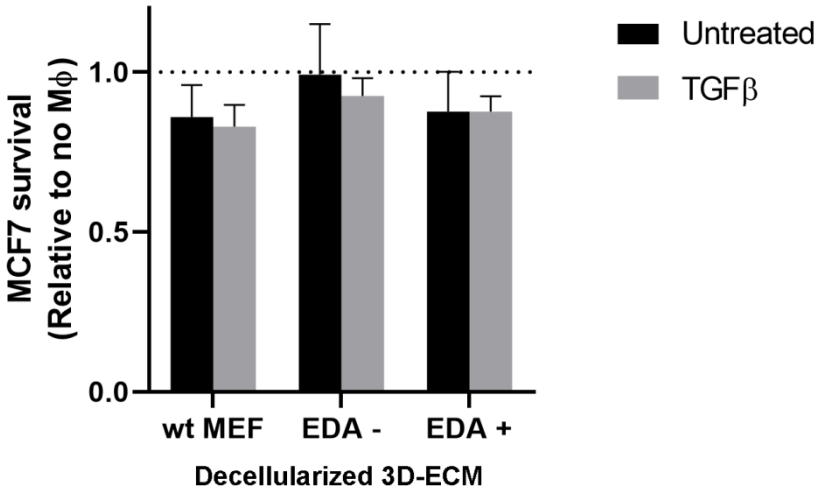

Figure 43: Macrophage activity is independent of the presence of fibronectin EDA in the 3D-ECM used as a substrate. The indicated MEF lines untreated and treated with 5ng/mL TGFβ were allowed to produce 3D-ECMs Matrices were decellularized and macrophages were seeded on top of half of the matrices. 24 hours later, MCF7 cancer cells were seeded on all matrices. Cultures were fixed with 4% PFA after 48 hours and analyzed by IF with anti-

F4/80 (green)and DAPI (red). Images were obtained using fluorescence microscopy and number of surviving MCF7 cells was quantified as intact nuclei with cytoplasm negative for F4/80. Plotted bars indicate the ratio of MCF7 surviving in the presence of macrophages relative to the absence.

5.3. Tumor cells are more aggressive on matrices enriched with fibronectin EDA

Besides indirectly regulating tumor cell aggressiveness by altering stromal cell behavior, ECM can directly control key characteristics of epithelial malignant cells such as the orientation in their movements and their invasiveness. Therefore, we aim to study and quantify if enrichment of EDA+ fibronectin in the matrix promotes malignant tumor cell behavior.

5.3.1. ECM fibronectin EDA content facilitates increased oriented cell movement

Tumor cells become malignant when they lose control of their proliferation and start spreading into the neighboring tissues in an invasion process that can be either individual or collective. We used MDA-MB-231 cells derived from human breast adenocarcinoma in order to study if fibronectin EDA matrices modulate individual motility, as they lack E-cadherin expression and present elevated individual cell migration and invasion. As mentioned in the introduction, this tumor cell line acquired an oriented migration on decellularized matrices generated by TGFβ treated Control but not *Snai1* KO MEFs, as they track the aligned fibers[61].

MDA-MB-231 were seeded on decellularized ECM derived from the three EDA genetically modified cell lines and their migration was imaged and quantified (Figure 44a). MDA-MD-231 presented a higher percentage of oriented movements when moving on matrices derived from EDA+ MEFs compared to EDA- (Figure 44b). This result relates to the findings in Figure 29, as EDA+ MEF derived ECM presents increased fiber alignment, leading to the increased oriented migration. EDA fibronectin presence in the ECM did not induce increased migration velocity.

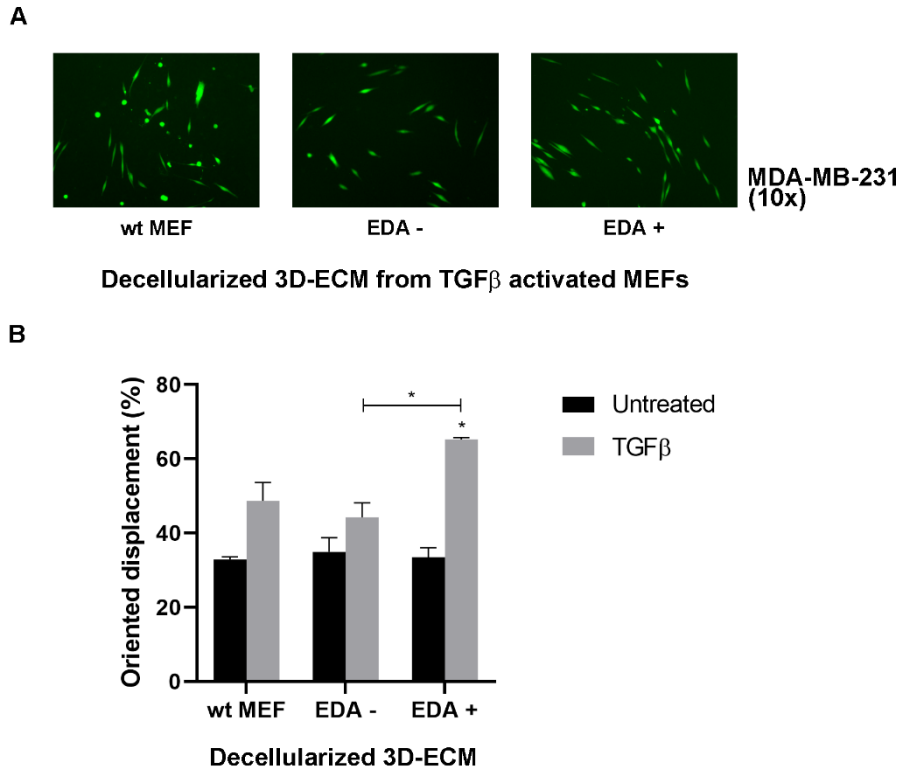

Figure 44: Oriented MDA-MB-231 migration depends on 3D-ECM fibronectin EDA. *(A) Immunofluorescence of migrating tumor cells.* The indicated MEF lines untreated and treated with 5ng/mL TGFβ were allowed to produce 3D-ECM. Matrices were decellularized and MDA-MB-231 tumor

cells labelled with Cell Tracker were seeded on top. At least 24 hours later, cell migration was recorded overnight by taking images every 15 minutes with life microscopy. *(B) Quantification of the tumor cell oriented displacement.* Cell movement was tracked using ImageJ software and displacement features, such as the angle of each displacement, were measured. Oriented migration was plotted as the percentage of cell movements in the maximum orientation (up to 21˚ deviation from the mode).

5.3.2. Irigenin treatment of ECM producing fibroblasts leads to disruption of the EDA induced increase in oriented migration

Even though Irigenin clearly reduced the tumor stroma fraction (Figure 41), it only induced a slight decrease in the alignment of *in vivo* like 3D-ECM produced *in vitro* (Figure 35). As ECM alignment closely correlated with tumor cell oriented migration (Figure 44), we expected Irigenin partially interfering with the orientation of the migration.

To confirm this, we seeded MDA-MB-231 on decellularized 3D-ECM generated from MEFs WT and EDA+ treated with TGFβ in the presence or absence of Irigenin. Fitting with the small alignment decrease induced by Irigenin, analysis of the cell movements from overnight time-lapse recording revealed a partial reduction of oriented movement by Irigenin on EDA+ ECMs (Figure 45a).

We further tested the action of Irigenin on oriented migration on matrices already polymerized. For that, we produced aligned 3D ECM from WT and EDA+ MEFs in the presence of TGFβ and added Irigenin only during the migration assay. The analysis of the videos indicated

that Irigenin could not disrupt the oriented migration on previously aligned matrices (Figure 45b).

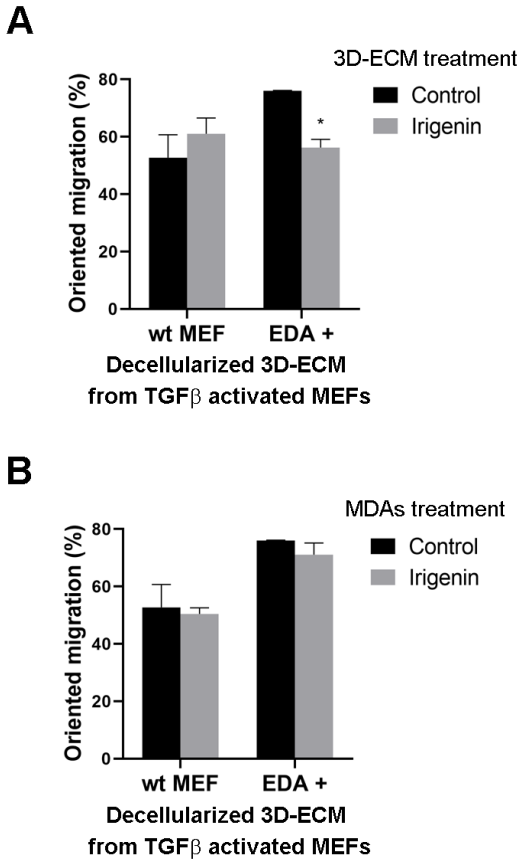

Figure 45: Irigenin alters 3D-ECM formation leading to a decrease in the oriented migration of tumor cells. *(A) Quantification of tumor cell oriented migration on Irigenin treated 3D-ECM.* 3D-ECM were produced by the indicated MEF lines activated with 5ng/ml of TGFβ and either treated or untreated with 50µM Irigenin. ECMs were decellularized and MDA were seeded on top and allowed to migrate. Migration was recorded and oriented movement was quantified as percentage of cell movements towards the same direction (up to 21˚ deviation from the mode). *(B) Quantification of Irigenin treated tumor cell oriented migration on 3D-ECM.* 3D-ECMs were produced by the indicated MEF lines activated with 5ng/ml TGFβ. ECMs were decellularized and MDA were seeded on top, either treated or left untreated with 50µM Irigenin, and allowed to migrate. Migration was recorded and

oriented movement was quantified as percentage of cell movements towards the same direction (up to 21˚ deviation from the mode).

5.3.3. Fibronectin EDA rich ECMs induce increased individual tumor cell invasion

Invasion of individual MDA-MB-231 cells through 3D-ECMs with or without fibronectin EDA was measured using invasion inserts. For that, decellularized 3D-ECM from wild-type, EDA- and EDA+ MEFs were produced on the insert membrane in the presence of TGFβ and tumor cells were then seeded on top and stimulated to invade towards the lower chamber using a FBS gradient. We found a higher number of MDA-MB-231 invading in EDA+ ECM compared to EDA- (Figure 46). Similar to the result obtained in oriented migration, tumor cells seeded in matrices generated by wild-type MEFs display an intermediate invasive behavior.

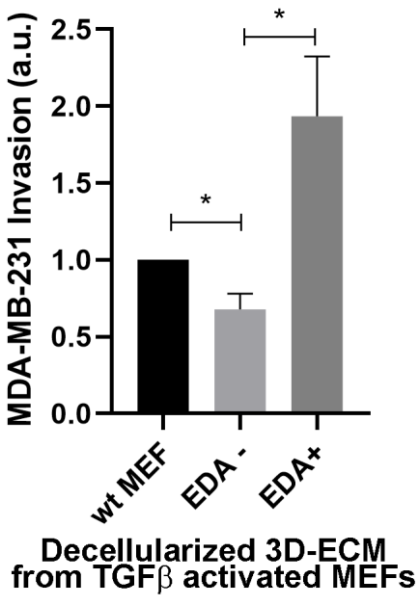

Figure 46: MDA-MB-231 invasion is increased on fibronectin EDA rich 3D-ECMs. The indicated MEF lines were allowed to produce 3D-ECM on top of the membrane of invasion inserts while activated with 5ng/mL TGFβ. ECMs were decellularized and MDA were seeded on top. DMEM media with 0.1% FBS was placed in the upper chamber and DMEM 10% in the lower as a chemoattractant. Cells were allowed to invade for 16 hours and fixed with 4% PFA. Invading cells were stained with DAPI and quantified.

5.3.4. MDA-MB-231 invasion trough 3D-ECM with fibronectin EDA is reduced if matrices are produced in the presence of Irigenin

We covered invasion inserts with decellularized 3D-ECMs produced by TGFβ activated fibroblasts in the presence or absence of Irigenin and MDA-MB-231 were seeded and allowed to invade. We find that in ECM produced by EDA+ MEFs, Irigenin treatment reduced tumor cell invasive capabilities compared to the untreated control (Figure 47).

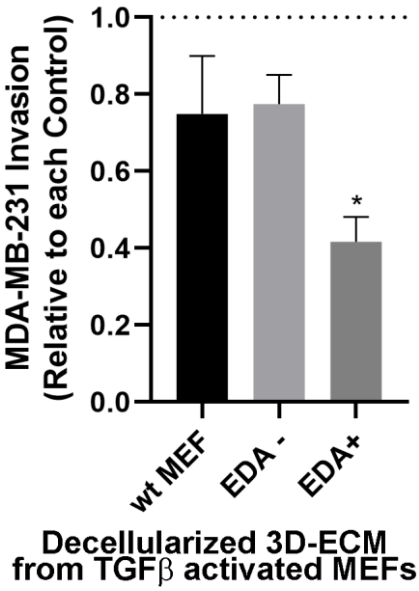

Figure 47: MDA-MB-231 invasion is decreased on fibronectin EDA rich 3D-ECMs produced in the presence of Irigenin. The indicated MEF lines were allowed to produce 3D-ECM on top of the membrane in the presence of 5ng/mL TGFβ and either treated or left untreated with 50μM Irigenin. ECMs were decellularized and MDA were seeded. DMEM media with 0.1% FBS was placed in the insert with the cells and DMEM 10% was placed beneath as a chemoattractant. Cells were allowed to invade for 16 hours and fixed with 4% PFA. Invading cells were stained with DAPI and quantified. Bars show the invasion in the presence relative to absence of Irigenin.

5.3.5. Presence of fibronectin EDA in the ECMs regulates collective tumor cell migration

We used the EpRas tumor cell line in order to study EDA effects over collective tumor cell migration and invasion. They are mouse cells derived from the mammary epithelial cell line EpH4 by inducing stable expression of the Ha-Ras oncogene. This cell line has a highly epithelial

phenotype, with high E-cadherin expression, and allows us to study collective movement.

EpRas were seeded on untreated glass coverslip or covered with decellularized 3D-ECMs derived from the three EDA genetically modified MEFs activated with TGFβ and their movements were recorded in bright field using life microscopy overnight (Figure 48a). Eventually, samples were fixed and used for immunofluorescence using phalloidin to study the cell colonies arrangement (Figure 48a). While these cells formed circular epithelial colonies when seeded directly on glass coverslips, they formed elongated colonies on 3D-ECMs. High amplification images of phalloidin immunofluorescence revealed finer details of colony organization (Figure 48b). Cells seeded on EDA+ matrices organized in compact colonies with smooth borders, often compactly moving in a main direction following leader cells. When seeded on EDA- matrices, however, compactness of the colonies is reduced as cell to cell interaction is reduced and cells located in the edges of the colony tend to extend prolongations outwards in every direction instead of having well defined leader cells.

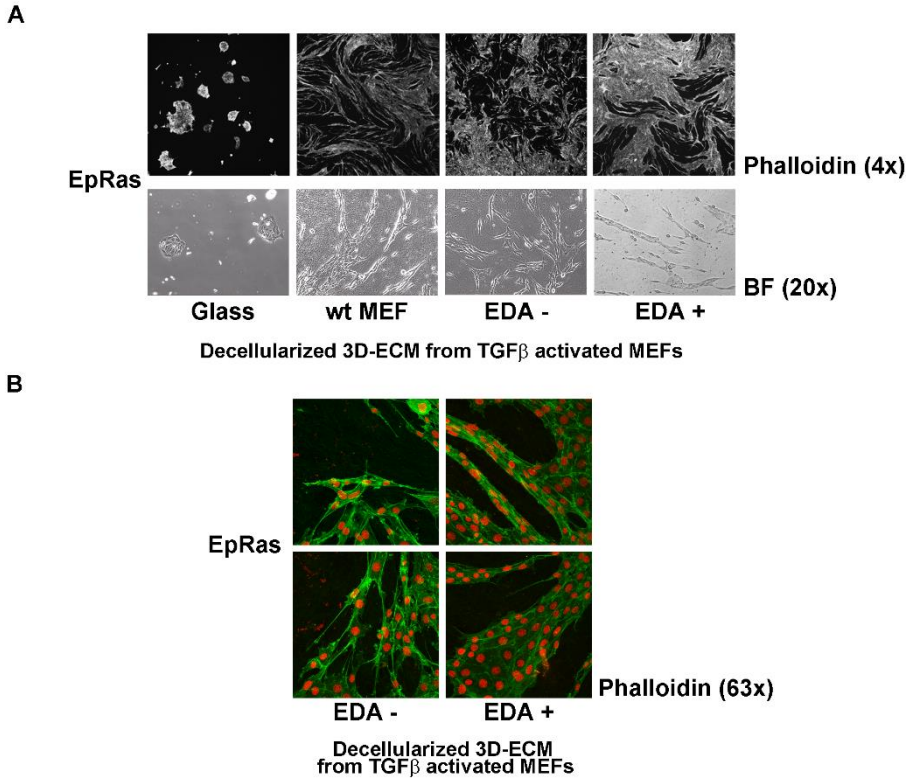

Figure 48: EpRas collective migration is affected by presence of fibronectin EDA in the 3D-ECM. *(A) Phalloidin immunofluorescence and bright field of migrating tumor cells.* The indicated MEF lines were allowed to produce 3D-ECM treated with 5ng/mL TGFβ. Matrices were decellularized and EpRas tumor cells were seeded on top. At least 24 hours later, cell migration was recorded overnight in a life microscope by taking images every 15 minutes. Bright Field (BF) images correspond to images taken during the recording. After at least 48 hours, cells were fixed with 4% PFA and analyzed by IF with Phalloidin (gray). *(B) Phalloidin immunofluorescence details.* Confocal pictures of the IFs described in A showing phalloidin (green) and DAPI (red).

5.3.6. Fibronectin EDA rich 3D-ECMs induces increased EpRas invasion

Invasion of EpRas cells through decellularized 3D-ECM produced by TGFβ activated fibroblasts was quantified in invasion inserts as performed with MDA cells. The results obtained mimic those of MDA-MD-231 (Figure 46). We found a higher amount of EpRas cells that crossed the fibronectin EDA matrices compared with EDA- (Figure 49). Invasion through 3D-ECMs generated by wild-type was similar to that in EDA+ matrices.

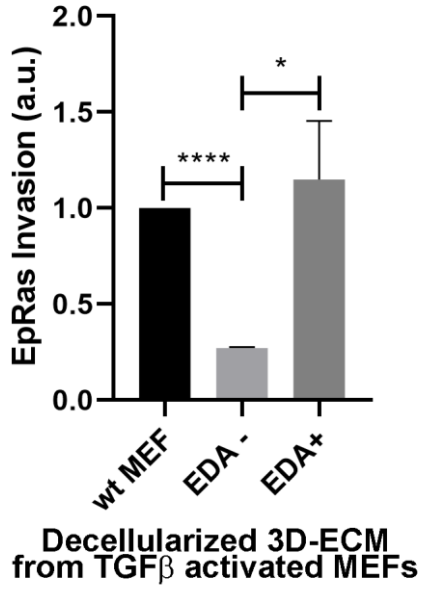

Figure 49: EpRas invasion is increased on 3D-ECMs containing fibronectin EDA. The indicated MEF lines were allowed to produce 3D-ECMs on top of the membrane of invasion inserts while activated with 5ng/mL TGFβ. ECMs were decellularized and EpRas were seeded on top. DMEM media with 0.1% FBS was placed in the upper chamber and DMEM 10% in the lower as a chemoattractant. Cells were allowed to invade for 48 hours and fixed with 4% PFA. Invading cells were stained with DAPI and quantified.

5.3.7. EDA+ generated 3D-ECM is less susceptible to degradation

The differences of individual and collective migration and invasion on EDA+ and EDA- matrices suggest different interaction between the tumor cells and these matrices. To evaluate their interactions, we set cocultures of MEFs and epithelial tumor cells. We added the MEFs to glass coverslips previously plated with breast MCF7 or colon HT-29 M6 human cancer cells.

In the coculture with MCF7, tumor cells grew expansively and forced fibroblast accumulation in reduced areas interconnected by lines of fibroblasts as detected through fibronectin immunofluorescence (Figure 50). Fibronectin fibers in cocultures with MEF EDA- were often discontinued, potentially suggesting degradation taking place.

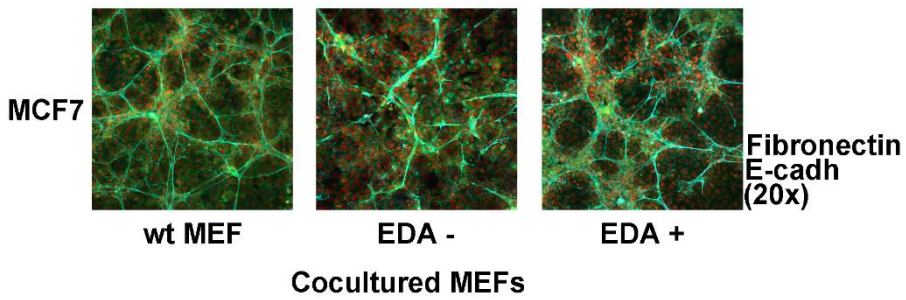

Figure 50: MCF7 prevent EDA-lacking fibronectin deposition around them. MCF7 tumor cells were seeded on glass coverslips and allowed to proliferate for 72 hours. The indicated MEF lines were then seeded on the same coverslips and cocultures were maintained for up to 6 days. Cells were fixed with 4% PFA and analyzed by IF with anti-fibronectin (cyan), anti-E-cadherin (green) and DAPI (red). Images were obtained through confocal microscopy.

In the coculture with HT-29 M6, tumoral cells grew as isolated distinct colonies, allowing us to easily differentiate epithelial cells from the cocultured fibroblasts. Fibronectin fibers of EDA+ MEFs tightly circled the colonies while clear gaps were often present in cocultures with EDA- MEFs. Coculture with wild-type MEFs presented an intermediate phenotype (Figure 51a). Tridimensional reconstructions performed from confocal imaging clearly show the differences between EDA+ and EDA-, while highlighting the existence of broken fibronectin fibers in the EDA- coculture (Figure 51b). The quantification of the empty areas surrounding the epithelial colonies with ImageJ software reflects the visual differences, with EDA- coculture presenting almost fourteen-fold bigger empty holes than EDA+ (Figure 51c). All data obtained suggested differences in tumor cell induced matrix degradation.

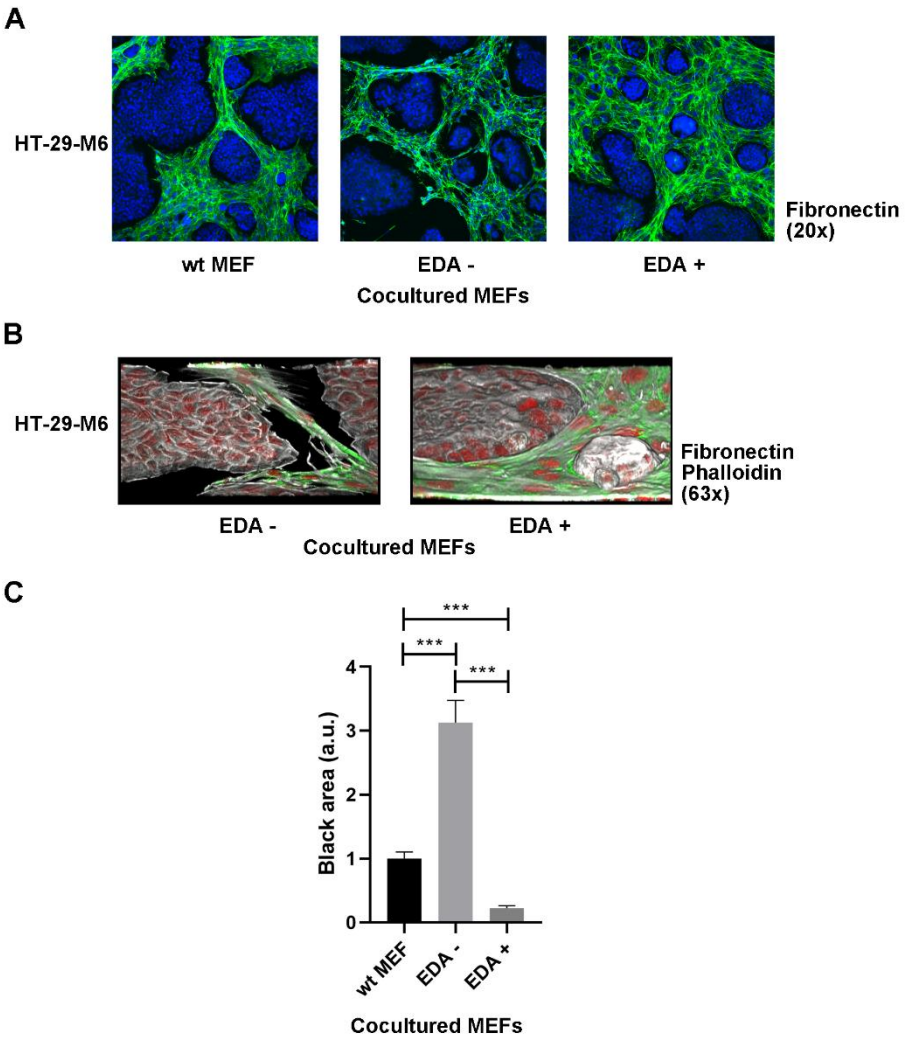

Figure 51: HT-29 M6 colonies prevent EDA-lacking fibronectin deposition around them. *(A) Fibronectin immunofluorescence of cocultures.* HT-29 M6 tumor cells were seeded on glass coverslips and allowed to proliferate as epithelial colonies for 72 hours. The indicated MEF lines were then seeded on the same coverslips and cocultures were maintained for up to 6 days. Cells were fixed with 4% PFA and analyzed by IF with anti-fibronectin (green) and DAPI. Images were obtained through fluorescence microscopy. *(B) Fibronectin and Phalloidin immunofluorescence detail.* Images were obtained through confocal microscopy every 0.5μm and Z-stack reconstruction was obtained through ImageJ software. *(C) Quantification of immunofluorescence black areas.* Black area surrounding each tumor cell colony was quantified on

ImageJ. Plotted bars indicate the measure of the black areas relative to the perimeter of the colony.

To test whether matrices of the cocultures were differently resistant to metalloproteinases activated by the presence of tumoral cells, cocultures with HT-29 M6 were performed in the presence of the unspecific metalloproteinase inhibitor GM6001 (Figure 52a). As suspected, the addition of GM6001 to the coculture significantly reduced fibronectin degradation in EDA-, taking the black area surrounding tumor cell colonies to EDA+ levels (Figure 52b).

5.3.8. EDA- MEF do not produce increased levels of Metalloproteinase 2

As GM6001 is capable of inhibiting all metalloproteinases, we aimed to pinpoint which MMP is responsible for degrading EDA lacking ECM. We performed zymography using conditionate media from cocultures as well as from each MEF and tumor cell line alone. The results obtained show that MEFs are the only producers of MMP2 both in its active and inactive forms (Figure 53). Unfortunately, our results show that compared to EDA+ MEFs, EDA- MEFs are not producing increased levels of either pro-MMP2 or its active form.

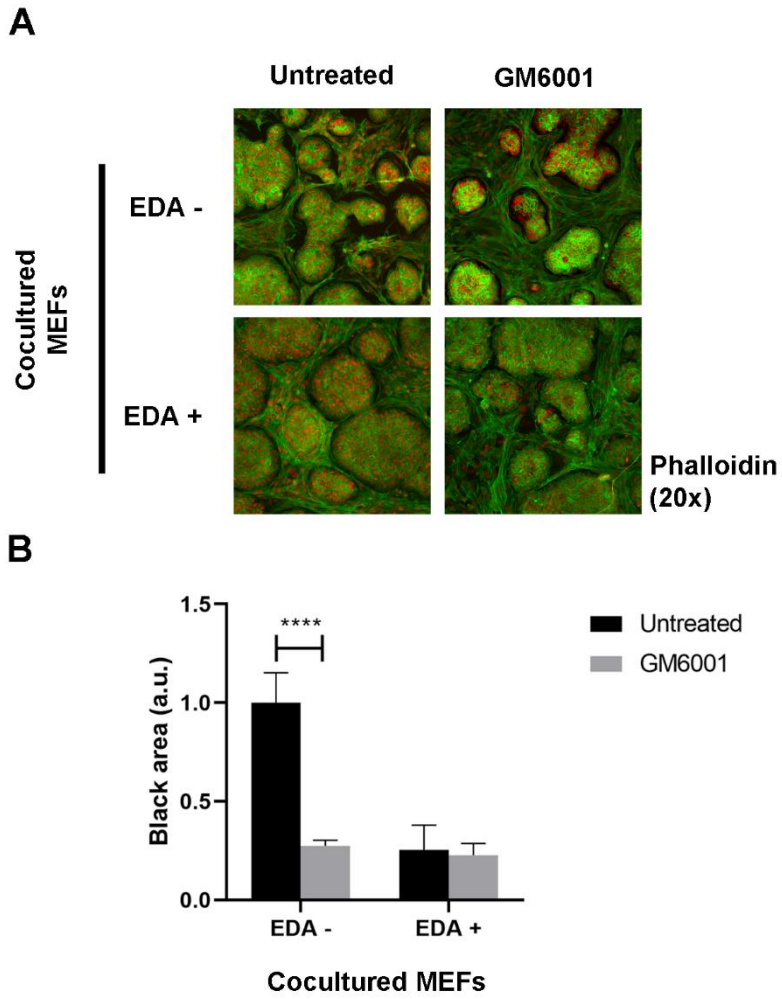

Figure 52: The metalloproteinase inhibitor GM6001 rescues the EDA-lacking fibronectin deposition around HT-29 M6 colonies. *(A) Phalloidin immunofluorescence of cocultures.* HT-29 M6 tumor cells were seeded on glass coverslips and allowed to proliferate as epithelial colonies for 72 hours. The indicated MEF lines were seeded on the same coverslips and 25µM GM6001 treatment was added were indicated. The coculture was maintained for up to 6 days. Cells were fixed with 4% PFA and samples were analyzed by IF with Phalloidin (green) and DAPI. Images were obtained with fluorescence microscopy. *(B) Quantification of black area surrounding epithelial colonies.* Black area surrounding each tumor cell colony was quantified on ImageJ. Plotted bars indicate the measure of the black areas relative to the perimeter of the colony.

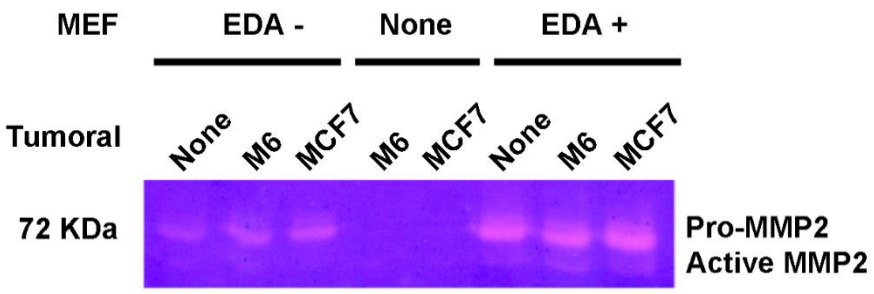

Figure 53: MEFs EDA+ secrete higher amounts of MMP2 to the media. Cocultures of indicated tumor cells and MEF lines were prepared by platting MEFs 24 hours before tumor cells. After 8 hours, media was replaced by 0% FBS DMEM and cocultures were allowed to grow overnight. Then, conditioned media was harvested, concentrated 10x, separated by SDS-PAGE using a gel containing gelatin, and MMP2 detected by zymography.

5.3.9. *Snai1* KO MEF produced ECM is more sensitive to degradation

We also studied degradation of the ECMs in cocultures in the context of SNAIL1 lacking MEFs. Since SNAIL1 favors inclusion of EDA, it should potentiate the resistance of the ECM to metalloproteinases.

Accordingly, we found more fibronectin empty areas surrounding tumoral cell colonies in cocultures with *Snai1* KO MEF than Control MEFs (Figure 54). Metalloproteinase involvement was also observed, as GM6001 treatment decreased the black area generated, clearly reducing *Snai1* KO degradation levels to Control MEFs like.

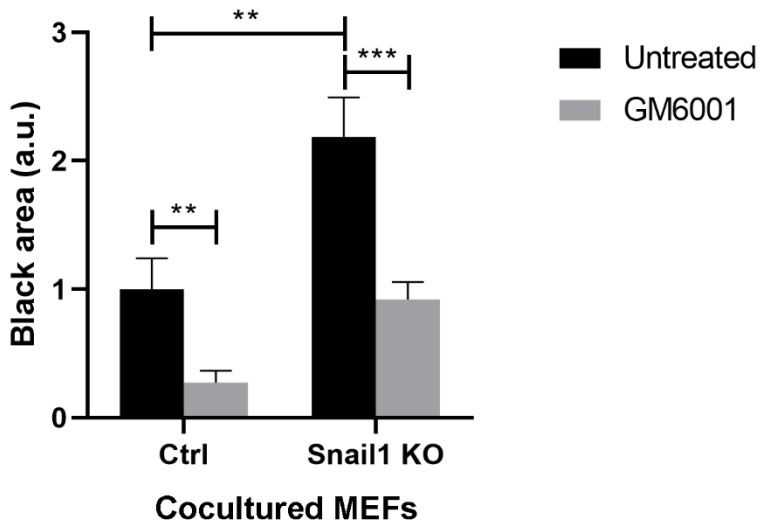

Figure 54: HT-29 M6 colonies prevent the deposition of fibronectin secreted by *Snai1* KO MEFs around them in a GM6001 dependent manner. HT-29 M6 tumor cells were seeded on glass coverslips and allowed to proliferate as epithelial colonies for 72 hours. The indicated MEF lines were seeded on the same coverslips and left untreated or treated with 25µM GM6001. Cocultures were maintained for up to 6 days and then fixed with 4% PFA and analyzed by IF with anti-fibronectin (green) and DAPI. Black area surrounding each tumor cell colony was quantified on ImageJ by measuring the black area relative to the perimeter of the colony.

5.4. Tumors with EDA fibronectin rich stroma are more aggressive

5.4.1. An EDA fibronectin rich stroma leads to increased tumor growth

Given all the studied effects of an EDA fibronectin rich 3D-ECM on both tumoral and stromal cells, we decided to test its relevance using an orthotopic *in vivo* model. We injected AT-3 mammary tumor cells and either MEFs EDA- or EDA+ in a 1:1 relation into inguinal mammary

fat pads of NOD-SCID gamma mice. Tumors were monitored, allowed to grow and surgically resected when the average length was 0.2-0.4cm. Tissue sections were used to perform Hematoxylin and Eosin staining (not shown) as well as fibronectin immunohistochemistry (Figure 55a). Upon resection, accurate primary tumor measurements were performed to calculate their volumes. Significant differences were observed, with tumors generated by AT-3 and EDA+ MEFs growing twice as much as those without EDA fibronectin in their stroma (Figure 55b).

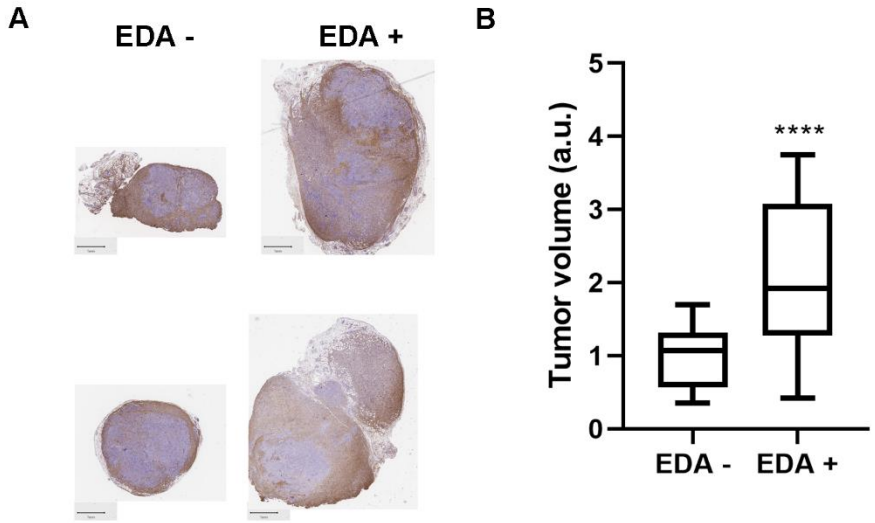

Figure 55: EDA fibronectin rich stroma induces enhanced primary tumor growth. *(A) Fibronectin immunohistochemistry of primary tumor sections.* $5x10^4$ AT-3 and either $5x10^4$ EDA- MEF or $5x10^4$ EDA+ MEF were co-injected orthotopically into the inguinal mammary fat pad of NOD-SCID gamma mice. Tumors were all resected at the same time once they started reaching 0.5cm approximately. Samples were measured, and immunohistochemistry was performed on 4% PFA-fixed paraffin embedded tissues. Bars correspond to 1mm. *(B) Tumor volume quantification*. The three main dimensions of resected primary tumors were measured prior to fixation. Tumor volume

was calculated and all data obtained is represented as box plots relative to average tumor volume of EDA- MEF co-injected tumor.

5.4.2. Primary tumor stroma lacking EDA fibronectin blocks lung metastasis generation

After surgical resection of primary tumors, mice were kept alive for 7 weeks to allow the growth of lung metastasis and then were humanely sacrificed. Lungs were extracted and hematoxylin and eosin staining were performed to study the presence of metastatic foci (Figure 56a). While 7/11 animals injected with AT-3 and EDA+ MEFs developed at least one metastasis foci, none of the animals injected with AT-3 and EDA- MEFs did (Figure 56b).

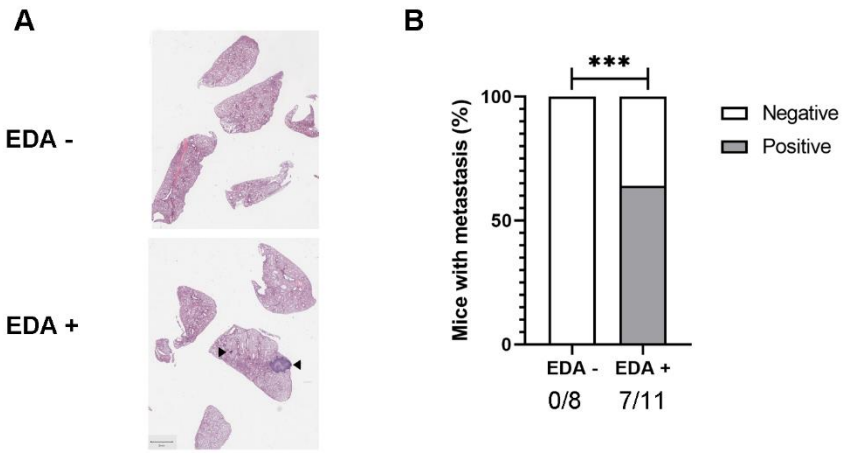

Figure 56: EDA fibronectin lacking stroma in primary tumors restricts metastasis formation. *(A) Hematoxylin and Eosin staining of lung sections.* Mice were humanely sacrificed at least one and a half months after primary tumor resection and lungs were extracted. Lungs were fixed in 4% PFA, embedded in paraffin and paraffin sections were stained with Hematoxylin and Eosin. Metastasis are signaled by black arrowheads. *(B) Quantification of presence of metastatic foci.* Lung hematoxylin and eosin staining were used

to detect presence of metastatic foci. Lungs with at least one metastasis are indicated as positive.

This data together with previous results showing a role for EDA fibronectin in inducing tumor cell invasion reinforces the relevance of EDA fibronectin in tumor progression and suggests a protective role for the lack of EDA.

DISCUSSION

1. CHARACTERIZATION OF THE SNAIL1-FIBRONECTIN EDA CORRELATION

Previous results in our laboratory have shown that SNAIL1 is essential for fibroblasts activation into myofibroblasts. We characterized in detail SNAIL1 relevance towards the formation of an aligned and stiff ECM, and we have related fibroblastic lack of SNAIL1 to decreased fibronectin production, disruption of fibrillogenesis and an overall decreased fibroblast activation leading to reduced tensional capabilities.

In an effort to characterize the promoters being targeted by SNAIL1 and study the mechanisms behind SNAIL1 mediated fibroblast activation, our group has performed SNAIL1 ChIP-seq. Unfortunately, the use of available SNAIL1 antibodies was unsuccessful as only background signal, comparable to *Snai1* KO MEFs, was obtained. During the present project, in an attempt to solve this limitation, we developed CRISPR Knock-In mutants inserting a tag (FLAG 3x) downstream of *Snai1*. However, the antibody against the inserted tag did not improve the ChIP signal. Nevertheless, a new commercial antibody targeting SNAIL1 with high specificity and efficiency was obtained, allowing us to perform the techniques presented in this project.

The description in our lab of a SNAIL1 interaction with PRMT1 and PRMT4 offered a new approach for studying SNAIL1 down-stream effects, as the analysis of SNAIL1-dependent arginine methylation

through mass spectrometry generated a list of proteins enriched in mRNA processing and splicing machinery. These results suggest that SNAIL1 may control splicing in myofibroblasts by a molecular mechanism other than that described in EMT. Several reports relate SNAIL1 to repression of splicing factors transcription, promoting EMT by inducing the shift from epithelial to mesenchymal isoforms of key genes[136–138]. These observations prompted our team to perform deep RNA-seq to study SNAIL1 regulation of transcription and splicing.

Analysis of the obtained RNA-seq data was carried out comparing TGFβ treated control and KO *Snai1* MEFs with the SANJUAN pipeline designed in the laboratory of Dr. Juan Valcárcel (Gene Regulation, Stem Cells and Cancer at CRG, Barcelona) to detect splicing events. We identified more than 300 SNAIL1 dependent events, including many genes related to cellular architecture, either involved in the cytoskeleton (*Anln, Macf1, Tpm2, PPP1R12A, Flnc and Flnb*) or the extracellular matrix (*Fn1 and Col5α1*).

The SNAIL1 dependent splicing event affecting inclusion of the extra domain A (EDA) into fibronectin mRNA was chosen for further study. The transcription factor SNAIL1 is physiologically expressed during development and pathologically during wound healing, fibrosis and cancer[139]. This expression pattern perfectly fits with that of the fibronectin isoforms including EDA[94]. However, a direct correlation or an SNAIL1 splicing regulation has never been reported.

Since fibronectin isoforms including EDA have also been linked to myofibroblast activation, a circular feedback pathway for SNAIL1

expression and fibroblast activation depending on fibronectin EDA can be envisioned. Furthermore, it offers a role for fibronectin EDA in modulating the tumoral stroma architecture, which we have previously attributed to be SNAIL1 dependent. Our initial work has focused in validating the existence of a correlation between these two molecules.

1.1. SNAIL1 is required for fibronectin EDA expression and both molecules correlate in cancers

Based on the data collected in the first results chapter of this manuscript, SNAIL1 strongly induces fibronectin EDA production by positively regulating EDA alternative splicing. Using various fibroblast cell lines, we demonstrate that SNAIL1 depletion, both permanent and transient, negatively affects EDA splicing both at the RNA and protein level. The detected SNAIL1 dependent increase in fibronectin EDA goes beyond the already described effect of SNAIL1 in inducing fibronectin transcription[53]. Interestingly, SNAIL1 depletion not only prevented TGFβ induced EDA inclusion but also reduced the basal inclusion percentage[125]. We further described the SNAIL1 capability to promote EDA inclusion by overexpressing the transcription factor in a highly epithelial cell line, with negligible basal levels of both SNAIL1 and fibronectin EDA expression. This data unveils SNAIL1 as a potent regulator for EDA inclusion that mediates the TGFβ induced increase.

Since the presence of SNAIL1 expressing myofibroblasts in primary tumors induces a pro-metastatic environment[61], we wanted to confirm that SNAIL1 and fibronectin EDA correlate in tumors, beyond

the effects detected in cell cultures. We have first interrogated a physiological model by using a PDX collection made available to us by Dr. Joaquin Arribas' lab (VHIO, Barcelona, Spain) and found that protein levels for SNAIL1 and fibronectin isoforms including EDA correlate. Concerns regarding PDXs abilities to recapitulate the stroma of the original tumors have been raised since during PDX engraftment in mice human stromal cells are replaced by their mouse equivalents[140]. This stromal substitution in PDXs has been considered a limit, potentially affecting tumor biology. However, it has been proven that PDXs maintain close similarities to their tumor of origin in terms of tissue architecture, molecular features and response to treatment, producing data matching that of the original patient[141]. These similarities suggest that PDXs maintain the basic tumor-stroma mediators intact, making them good study models[142]. Importantly to our study, proteomic analysis of paired tumors and PDX show conservation of the original stromal profile[143,144]. Despite these considerations, we have further analyzed human tumor data, which should support PDX reliability and confirm the correlation.

Available data in public databases for five types of solid tumors was used. For all these tumors, a relevant role for stroma in tumor progression and malignancy has been described: breast[145–147], lung[148,149], kidney[150], bladder[151] and skin[152]. Our approach was to separately interrogate tumors in their initial and more advanced stages, as it has been reported that fibronectin EDA levels are higher in malignant than benign tumor masses[153]. For all the studied cancers we found a basal percentage of tumors with high EDA expression

independently of SNAIL1 levels and stage. Only in advanced stages, tumors with elevated SNAIL1 levels present increased percentage of high EDA inclusion. This data likely points to other splicing regulatory mechanisms independent of SNAIL1 being in place. However, in advanced tumors, where signaling such as TGFβ are preeminent[154], SNAIL1 action on splicing is turned on. Other studies have already shown that EDA isoforms are increased in advanced stage tumor samples for colorectal cancer[155]. This same study finds that tumor tissue EDA levels negatively correlate with both disease free survival and overall survival. Similar discoveries for SNAIL1 expression correlating with bad prognosis have been made on this same tumor type[22].

While we found a strong correlation in PDX and tumor data analyses, all used data relates to extracts from the whole tumor, including both parenchyma and stroma. However, parenchymal contribution to both total fibronectin EDA and SNAIL1 levels is likely insignificant, as even though tumoral SNAIL1 expression was originally attributed to the parenchyma, it has been demonstrated that CAFs are the main producers[22]. In fact, a crosstalk has been described were CAFs induce malignant properties and EMT in the tumor-stroma interface[156] and, in turn, receive chemical signals such as TGFβ that promote further fibroblast activation[157], inducing SNAIL1 expression among others. Therefore, most SNAIL1 positive tumors express it in both compartments. Nevertheless, we seek to analyze tumor tissue samples through immunohistochemistry and confirm our hypothesis that SNAIL1 expressing stroma bears a higher EDA fibronectin content. We

are currently working in collaboration with Dr. Alberto Rodríguez (Thoracic surgery service, Hospital del Mar) to obtain a collection of human lung tumor samples to study.

1.2. SNAIL1 as a splicing regulator

SNAIL1 is a transcription factor with key roles in EMT and fibroblast activation, directly repressing E-cadherin expression as well as other epithelial genes and inducing the expression of several mesenchymal genes, including fibronectin. As mentioned above, our SNAIL1 gain and loss of function approach in cell cultures and the correlations observed in patient tumor samples introduce a new role for SNAIL1 in regulating splicing in fibroblasts. Zinc-finger proteins are described as DNA-binding transcription factors. However, their binding capabilities have been shown to be not restricted to double-stranded DNA but also proteins and RNA[158,159]. Here, we present evidence for an RNA-binding ability for SNAIL1, as shown through OOPS.

To us, this capability, paired with the existence of an E-box, canonically recognized by SNAIL1 zinc-finger domain, in the EDA coding region just upstream of the already described exonic splicing enhancer, offered a possible explanation for SNAIL1 role in EDA splicing regulation. We speculated SNAIL1 may directly bind to the RNA in this EDA region to regulate the binding and/or activity of splicing factors. However, our RIP results unveiled no SNAIL1 highly specific binding to the EDA coding RNA, discarding this initial hypothesis.

In contrast, ChIP data showed specific enrichment of the DNA region coding for EDA in SNAIL1 immunoprecipitates. Given this result, we speculated that SNAIL1 recruitment to the DNA is what regulates EDA splicing, for instance by controlling the access of splicing factors to the RNA. Indeed, the recruitment of SNAIL1 takes place in a TGFβ dependent manner, fitting with our previous argument that SNAIL1 mediates the TGFβ-induced splicing (see above, Discussion chapter 1.1). Therefore, while we describe by OOPS that SNAIL1 has RNA-binding capacity, we conclude that strong direct interaction with the EDA RNA is not occurring and is therefore irrelevant to control its alternative splicing. Further studies would be necessary to assess RNA targets for SNAIL1 and the meaning of the detected interaction.

As mentioned in the introduction, the splicing factor SRSF1 positively regulates EDA inclusion in a TGFβ manner. According with our hypothesis that SNAIL1 recruitment to the DNA regulates the access of splicing factors to the RNA, we found a SNAIL1 dependent recruitment of SRSF1 to the EDA coding mRNA. In addition, we have detected a TGFβ dependent SRSF1 binding to the EDA coding DNA, likely a result of cotranscriptional splicing that allows precipitation of genomic regions with crosslinked nascent RNA-binding proteins[160]. On the other hand, SRSF1 binding to the constitutively included fibronectin exon 7 was not detected to be TGFβ dependent, suggesting the existence of different recruitment mechanisms controlling SRSF1. Thus, our model for the alternative splicing of exon 33 is that through a TGFβ dependent SNAIL1 binding to the DNA region coding for the

EDA, the factor allows the recruitment and binding of SRSF1 to the pre-mRNA, ultimately leading to increased exon inclusion (Figure 57).

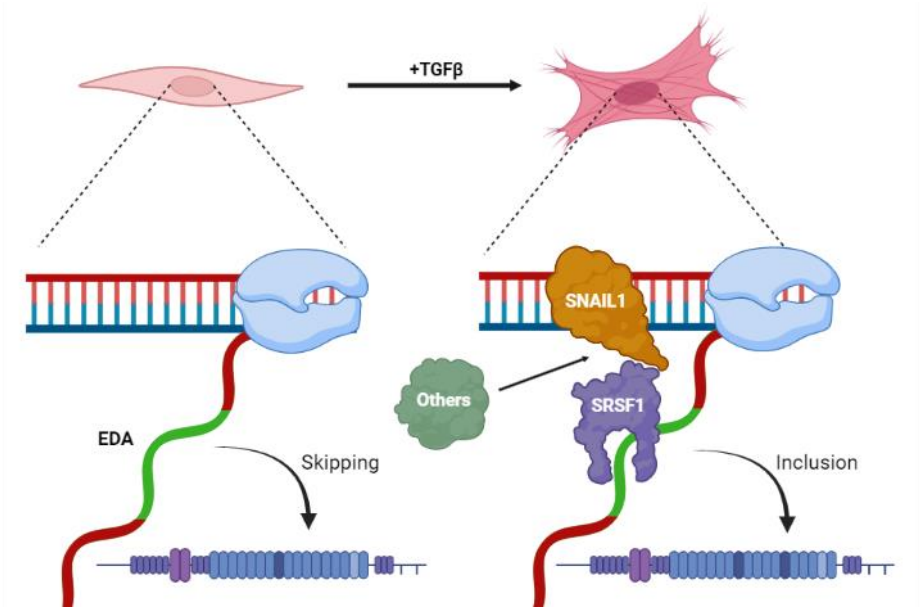

Figure 57: TGFβ regulated EDA splicing. Working model for SNAIL1 regulated EDA splicing. Upon TGFβ induced fibroblast activation, SNAIL1 binds to the DNA coding for fibronectin extra domain A, inducing the recruitment of SRSF1 to the nascent RNA. Increased SRSF1 has been shown to induce inclusion of the EDA coding exon into mRNA and into the translated protein. SRSF1 recruitment by SNAIL1 may be direct or indirect, depending on other factors. Image created in BioRender.

Our data showing that SNAIL1 and SRSF1 coimmunoprecipite, together with the data that the complex disappears in the presence of exogenous RNase, reinforces the existence of a cotranscriptional splicing complex including DNA and RNA binding proteins linked by nascent RNA and discards a direct interaction between SNAIL1 and SRSF1. With the present data we do not solve how SNAIL1 facilities the binding of SRSF1. It is possible that SNAIL1 presence determines the

conformation adopted by the nascent RNA allowing the accessibility of SRSF1 to its RNA binding site. Additionally, it is also plausible that regulatory methylation of some of the components of the splicing complex is SNAIL1 dependent. In the next chapter, we discuss this and other SNAIL1 dependent methylation possibilities that we have not explored.

1.3. A role for SNAIL1 mediated methylation in alternative splicing regulation

Previous reports by our group describe the formation of a transcription activator complex in the promoter of fibronectin, which includes SNAIL1 and the arginine methyltransferases PRMT1 and PRMT4. The data suggests that PRMTs induced asymmetric methylation of the histones in the promoter region regulates transcription for fibronectin[161]. Besides inducing transcription, this complex may be relevant in splicing regulation. Importantly, a coupling between transcription and splicing has been characterized, as the C-terminal domain (CTD) of the RNA polymerase II (Pol II) serves as a platform for binding of RNA maturation factors, including splicing factors. Minigene studies have shown that fibronectin promoter structure influences SRSF1 mediated EDA splicing, with changes both in sequence and histone modification altering the splicing rate[105,162]. Both PRMT1 and PRMT4 activities have been linked to regulation of not only transcription but also splicing through specific methylation of histones, splicing factors and other RNA binding proteins[163,164].

PRMT1 regulates splicing through methylation of the RNA-binding splicing factor recruiter RBM15, leading to its degradation via ubiquitination[163]. Additionally, PRMT1 has been shown to methylate SRSF1 in three different Arginine residues, regulating SRSF1 subcellular distribution and, by extension, its activity in splicing regulation[165]. However, we have not detected significant changes neither in the total SRSF1 amounts nor in its cellular distribution upon TGFβ treatment and/or SNAIL1 depletion. In contrast, although not documented, we can speculate that arginine methylation of SRSF1 may change the ability of the factor either to bind some RNA sequences or to exert its regulatory function.

PRMT4 methylates many proteins of the RNA processing machinery, regulating their protein-protein binding and their capability to assemble the spliceosome. PRMT4 direct interaction with splicing factors has also been described[164]. While no interaction between PRMT4 and the Pol II CTD is reported, it does methylate CTD-binding proteins such as elongation factors[166]. The methylation status of this factors determines their ability to regulate Pol II elongation rate[166,167], a key factor in EDA alternative splicing, as slow transcription favors its inclusion[168]. SNAIL1 binding to promoters always localizes near the transcription start site[53] and, therefore, near the Pol II binding site. This proximity may facilitate PRMTs interaction with CTD associated proteins in the context of fibronectin.

This body of data, coupled with our reporting of SNAIL1-PRMT1-PRMT4 dependent methylation of the fibronectin promoter[161],

suggests a potential mechanism for SNAIL1 EDA splicing regulation. We discard that TGFβ/SNAIL1 induced PRMT methylation of the *Fn1* promoter results in SRSF1 recruitment to the transcriptional complex as we detect no binding of SRFS1 in the promoter. In contrast, we cannot discard the DNA methylation dependent recruitment of other splicing factors or the methylation of those already bound to the CTD. Fitting with this possibility, splicing factors SRSF2 and SRSF3, but not SRSF1, present arginine methylation in a SNAIL1-dependent manner, as detected through mass spectrometry (unpublished data).

Alternatively, we can speculate on the possibility that SNAIL1 regulates EDA splicing through PRMTs recruitment to the EDA coding region and arginine methylation of histones or other protein components. This event could be concomitant with SNAIL1/PRMT recruitment in the fibronectin promoter and the regulatory methylation mentioned above. Some studies have linked DNA methylation with alternative exon inclusion, such as the H3K36me3 methylation state of exon 7 of PBX1[130]. Histone methylation regulates splicing either by the modulation of the Pol II elongation rate or acting as a recruitment platform for splicing factors[169]. Even though asymmetric arginine methylation in histones has not been related to any of this roles, we speculate SNAIL1-PRMT induced methylation of EDA coding DNA might reduce the elongation rate, facilitating its inclusion[168].

Further experiments are required to validate these hypotheses. For instance, Chromatin Immunoprecipitation assays for the PRMT1/4 dependent methylation marks (H4R3me2a and H3R17me2a) in control

and SNAIL1 depleted fibroblasts would reveal if these histone modifications are present in the EDA region and if they are TGFβ/SNAIL1 dependent. Similarly, RNA Immunoprecipitation for SRSF1 in MEFs KO for PRMT1 and PRMT4, readily available at our lab, may confirm their role in regulating fibronectin alternative splicing.

As stated in the introduction, aberrant alternative splicing is frequent in cancer, mainly through mutations on splicing regulation elements. Here, we present a different alteration promoting cancer progression where a natural wound healing related alternative splicing is sequestered by a pathological sustained expression of SNAIL1 in CAFs. We consider that a more detailed knowledge of this mechanism will offer new molecular data in splicing regulation and therapeutic targets given that EDA plays a crucial role in preventing metastasis formation, as we will further discuss in the next chapters.

2. FIBRONECTIN EDA ENABLES TUMORAL PROGRESSION

Aberrant expression of fibronectin EDA has been widely reported for advanced stage tumors[98,99]. However, its exact roles in tumor progression and stromal regulation remain poorly defined. Based on the discussed SNAIL1 regulation of EDA inclusion, our group findings regarding SNAIL1 roles and the existing literature on EDA, we hypothesized a role for EDA in inducing a permissive stroma leading to increased tumoral cell invasiveness and fibroblastic activation. To test this notion, we used genetically modified MEFs supplied by Dr. Andres

Muro's lab (ICGEB, Trieste, Italy) to perform *in vivo* experiments using immunodeficient NSG mice.

2.1. Lack of fibronectin EDA in the tumoral stroma exerts a protective effect

Metastatic breast tumors were generated by coinjection of AT-3 tumoral cells and fibroblasts. We used either MEFs EDA- or EDA+ to condition the tumoral stroma. Our approach led to two discoveries regarding EDA effects on tumoral development: a differential primary tumor growth rate and a complete lack of metastasis in the absence of EDA.

Tumors with a fibronectin EDA rich stroma grew up to twice as fast as those without EDA, in line with *in vivo* data showing that fibronectin EDA is expressed in tissues where cells actively proliferate[118]. Few reports actively link EDA to proliferation induction. Use of substrates coated with fibronectin EDA was presented as an inductor of cell cycle[118] and conditioned media from the same EDA+ MEF cell line used for our study was shown to induce embryonic stem cell proliferation[170]. While relevant, both studies rely on data obtained from fibronectin either deposited as an artificial coating or administered in a soluble state rather than incorporated into fibers of the ECM by the cells that produced it. We studied the direct role of fibronectin EDA incorporated into matrices on proliferation by growing tumor cells on 3D-ECMs generated by MEF EDA+ and EDA- and no significant changes in the tumor cell growth were obtained (data not shown). Our observations suggest that neither the polymerized

fibronectin EDA fibers nor the extracellular matrix deposited around them are mechanical inductors of cell proliferation. Instead, this effect arises from soluble factors secreted by fibroblasts in contact with EDA, present both in our orthotopic tumors with MEFs EDA+ and in the supernatants of fibroblasts incubated with soluble EDA[170].

Analysis of the lungs of mice 7 weeks after resection of the primary tumor allowed us to study the formation of metastasis, as the lungs are the preferred target to metastasize in this model. We found a striking absence of metastasis in those mice injected with tumoral cells with EDA- MEFs, revealing a protective phenotype from the stroma lacking fibronectin EDA. A similar protection was described in the same murine model when coinjection of *Snai1* KO MSC with tumoral cells also resulted in the total abrogation of metastasis[65]. However, no differences in tumor growth were detected, showing that increased invasive capabilities are unrelated to tumor growth. Therefore, we expect fibronectin EDA induction of invasion independently of its action on tumor growth.

In the next chapters, we discuss our data related to fibronectin EDA induced changes in the physical properties of the matrix, which support the ability of fibronectin EDA to induce metastasis beyond promoting tumor cell proliferation.

2.2. Architectural role of fibronectin EDA

In order to better understand the underlying mechanisms regulating metastasis by EDA inclusion or exclusion, we took advantage of *in vivo* like 3D-ECM derived from MEFs with genetically modified fibronectin splicing. These 3D-ECMs are a useful model to study the physical properties of the stroma such as architecture and mechanical properties[19,42] and the characteristics of the fibroblasts embedded within. Decellularization and recellularization procedures on synthetized matrices offer a model to study ECM effects on additional cell types in a controlled manner. The fact that presence/absence of fibronectin EDA did not affect overall matrix deposition, as we obtain 3D-ECM from all MEFs lines, allowed us to study the effect of TGFβ in all conditions.

Matrix organization was estimated through the alignment of both fibronectin fibers and the embedded MEFs nuclei, two connected parameters as fiber polymerization and organization is directed by fibroblasts (and nuclei) orientation. In non-activated conditions, the fiber and nuclei alignment were isotropic, independently of the fibronectin isoform expressed. Upon TGFβ treatment, anisotropy was induced in a fibronectin EDA dependent manner. The same failure to support anisotropy was reported in ECMs from MEFs KO for *Snai1*[61]. This similarity suggests that the effect in *Snai1* KO is mediated by the decrease in EDA inclusion we have described in these KO MEFs.

Not only EDA containing fibers are more coordinated in their alignment, but they are also more persistent in the direction, as

revealed by decreased fiber curvature and branchpoints. As fibronectin fibers act as templates to other extracellular fibers, we expected that collagen deposition and properties related to it, such as ECM rigidity, will be dependent of the presence/absence of fibronectin EDA. Indeed, our data showed overall collagen deposition changes visualized by SHG and Masson's trichrome staining and an EDA dependent increase of ECM rigidity, as measured through the substrate Young's modulus.

As mentioned in the introduction, both anisotropy and rigidity have been related to tumor malignance. Rigidity is a particularly relevant risk factor in tissues. For instance, in breast tissue a high mammographic density has been reported to increase the risk of breast cancer up to 6 fold[58]. Previous studies by our group have already described a role for SNAIL1 in matrix stiffness in response to TGFβ. Similar to matrix alignment, our data points that the observed increase of rigidity might be mediated by SNAIL1 regulation of EDA splicing.

2.3. Fibronectin EDA matrices orient cell movement and permit invasion

As mentioned, an aligned ECM has been linked to tumor cell malignancy[41]. In primary breast tumors, fibronectin[61] or collagen[24] fiber alignment in a perpendicular manner to the tumor surface is related to a bad patient prognosis. Our data supports a role for both alignment and fibronectin EDA in inducing tumor cell migration and invasion. These results match those previously obtained for *Snai1* KO

MEFs. In the present work, we have gone deeper and we analyzed both individual and collective cell movements.

For single tumor cell migration, we used breast cancer tumor cells MDA-MB-231, a highly mobile E-cadherin negative cell line. The registered movements clearly tracked the ECM fibers while the percentage of fast moving cells was barely altered by the EDA composition of the matrix. In our cell cultures, the preferred fiber alignment orientation (and therefore of the tumoral cell movement) is essentially random, as no gradients exist. *In vivo*, gradients of extracellular cues condition the orientation of fibroblasts and their alignment in a perpendicular manner to the tumor surface, allowing the tumor cell escape[171]. Therefore, aligned fibronectin EDA tracks can be interpreted as mediators of tumor escaping movements.

Collective migration is likely one of the main modes of migration for tumoral cells during metastasis in many solid tumors[172,173]. This migration model relies on tumoral cells taking the role of leaders, while the others act as followers[29]. These roles have been described to rotate, likely due to the metabolic strain suffered by the leaders[174]. Cell groups migrating through fibronectin EDA containing ECM presented clear leader cells, located in the tip of the group and dragging the rest of the colony, that collectively moved in the specific orientation traced by the fibronectin fibers (as seen through bright field imaging). Comparatively, cell groups migrating through ECM lacking fibronectin EDA presented various cells along the colony borders that start acting as leaders, tugging the colony towards

different directions, likely because the matrix fails to condition a predetermined direction movement. This cell behavior, in turn, led to cell groupings disaggregating towards different directions, an event we barely ever detected in the presence of fibronectin EDA.

Besides cell movement changes, we clearly detected that fibronectin EDA containing matrices are more effectively invaded by single and collectively migrating cells. Among other factors, invasion depends on substrate rigidity and topology. These matrix properties have been related to the induction of hybrid EMT states, linked to increased invasive features[175,176]. Additionally, we cannot discard a direct role for EDA in initiating EMT, as fibronectin EDA produced by tumoral cells is capable to promote some EMT features autocrinely[135]. Therefore, fibronectin EDA containing ECM presents the necessary topological and mechanical conditions combined with the motif-directed cues to generate the ideal conditions for invasion.

Another factor determining efficient invasion through matrices is the tumoral cells capacity to remodel and degrade the ECM through metalloproteinases. In contrast with this idea, we found that fibronectin lacking EDA is more easily degraded by tumoral cells than homomeric fibronectin EDA fibers. However, our results suggest that the degradation resistance of fibronectin EDA leads to the preservation of aligned fibers useful to guide tumor cell movement and support the forces required for cell displacement. Thus, we do not discard that metalloproteinases play a role in the metastatic invasion, as other elements of the ECM besides FN1 may have been targeted.

Indeed, it is likely that in permissive tumoral environments, MMPs can be effective in releasing matrix tethered growth factors and degrading parts of the ECM while preserving the EDA containing fibers guiding tumor cells towards blood or lymphatic vessels.

It is worth noting that matrix degradation experiments were performed using cocultures of matrix producing MEFs with HT-29 M6, not any of the cell lines used to test migration and invasion, due to their characteristic growth in tight, concrete colonies. Cocultures with MCF7, which expand over fibroblasts complicating quantification, show an accumulation of thin fibronectin fibers that disappear in EDA- conditions, in line with higher degradation sensitivity. Further experiments with additional tumor cell lines are being performed by Martín Jimenez, in the context of his master's project, to test the general validity of our observations. Additional experiments to discern whether either MMP-2 or MMP-9 mediate this degradation are also being carried out. Alternatively, it has also been described that some metalloproteinases activation from their inactive state requires tumor cells to directly interact with fibroblasts[177]. Therefore, metalloproteinases role in our oriented migration and invasion experiments on decellularized matrices may be reduced, as we do not model this interaction.

We also detected differences when comparing individual and collective invasion on 3D-ECM synthesized by wild-type and EDA+ MEFs. While single cells invade 3D-ECMs synthesized by TGFβ activated EDA+ MEFs almost twice as much as those synthesized by

wild-type MEFs, collectively moving cells essentially invade identically both matrices. Although this differences might arise from intrinsic differences in the cell lines used (MDA-MB-231 vs EpRas), other factors are likely to be involved.

Individual invasion depends on tumor cells capability to squeeze through the already created paths in the ECM relying on Rho kinases, integrins and actomyosin to induce the necessary deformations on the cytoskeleton[178–180]. The ECM synthesized by TGFβ-treated EDA+ MEFs is not only more aligned than the wild-type MEF synthesized, but also presents a lower curvature and lower amount of branchpoints (Figure 58). These differences translate into EDA generating easy, aggressive pathways for single tumoral cells to invade. Meanwhile, the decreased persistence in the fiber direction and increased obstacles in the way lead to reduced invasion through wild-type MEF synthesized 3D-ECM. On the other hand, collectively invading cells are less likely to be affected by these parameters as they present more points of interaction with the matrix and have an increased capacity to remodel their surroundings as they invade.

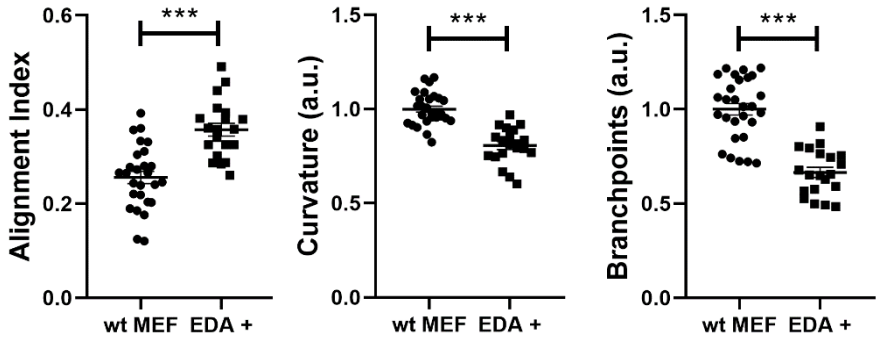

Figure 58: Quantification of fibronectin fiber parameters through TWOMBLI. Images from matrices generated by the indicated MEFs treated with TGFβ were analyzed using the ImageJ macro TWOMBLI and data obtained was plotted showing all individual measurements, mean and SD. Arbitrary units are provided by the plugin and are expressed as relative to wild-type MEFs.

2.4. Fibronectin EDA regulates stromal activation

In vivo like 3D-ECM produced *in vitro* were also used to assess the effect of fibronectin EDA on stromal activation. Mechanical properties such as rigidity are key factors in regulating fibroblast activation into myofibroblast. Focal adhesions (FAs) are large molecular assemblies that transmit mechanical forces and molecular signals from the extracellular matrix towards the interior of the cell[181], but also propagate cell generated forces towards the ECM. In these cellular locations, different integrins interact with a variety of partners in the ECM. Classically, integrin $\alpha5\beta1$ interacts with the RGD sequence of fibronectin and integrin $\alpha4\beta1$ specifically with the EDA domain. Upon interaction, integrins recruit vast protein complexes to the membrane that connect them to the cytoskeleton. Generally, increased FA size has been shown to predict slower migration as it has been related to

an actin increased rate of assembly and/or a decrease on disassembly[182,183]. We studied focal adhesions in fibroblasts expressing fibronectin EDA+ or EDA- isoforms embedded in their own matrices. We found fewer but larger FAs on fibroblasts embedded on ECM lacking EDA suggesting that these fibroblasts move less efficiently. Specifically for fibroblasts, some reports suggest FAs length is strictly modulated by substrate rigidity and they need to reach a minimum length to become able to induce α-SMA incorporation into stress fibers[184]. As we detect widespread α-SMA incorporation into stress fibers in fibroblasts embedded in both matrices, generated by TGFβ-activated MEFs expressing EDA- and EDA+, we conclude that the minimum focal adhesion length is achieved in both cases and the total length better reflects fibroblast mobility than rigidity.

We studied the consequences of stress fiber formation through their effect on nuclei elongation, a classical response to mechanical stress that has been associated to regulation of gene transcription through YAP and TAZ[185], a transduction signal turned on in activated fibroblasts[186]. We report that α-SMA containing stress fibers in TGFβ treated MEFs EDA- embedded in their own ECM, do not translate into nuclei remodeling, likely indicating lower forces being transmitted due to the decreased matrix rigidity. Overall, the changes in FAs, α-SMA fibers, nucleus shape and orientation of fibroblasts EDA+ embedded into their 3D-ECMs show the fibronectin EDA imposes structural and mechanical changes that are mechanosensed and act as a positive feedback signal fully activating fibroblasts.

To confirm the role of the ECM including fibronectin EDA on fibroblast activation, we set up a more direct experimental approach. We estimated the potential of matrix to induce fibroblast activation by seeding naïve fibroblasts on decellularized matrices and measured activation as the percentage of fibroblasts incorporating α-SMA into stress fibers. We detected a clear EDA dependent fibroblast activation over the basal levels in two different fibroblastic cell lines. Therefore, our data confirms that fibronectin EDA in the context of a cell-synthesized ECM induces fibroblast activation. Interestingly, fibroblast activation was also observed in non-aligned matrices with fibronectin EDA generated in the absence of TGFβ, differentiating this effect from that over cell migration. Thus, fibrillary fibronectin EDA is effective in activating fibroblasts independently of its organization, an observation that fits with the reported data using recombinant fragments or full fibronectin in a non-fibrillar state. Fitting with this EDA requirement, matrices generated by EDA- MEFs failed to induce fibroblast activation over the basal levels even if generated in the presence of TGFβ.

Remarkably, matrices produced by wt MEFs including both isoforms activate fibroblasts only when produced in the presence of TGFβ. We have shown that untreated wild-type MEFs in culture present close to 50% inclusion of EDA and still, matrices generated by these MEFs activate fibroblasts at the same basal levels as matrices generated by EDA- MEFs. We predict that EDA present in non-aligned heteromeric fibers (including both isoforms) is masked while alignment of these fibers induces conformational changes that increase EDA availability. Thus, in non-modified fibroblasts, such as those naturally present in

the tumor microenvironment, TGFβ/SNAIL1 promotes EDA inclusion, leading to increased fibronectin fiber alignment, increasing EDA availability to naïve fibroblasts. In accordance with these results, we have shown that *Snai1* KO MEFs produce reduced amounts of fibronectin EDA isoforms, fail to align matrices even in the presence of TGFβ and fail to activate fibroblasts.

As proposed, our data supports that fibronectin EDA cooperates with TGFβ in activating fibroblasts through a positive feedback loop. Using the 3D-ECM model, we show that transient TGFβ treatment (2 days+4 days without treatment) in a homomeric EDA including fiber context leads to a complete activation (maximum organization comparable to that of a continual TGFβ administration). In contrast, in a heteromeric context, the response to transient TGFβ administration is weaker. It is expected that a two-day pulse of TGFβ is not enough to induce the conformational changes necessary to expose the masked EDA that support alignment, rigidity and fibroblast activation. Moreover, EDA availability was found to be crucial for the storage of cell secreted latent TGFβ into the matrix also involved in the feedback loop[90].

In an effort to characterize how wide the effects for fibronectin EDA are on stromal activation, we tested for a potential role in macrophage activation taking advantage of a model already set up in our group. Although no role was detected specifically for fibronectin EDA, we did find SNAIL1 dependent ECM remodeling regulates macrophage activity. While roles for SNAIL1 in regulating macrophage activity and polarization have been described, these have always been related to

SNAIL1 expression in cancer or immune cells regulating inflammatory cytokine and chemokine expression[187]. To our knowledge, this constitutes the first report for SNAIL1 regulation of the ECM altering macrophage activity.

Overall, we have shown a very relevant role for EDA in tumoral progression, where the lack of this domain exerts a protective function *in vivo*. Additionally, mimicking *in vivo* conditions, we have deepened the knowledge of specific tumoral processes influenced by fibronectin EDA, offering potential new targets of study for therapies aiming to disrupt EDA signaling.

3. FIBRONECTIN EDA INHIBITORS POTENTIAL

3.1. Antisense oligonucleotides deserve further attention

Use of antisense oligonucleotides (AONs) to regulate alternative splicing for disease treatment is still in its early days. Drugs based on this approach have been approved to treat very few diseases such as spinal muscular atrophy, neuronal ceroid lipofuscinosis 7 and Duchenne muscular dystrophy[188]. Their use for cancer therapy is still under investigation, with no drug approved yet. However, some reports indicate their effectiveness in regulating an array of targets *in vitro*[89]. We reasoned that the existing data regarding EDA inclusion regulation, strongly dependent on the capacity to bind the ESE of splicing factors such as the SRSF1, made this particular splicing event a good potential target for an antisense oligonucleotide approach.

Our results confirmed that the use of these AONs to target both the ESE and the ESS partially reduced EDA inclusion. The reduction in EDA inclusion obtained upon ESS targeting is consistent with the previously mentioned role as an indirect ESE for the murine sequence homologous to the human ESS[104]. Although we failed to demonstrate long term effects in our test on 3D-ECM organization and shifted the focus of our research towards alternative approaches, further experimental setups might show a pharmacological potential for these AONs against permissive stroma. For instance, as our approach consisted in only an initial dose of AONs, increasing the number of administrations during the experiment, although technically challenging, might offer encouraging results. Otherwise, since our mouse model detects a drastic effect on lung metastasis by eliminating EDA from the primary tumor stroma, it could be useful to set up a treatment regimen for this *in vivo* model.

3.2. Irigenin and CLI-095, two promising alternatives

During the development of this project, we have tested the effects of two different molecules with the capacity to block EDA signaling on fibroblast activation: CLI-095 and Irigenin.

CLI-095 unspecifically blocks the TLR4 pathway by binding to its intracellular domain. Other groups have already tested CLI-095 to block EDA signaling, as it has been shown to be capable of activating TLR4. However, the published works use this inhibitor against EDA in healthy or fibrotic contexts but not cancer[189–192].

Irigenin is a fairly novel drug, as no reports concerning its potential therapeutical capabilities exist before the year 2000. Since then, an array of studies has been published reporting on its antioxidative capabilities and, importantly, proposing its capability to interact with the C-C loop formed by EDA, disrupting its folding[135].

3.2.1. Irigenin, the best candidate to suppress a fibronectin EDA induced permissive stroma

Using the 3D-ECM model, we detected small effects blocking ECM alignment for both inhibitors but a higher effect blocking fibroblast activation by matrices. This difference can be due to the fact that whereas naïve fibroblasts are challenged to be activated by the 3D-ECM without addition of exogenous TGFβ, the alignment experiment requires TGFβ inclusion as an inductor. Therefore, in the alignment studies, the inhibitors could not compete with the exogenous TGFβ signaling on the fibroblasts.

Considering the activation of fibroblasts on decellularized matrices, we found that Irigenin completely inhibited fibroblastic activation dependent of fibronectin EDA. In contrast, the effect of CLI-095, while reproducible, was not so clear. Additionally, administration of both inhibitors did not have additive or synergistic affects. This can be explained by the fact that Irigenin directly interacts with EDA, disrupting its folding and preventing its recognition both by integrins and by TLR4, the pathway inhibited by CLI-095.

Our data on CLI-095 and Irigenin capacity to prevent fibroblast activation validates previously published experimental approaches. Bhattacharyya S. et al. induced activation of fibroblasts by incubation with full length soluble fibronectin EDA which was inhibited with CLI-095[189]. For Irigenin, Kwon A. et al. activated CAFs with both conditioned medium and recombinant fragments of the EDA and its flanking exons and abrogated this inhibition with Irigenin[193].

To test the blocking effect of Irigenin in a more physiological landscape, we decided to test Irigenin *in vivo* using a metastatic cancer model. Experimental conditions for the Irigenin administration were decided based on data from Kwon A. et al. In our approach, tumor cells were coinjected with MSCs instead of MEFs as they are not transformed cells, avoiding the introduction of an uncontrollable growth variable. Interestingly, Irigenin administration after tumoral induction resulted in a significant reduction of the tumor stromal component. As previously commented, a higher percentage of stroma has been correlated with worse prognosis for patients of a variety of tumor types. Therefore, Irigenin might be playing a protective role by affecting fibroblast activity.

3.2.2. Irigenin has the potential to prevent tumor malignancy

Our data showing interference of Irigenin with migration and invasion supports a possible anti-metastatic action of the drug. For oriented single-cell migration measurements, two different Irigenin treatments were tested. In one, the treatment aim was to interfere with the 3D-ECM properties by adding the drug while TGFβ-activated EDA+ MEFs

were synthesizing it. In the other, its objective was to directly interfere with the migration by adding the drug simultaneously with the tumoral cells on the decellularized matrices. Strikingly, only Irigenin treatment during ECM deposition led to a reduced oriented migration comparable to basal migration on wild-type MEF derived ECM. The absence of effect upon direct treatment of the tumoral cells on decellularized 3D-ECM strongly suggests the reduction in oriented migration depends on some property of the ECM and not on the tumor cells capacity to sense EDA. The detected reduction in oriented migration in Irigenin treated ECM is larger than the Irigenin dependent reduction of ECM alignment (25 vs 15%) which, a priori, was expected to be the matrix property guiding migration. Besides the already discussed decrease in alignment, TWOMBLI analyses of ECM produced by EDA+ MEFs with and without Irigenin revealed increased lacunarity. An increase in this parameter, associated to the size of the gaps without fibers, might justify the loss of oriented movement, as tumor cells move more freely around the ECM, without the guidance of the fibronectin fibers. Additional studies to assess this and other parameters such as matrix stiffness upon Irigenin treatment might offer a more complete perspective into fibronectin EDA induction of oriented migration.

Invasion experiments were performed administering Irigenin during ECM production, as this worked best in disrupting oriented migration. Irigenin achieved a 60% reduction of invasion of MDA-MB-231 cells through EDA+ MEF synthesized ECM. Irigenin has been used to inhibit tumoral cell sensing the fibronectin EDA generated by themselves[135].

In this context, a reduction in EMT markers was detected upon Irigenin administration. While we have made attempts in studying such a reduction using the collectively migrating EpRas cells through IF of E-cadherin, N-cadherin and Epcam, no relevant results have been obtained yet.

We attempted to study the consequences of this prometastatic fibronectin EDA role by evaluating Irigenin effect over metastasis formation in the *in vivo* model. However, an uncontrollable complication of the experimental setup was the regrowth of primary tumors after the resection. Typically, upon such occurrence, animals have to be discarded from the experiment, as the regrowth tumors do not receive treatment and present a much higher metastasis count than those without such regrowth. Unfortunately, even after improving the resection protocol, this complication was highly prevalent for animals in these experiments (both Control and treated with Irigenin) and clear conclusions could not be reached.

Kwon A. et al. coinjected cancer cells with MEFs mutated for their gene of interest and found a reduction in tumor volume upon Irigenin treatment, an occurrence we did not detect. Besides the differences in the used fibroblastic cell line, their experimental design does not include the condition where tumors generated from coinjection with wild-type fibroblasts are treated with Irigenin, so our results are not directly comparable. Despite this limitation, their additional results show an Irigenin dependent reduction of the appearance of lung

metastasis, a piece of data we could not obtain, suggesting that, indeed, Irigenin has the potential to prevent tumor malignancy.

Overall, the results obtained using Irigenin as a specific EDA blocking agent indicate that it can be used to generate a restrictive stroma by attenuating fibroblast activation and altering ECM architecture and to disfavor tumor progression by disrupting tumoral cell migration and invasion. Therefore, our results encourage further testing for Irigenin to be used as a tumoral treatment *in vivo.*

4. PROPOSED MODEL FOR FIBRONECTIN EDA EFFECTS OVER TUMORAL PROGRESSION

Our work presented here describes roles for a TGFβ/SNAIL1 regulated inclusion of EDA in fibronectin in a tumoral context. A simplified model of fibronectin EDA effect in tumor progression through fibroblast activation and induction of a permissive stroma leading to tumoral cell migration is presented in figure 59. Our pharmacological treatment approach suggests these effects could be reverted and a restrictive stroma could be forced.

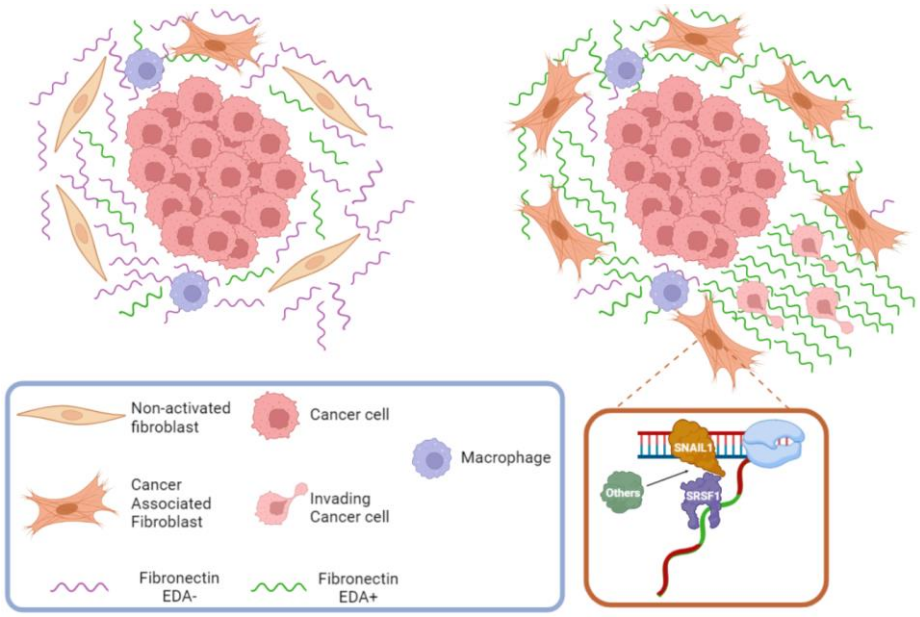

Figure 59: Simplified model of the effect of fibronectin EDA in the tumor microenvironment. Fibroblasts synthesize an ECM containing isoforms of fibronectin including and excluding the EDA. During initial tumor stages the ECM, richer in fibronectin without EDA, is organized and contains the tumoral cells. Upon activation of the fibroblasts into myofibroblasts through TGFβ signals coming from the tumoral cells, SNAIL1 expression rises, leading to increased EDA inclusion rate. Increased fibronectin EDA generates more permissive stroma with a stiffer, more aligned ECM, leading to increased fibroblast activation in a self-sustained loop and to increased cancer cell invasion and metastasis. Image created in BioRender.

CONCLUSIONS

1. SNAIL1 induces the alternative inclusion of the EDA coding exon 33 into the fibronectin mRNA in fibroblasts and colon cancer cells.
2. High SNAIL1 protein expression correlates with high EDA inclusion into the fibronectin mRNA in a breast cancer PDX cohort and in patient samples from advanced stages of breast cancer.
3. Elevated SNAIL1 protein expression correlates with high EDA inclusion into the fibronectin mRNA in 4 other solid tumor types in advanced stages.
4. SNAIL1 recovers as an RNA-binding protein through OOPS.
5. SNAIL1 and SRSF1 coimmunoprecipitate in an RNA dependent manner.
6. SNAIL1 and SRSF1 bind the EDA coding DNA region in a TGFβ dependent manner and SRSF1 binds the EDA coding mRNA in a SNAIL1 dependent manner.
7. Fibronectin EDA sustains TGFβ induced ECM anisotropy and stiffness.
8. Fibronectin EDA presence in the ECM activates naïve fibroblasts. The inhibitors CLI-095 and Irigenin can block this response.

9. Fibronectin EDA presence in the ECM induces single and collective tumor cell invasion. Irigenin can inhibit single tumor cell invasion.
10. Irigenin reduces the stromal compartment in primary orthotopic breast tumors.
11. Fibronectin EDA absence in the stroma of primary breast tumors reduces tumor growth and blocks the appearance of lung metastasis.

MATERIALS AND METHODS

1. CELL CULTURE

1.1. Stable cell lines

Cells were grown and maintained in Dulbecco's modified Eagle's medium (DMEM) (Invitrogen) high glucose supplemented with 10% FBS (Gibco), 2mM glutamine, 4,5g/L of Sodium Pyruvate, 56U/L penicillin, 56U/L streptomycin and non-essential amino acids. Cell cultures were maintained at 37°C in a humid atmosphere containing 5% CO_2.

MDA-MB-231, MCF7, HT-29 M6 and NIH-3T3 cells were acquired from the repository stock of our center. Mouse embryonic fibroblasts control and *Snai1* KO (MEFs), mouse Mesenchymal stem cells and HT-29 M6 overexpressing SNAIL1 were previously established in our laboratory[58,127].

Mouse embryonic fibroblasts wild-type, EDA- and EDA+ were kindly provided by Dr. Andrés Muro lab, International Centre for Genetic Engineering and Biotechnology (Trieste, Italy). BJ human fibroblasts were kindly gifted by Dr. Cristina Peña lab, Hospital Universitario Puerta de Hierro (Madrid, Spain). EpRas tumor cell line was provided by Dr. Antoni Celià lab, Institut Hospital del Mar d'Investigacions Mèdiques (Barcelona, Spain). They were originally generated by Dr. Robert Weinberg lab, Whitehead Institute for Biomedical Research (Cambridge, USA). AT-3 tumor cell line was kindly gifted by Dr. José Yélamos lab, Institut Hospital del Mar d'Investigacions Mèdiques (Barcelona, Spain).

1.2. Cell treatments

Cells were treated with different specific reagents, which are listed in Table 1.

Treatment	Supplier	Concentration
TGFβ	Peprotech	5ng/mL
Irigenin	Tebu Bio	50μM
CLI-095	InvivoGen	5μM
GM6001	Millipore	25μM
CellTracker Green CMFDA	Thermo Fisher	1μM

Table 1: Cell culture treatments

1.3. Cell transfection

For transient transfection with siRNA or AONs, MEFs were grown to 60–80% confluence. Cells were transfected in DMEM without antibiotics using the DharmaFECT transfection agent. For siRNA, transfected cells were kept in medium without antibiotics for 24 hours and then complete medium for extra 24 hours before testing gene expression by RT-qPCR or 48 for protein analysis by WB. Transfected siRNAs are specified in Table 2.

siRNA	Supplier
siCtrl	D-001810-02-50, Dharmacon
siSnai1	L-010847-01-0005, Dharmacon
siKhsrp	L-054914-00-0005, Dharmacon

Table 2: Transfected siRNA

Antisense Oligonucleotide (AON) where designed using 2' O-Methyl RNA bases and phosphorothioate bonds. The same transfection protocol was applied. Cells were kept in complete media for 48 hours before using them to produce 3D-ECM. The different AONs used are indicated in Table3.

1.4. Cell infection

Retrovirus containing a pBABE empty and pBABE *Snai1*-HA plasmid were used to induce stable expression of SNAIL1-HA in MEF cells. MEF were grown up to 50% confluence and virus were added dropwise to complete medium. Culture medium was renewed 24 hours after infection and puromycin 1mg/mL was added to select infected cells.

AON	Sequence	Supplier
AON #1, Scramble	5'- AGUGCGCCGUACCGCCUUGGC	IDT
AON #2, EDA ESE	5'- UGCAGUGUCGUCUUCACCAUC	IDT
AON #3, EDA ESS	5'- GCCUGAGGCCCUGCAGCUCUG	IDT
AON #4, 5'SS	5'- AUGUCUGUUAGGCAAAUUAAU	IDT
AON #5, 3'SS	5'- UGCGGUUAACGAUAUACCUGU	IDT

Table 3: Transfected AONs

2. *IN VITRO* EXPERIMENTS

2.1. Three-dimensional extracellular matrices

Three-dimensional ECMs were generated following a previously-described protocol[194]. For 24 wells plates, 1-3x10^5 fibroblasts were seeded on gelatin cross-linked glass coverslips and for invasion experiments, 10^5 fibroblasts were seeded in gelatin cross-linked invasion inserts, using 100µl of medium to prevent media leaking through the insert pores. After 24 hours, cell culture media was supplemented with 50µg/ml ascorbic acid and, where indicated,

5ng/ml TGFβ. To foster ECM deposition by the plated cells, media was replaced every two days for six days. In TGFβ pulse experiments, TGFβ was maintained in the cell culture media the first 2 days. Cultures were eventually washed with pre-warmed (37ºC) phosphate buffered saline (PBS) and either fixed with 4% Paraformaldehyde (PFA) and treated with NH_4Cl 50mM to quench PFA fluorescence for immunofluorescence analysis, or decellularized with 20mM NH_4OH and 0.5% Triton X-100 in PBS for later use as a cell culture substrate.

2.2. Fibroblast activation

For fibroblast activation experiments, approximately 40.000 MSC or NIH-3T3 were seeded on decellularized matrices blocked with heat-denatured 2% BSA. Samples were fixed with 4% PFA and NH_4Cl 50mM after an overnight (~16hours) to perform immunofluorescence. In experiments where inhibitors were used, they were added at the same time as the fibroblasts.

2.3. Macrophage activity

To obtain bone marrow-derived macrophages (BMDM), male C57Bl/6J 8-12-week-old mice were sacrificed, and the femoral and tibial bone marrow were flushed with a 25G syringe with complete medium. Cells were then filtered through a 100µm mesh and seeded in 5 100mm polystyrene dishes with complete medium supplemented with 25% (vol/vol) L929-conditioned medium (as a supply of Macrophage colony stimulating factor) and incubated for 7 days at 37ºC in 5% CO_2

atmosphere[195]. At this time more than 94% of cells were macrophages as assessed by F4/80 staining.

Approximately 40.000 BMDM were seeded on decellularized matrices blocked with heat-denatured 2% BSA. 40.000 MCF7 tumor cells were additionally seeded after 24 hours. As a control, equivalent amount of tumor cells was seeded directly on decellularized matrices. After 48 hours of coculture, samples were fixed with 4% PFA and NH_4Cl 50mM to perform immunofluorescence.

2.4. Migration assays

Tumor cells were labeled with a fluorescent marker previous to the assay. For that purpose, they were seeded on a 10cm round plate, allowed to reach 80% confluence, treated with 1μM Cell Tracker in DMEM medium 0% FBS for one hour, allowed to recover in DMEM 10% FBS for half an hour and trypsinized. Then, 10^4 cells were seeded on decellularized matrices blocked with heat-denatured 2% BSA. After at least 24 hours, a fluorescence microscope Zeiss Cell Observer HS was used to take representative images every 15 minutes for ~16 hours.

2.5. Invasion assays

Approximately $5x10^5$ cells were seeded on decellularized matrices produced in invasion inserts on 100μL DMEM medium 0,1% FBS. 500μL DMEM medium 10% FBS was placed in the lower chamber as a chemoattractant. MDA-MB-231 cells were allowed to invade the ECM

for 24 hours and EpRas were allowed to invade for 48 hours. After the invasion period, samples were fixed with 4% PFA. Non-invading cells were removed from the insert upper side with a cotton swab. Invasion insert membranes were removed and mounted on glass slides with DAPI Fluoromount G (SouthernBiotech). Invading cells were imaged and quantified with Image J.

3. CELLULAR AND MOLECULAR PROCEDURES

3.1. RNA extraction, reverse transcription and PCR

Cells were washed twice with cold PBS and then lysed in TRIzol reagent (Invitrogen). Lysates were mixed with 200μL chloroform, vortexed and incubated for 2 minutes. Then, samples were centrifuged at 12000g for 20 minutes at 4˚C. The aqueous phase of the samples was transferred to a new Eppendorf tube, mixed with 400μL isopropanol and incubated for 20 minutes at Room Temperature (RT) to precipitate RNA. Then, tubes were centrifuged at 12000g for 20 minutes at 4˚C. Supernatant was discarded and the pellet was washed with 70% ethanol and centrifuged at 12000g for 15 minutes at 4˚C. Ethanol was completely removed and the RNA pellet was resuspended in 20-50 μL water. Extraction results were quantified using a NanoDrop.

Reverse transcription was performed on 1-2mg RNA using the Transcription First Strand cDNA Synthesis Kit (Roche) following manufacturer's protocol.

PCR was performed using BioTaq DNA polymerase (Bioline) with specific oligonucleotides (Table 4) and 100ng cDNA. For semiquantitative PCR, PCR cycles were optimized from 20 to 30 to better visualize differences between samples. PCR products were separated by 2% agarose DNA electrophoresis and visualized using SYBR Safe DNA gel stain (Invitrogen).

Oligonucleotide	Sequence
***Fn1* exon 32**	CCCTGGTTCAAACTGCAGTG
***Fn1* exon 34**	GGTTGATTTCTTTCATTGGTCCTG

Table 4: Oligonucleotides used for PCR

For quantitative studies, qPCR was performed using the SYBR Green LightCycler 480 Real Time System (Roche). 5-20ng cDNA were amplified using specific oligonucleotides (Table 5).

Oligonucleotide	Sequence
Human *FN1* exon 33 Fw	TGCACGATGATATGGAGAGC
Human *FN1* exon 34 Rv	TGGGTGTGACCTGAGTGAAC
Human *FN1* exon 1 Fw	GGGAGCCTCGAAGAGCAAG
Human *FN1* exon 2 Rv	CGCTCCCACTGTTGATTTATCTG
Human and Mouse HPRT Fw	GGCCAGACTTTGTTGGATTTG
Human and Mouse HPRT Rv	TGCGCTCATCTTAGGCTTTGT
Mouse KHSRP Fw	GACTCAGGCTGCAAAGTTCA
Mouse KHSRP Rv	GTGCTCCAGTCAGAGACACG
Mouse *Fn1* exon 32 Fw	CCCTGGTTCAAACTGCAGTG
Mouse *Fn1* exon 33 Rv	TGTGGGCTTTCCCAAGCAAT
Mouse *Fn1* Promoter Fw	CTGCTCTTGGGGCTCAACC
Mouse *Fn1* Promoter Rv	AAGGAGATGGAAGGAGAGGACC
Mouse *Fn1* exon 7 Fw	GCTCCTTCACTGATGTCCGAA
Mouse *Fn1* exon 7 Rv	CTTCAGCCACTGCATTCCCA
Mouse *Fn1* exon 33 Fw	TTCCAATCAGGGGCTGGCTCTC
Mouse *Fn1* exon 33 Rv	TCGAGCCCTGAGGATGGAATCC

Mouse *Fn1* intron 32 Rv	GCAGAACTGCTTTGCATGGTA

Table 5: Oligonucleotides used for qPCR

3.2. Western Blot

Cells were washed twice with cold PBS and then lysed with lysis buffer (2% SDS, 50mM TRIS pH 7.5, 10% glycine). Lysates were boiled for 10 minutes and centrifuged 10 minutes at top speed to eliminate insoluble debris. Protein concentration was quantified by DC Protein Assay (Bio-Rad).

For extraction of proteins from tumor pieces, such as PDX samples, a volume of lysis buffer proportional to the piece weight was added and an 18G syringe was used to break the tissue. Then, the samples were boiled at 95˚C for 10 minutes. Afterwards, the samples were sonicated (Branson DIGITAL Sonifier UNIT Model S-450D) for two rounds of 15 seconds at a potency of 15%, with 30 seconds of resting between each round. The samples were kept on ice during all the process. Finally, we centrifuged the samples 5 minutes at maximum speed and collected and quantified the supernatant.

1 to 20μg protein were mixed with loading buffer (50mM TRIS pH6.8, 2% SDS, 10% glycerol, 0.1% bromophenol blue), boiled and loaded into an SDS-polyacrylamide gel. Samples were run in TGS buffer at 120V and transferred into a nitrocellulose membrane at 400mA for 90 minutes. Once proteins were transferred, membrane was blocked with TBS-Tween 20 (Tris-buffered saline) 1% BSA and incubated overnight with the primary antibody diluted in TBST 0.1% BSA (Table 6). After three washes with TBST membranes were incubated with Horseradish peroxidase (HRP)-conjugated secondary antibody 1h at room

temperature and washed again with TBS-Tween. The detection was carried out using Immobilon western HRP substrate (Millipore) and captured using the Alliance Q9 Advanced (Uvitec) chemiluminescence imager.

Protein	Host	Application	Dilution	Reference
E-CADHERIN	Mouse	IF	1:100	610182, BD Transduction Labs
EDA+FN1	Mouse	WB	1:500	ab6328, Abcam
EDA+FN1	Mouse	WB / IF	1:500 / 1:100	F6140, Sigma
F4/80	Rat	IF	1:100	14-4801-81, ThermoFisher
FN1	Rabbit	WB / IF	1:2000 / 1:1000	A0245, Dako
KHSRP	Rabbit	WB / IF	1:1000 / 1:100	ab140648, Abcam
LAMIN B	Rabbit	WB	1:2000	ab16048, Abcam
PAXILLIN	Mouse	IF	1:100	P13520, Transduction Labs
PYRUVATE KINASE	Goat	WB	1:2000	AB1235, Chemicon

SNAIL1	Rabbit	WB	1:1000	3879, Cell Signaling
SNAIL1	Mouse	IF	1:2	Hybridoma[156]
SRSF1	Mouse	WB / IF	1:1000 / 1:100	32-4500, ThermoFisher
α-SMA	Mouse	IF	1:100	A2547, Sigma
β-ACTIN	Mouse	WB	1:10000	A5441, Sigma
α-TUBULIN	Mouse	WB	1:10000	T9026, Sigma

Table 6: Antibodies used for Immunofluorescence and Western Blot

3.3. Immunofluorescence analysis

Cells were grown for at least 48 hours on ethanol-sterilized glass coverslips following a standard IF protocol. All steps were carried out at room temperature. Cells were fixed with 4% PFA for 10 minutes. PFA autofluorescence was quenched by incubating with 50 mM NH_4Cl in PBS for 5 minutes. Blocking and permeabilization were carried out at the same time with a solution of 1% BSA and 0,3% Triton X-100 for 1 hour. Coverslips were incubated overnight with specific primary antibodies (Table 6) in blocking + permeabilization solution, and then for 1 hour with the corresponding secondary antibody. In samples where phalloidin was used, it was added to the secondary antibody solution. Secondary antibodies and phalloidin were complexed with

Alexa fluorochromes. Nuclei were stained with DAPI for 10 minutes and coverslips were mounted with Fluoromount G (SouthernBiotech).

For 3D-ECM produced *in vitro*, the same protocol was followed. For nuclei alignment, measurements of the angle of the ellipse fitting with each nucleus were determined with ImageJ on DAPI images. Length, width and area of the ellipses were used for nucleus morphological analyses. Nucleus aspect ratio (AR) is defined as the ratio between nuclear length and width. Fibronectin fiber alignment was quantified on fibronectin immunofluorescent images using two ImageJ extensions. OrientationJ distribution tool of the OrientationJ plugin[196] was used setting both Min. Coherency and Min. Energy at 10%. TWOMBLI plugin[132] allowed quantifying other morphological patterns of the ECM, including the alignment. Optimal parameters to analyze our images were obtained by testing a small sample (Contrast Saturation: 0.35, Min Line Width: 10, Max Line Width: 10, Min Curvature Window: 50, Max Curvature Window: 50, Minimum Branch Length: 10, Maximum Display HDM:225, Minimum Gap Diameter: 0).

3.4. Collagen imaging

Fixed cellularized 3D-ECM produced *in vitro* were stained with Trichrome III blue staining kit (Roche) by the technicians of the pathological anatomy department of the Hospital del Mar.

Alternatively, fixed cellularized 3D-ECM produced *in vitro* were used to obtain second harmonic generation (SHG) images. The second harmonic was detected with an inverted multiphoton laser scanning

microscope (Leica TCS SP5) equipped with a pulsed (80 Mhz) and tunable Mai Tai Ti:Sapphire laser (Spectra Physics) set at 880nm. To collect the SHG signal from collagen, a 0.55 NA condenser with a BP 436/7 filter set above it was used.

3.5. Measurement of the micromechanical properties by Atomic Force Microscopy

Micromechanics of decellularized matrices were measured using a custom-built Atomic Force Microscope mounted on an inverted optical microscope (TE2000, Nikon). All the experiments were performed in PBS buffer with a pH of 7.4 at 37 ºC. Measurements were performed by doing force-displacement curves on the surface of the sample with V-shaped silicon nitride cantilevers (0.012N/m of nominal spring constant) ended with a 2.5µm radius spherical glass bead (Novascan Technologies). The vertical position of the cantilever was controlled by a piezoelectric actuator and measured with strain gauge sensors (Physik Instrumente), and a four-quadrant photodiode (S4349, Hamamatsu) was employed to measure the deflection of the cantilever. Elastic modulus was calculated from the force-displacement curves by adjusting the Hertz model for sphere-plane contact as described in Otero J. et al.[197] and computed at 0.5µm of surface indentation. Samples were probed in five randomly selected zones, and in each zone five different points were probed (separated at least 10µm between them) for a total of twenty-five force-curve measurements in each sample.

3.6. Immunohistochemistry

Harvested tissue samples were fixed in 4% PFA and embedded in paraffin. Sections of 4μm were obtained with a microtome and then subsequently dewaxed and rehydrated. Antigens were retrieved by boiling the samples in Tris/EDTA (50mM Tris/HCl, 1mM EDTA, and 10mM NaCl, pH 9.0) for 15 minutes. Endogenous peroxidase activity was quenched for 15 minutes with 3% hydrogen peroxide in PBS containing 1% sodium azide. After several rinses with PBS, sections were incubated with PBS containing 1% BSA and 0.3% Triton X-100 to block non-specific binding and then washed with PBS. Sections were incubated with the indicated antibodies overnight at 4°C. After several rinses with PBS, bound antibody was detected using anti-mouse or anti-rabbit Envision. Sections were counterstained with hematoxylin and mounted for microscopy analysis.

3.7. Immunoprecipitation Assay

Cells grown at approximately 80% confluence were washed twice with cold PBS and then lysed with RIPA buffer (1% NP-40, 0.5% Sodium deoxycholate, 0.1% SDS in PBS). Protein concentration was quantified by DC Protein Assay (Bio-Rad). 500μg of protein was diluted in a total volume of 500μL and either 1μL of primary antibody or the corresponding volume of Irrelevant IgG was added. After incubating the mix overnight at 4°C, 20μL of Gammabind G Sepharose (GE Healthcare) beads were added to each sample and incubated for 2 hours at 4°C. Samples were centrifuged at 380g at 4°C. Supernatants were discarded or saved as an Unbound fraction to assess

Immunoprecipitation efficiency. Beads were washed with PBS 0.1% NP-40 and centrifuged three times. Finally, 20μL of Loading Buffer were added to the beads, boiled and samples were loaded on SDS-polyacrylamide gels for protein electrophoresis and western blot analysis.

3.8. Chromatin Immunoprecipitation

Cells were seeded on culture dishes and allowed to grow in regular culture medium up to 80% confluence and, when indicated, treated with 5ng/mL TGFβ for 3 hours. Samples were cross-linked for 10 minutes at 37°C with 1% formaldehyde in DMEM. To stop the reaction, cells were incubated for 5 more minutes with glycine added at final concentration of 0.125M. Cells were washed twice with cold PBS and scrapped off with cold PBS containing Protease Inhibitors. Samples were centrifuged at 800g for 5 minutes at 4˚C and supernatants were removed. Cell pellets were resuspended in soft lysis buffer (20mM Tris pH 8.1, 85mM KCl, 0.5% NP-40, 5mM PIPES) at a rate of 500μL per 10^7 cells. Lysates were incubated 15 minutes on ice and then centrifuged for 5 minutes at 800g in 4˚C and the supernatants were discarded. Pellets were resuspended in nuclear lysis buffer (1% SDS, 10mM EDTA, 50mM Tris pH 8.1) and sonicated 15 rounds of 10 seconds (separated by 30 cooling seconds on ice) using 10% of the sonifier amplitude (Branson DIGITAL Sonifier UNIT Model S-450D) in order to generate DNA fragments ranging from 200 to 500 base pairs in length. Optionally, the length of the fragments was confirmed in a small volume of the sample by 2% agarose DNA electrophoresis. Samples

were centrifuged at 12000g for 10 minutes at 4˚C and supernatant was recovered.

As starting material for next steps of the procedure, a supernatant volume corresponding to $2x10^6$ cells was diluted 1:10 in dilution buffer (0.01% SDS, 1% Triton X-100, 16.7mM Tris pH 8.1, 1.2mM EDTA, 167mM NaCl). In order to reduce background, samples were incubated in constant rotation for 1 hour at 4°C with IgGs of the same species as the primary antibody that is going to be used and 30μL Gammabind G Sepharose beads. Beads were typically separated of the samples by 3 minute 350g centrifugation at 4°C.

10% of the beads free lysate was kept apart for the input and the remaining volume was cut in half and incubated overnight at 4°C with agitation with either 5-10μL of the specific antibody or the equivalent amount of IgG of the same species. In parallel, 30μL of beads for each sample was blocked overnight with BSA 0,5% in TBS. The next day, beads were washed with dilution buffer and added to samples, which were further incubated 4 hours at 4°C with rotation. Afterwards, three washes were performed on ice with each of the given buffers: low salt buffer (0.1% SDS, 1% Triton X-100, 2mM EDTA, 20mM Tris pH 8.1, and 150mM NaCl), high salt buffer (the same as low salt but 500mM NaCl) and LiCl Buffer (250mM LiCl, 1% Nonidet P-40, 1% Sodium deoxycholate, 1mM EDTA, and 10mM Tris pH 8.0). For each wash, samples were centrifuged at 350g for 3 minutes at 4˚C.

Recovered beads were incubated with 800rpm shacking in 100μL elution buffer (100mM Na2CO3, 1% SDS) at 37°C for 1 hour, separated

by centrifugation and discarded. NaCl was added to elutes and inputs at a final concentration of 200mM. Immunoprecipitates and inputs were then decrosslinked by incubation at 65°C overnight with 800 rpm shacking followed by digestion with proteinase K for 1 hour at 55˚C with shacking 800 rpm. DNA for quantitative PCR analysis was purified using the MinElute PCR Purification Kit (Qiagen).

3.9. RNA Immunoprecipitation

Cells on cell culture dishes were grown until 80% confluence, washed with warm PBS, trypsinized and recovered by centrifugation. Cells were then resuspended in 300μL lysis buffer (100mM KCl, 5mM MgCl2, 10mM Hepes pH 7, 0.5% NP-40, 1mM DTT, 1x RNase Inhibitor, 1x Protease Inhibitor) for each 15cm diameter plate, incubated 5 minutes on ice and snap-frozen in liquid nitrogen.

Thawed samples were sonicated in a Bioruptor Pico Sonicator (Diagenode) for 15 cycles of 30 seconds ON/OFF at 4˚C. Samples were centrifuged at 16000g during 10 minutes at 4˚C, supernatants recovered and their protein content quantified.

In parallel, antibody-complexed beads were prepared. 30μL of Gammabind G Sepharose beads per sample were washed in NET buffer (50mM Tris pH 7.5, 150mM NaCl, 0.1% NP-40, 1mM EDTA), blocked with 20μg tRNA, washed again and incubated for 2 hours at 4°C with rotation after adding the primary antibody or Irrelevant IgG. All centrifugations of beads were done at 350g and 4˚C.

Protein samples were precleared with unblocked beads for 30 minutes at 4C with rotation, centrifuged for 2 minutes at 350 g and supernatant was recovered. 6mg of protein was mixed with the previously blocked and Antibody-complexed beads and incubated for 2 hours at 4˚C with rotation. The mix was centrifuged and beads were washed 4 times with NET buffer.

Finally, beads were resuspended in 50μL NET with 2μL of blue glycogen and 150μL TRIzol and RNA extraction was carried out as described above.

3.10. Orthogonal organic phase separation

Orthogonal organic phase separation was carried out as described in Villanueva E. et al[198]. Cells were grown up to 80% confluence, washed with warm PBS and dried as much as possible before crosslinking with 300mJ/cm^2 UV in a GS gene linker UV chamber (BioRad). Cells were lysed and scraped in 1mL TRIzol, mixed with 200μL chloroform, vortexed and centrifuged at 12000g for 15 minutes at 4˚C. The aqueous and organic phase were discarded and the interphase was resuspended in 1mL TRIzol again. The whole procedure was repeated three times in total. The resulting interphase was washed with 900μL methanol, vortexed and centrifuged at 14000g for 10 minutes at room temperature.

After removing the supernatant, 100μL of 100mM TEAB, 1% SDS were added and the interphase was dissolved. Samples were sonicated in a Bioruptor Pico Sonicator (Diagenode) for 15 cycles of 30 seconds

ON/OFF at 4˚C and boiled at 95˚C for 5 minutes. After cooling for 2 minutes on ice, the remaining pellet was homogenized by pipetting. 10μg of RNase A were added and samples were incubated at 37˚C for 4 hours. 1mL TRIzol and 200μL chloroform were added and samples were centrifuged for 15 minutes at 12000 g at 4˚C. The organic phase was recovered and pelleted by mixing (1:4) with ethanol 100% and centrifuging. An additional washing with ethanol 80% was done and the pellet was allowed to dry completely. The pellet was resuspended in 100mL TEAB 100mM, 1% SDS buffer, boiled, quantified and studied through western blot.

3.11. Zymography

Cell conditioned medium was analyzed by following the gelatin zymography protocol described by Abcam. Serum free DMEM medium was collected from cell cultures after an overnight incubation and concentrated at 10X with Amicon® Ultra 4mL Centrifugal Filters (Sigma-Aldrich). For that, samples were centrifuged at 7500 g for 5 minutes.

Loading buffer was added to the samples and proteins were resolved by SDS-PAGE at 120 V in TGS buffer using gel containing 1mg/mL gelatin. The gel was washed twice for 30 minutes with a washing buffer (2.5% Triton X-100, 50mM Tris pH 7.5, 5mM $CaCl_2$, 1μM $ZnCl_2$), rinsed for 10 minutes in incubation buffer (1% Triton X-100, 50mM Tris pH 7.5, 5mM $CaCl_2$, 1μM $ZnCl_2$) and incubated in this buffer for 24 hours at 37˚C. The gel was then stained with the staining solution (40% methanol, 10% acetic acid, 5mg/mL Coomasie blue) for 1 hour. Excess

staining solution was washed off with water and destaining solution (40% methanol, 10% acetic acid) was applied until the background levels decreased enough to distinguish the specific bands.

4. *IN VIVO* PROCEDURES

Animals were maintained in a specific pathogen-free area and fed *ad libitum*. All the procedures were approved by the Animal Research Ethical Committee from the Parc de Recerca Biomèdica de Barcelona (Barcelona, Spain) and by the Generalitat de Catalunya.

4.1. Mammary orthotopic transplantation and resection

Synchronized primary tumors were generated in mice by implanting $5x10^4$ AT-3 tumor cells and either $5x10^4$ MSCs or $5x10^4$ MEF EDA+ or EDA- embedded in Matrigel. NOD-SCID (Non Obese Diabetic/Severe Combined Immunodeficiency) females at least eight weeks old were treated with buprenorphine 0.1mg/kg and anesthetized with isoflurane 2.5-3.5% on O_2 0,8 L/min, following the procedure approved by the ethical committee, and two inguinal mammary fat pads per mice were injected.

For mice injected with AT-3 and MEF, tumor size was externally monitored and they were surgically resected when reached 0.2-0.4cm. Mice injected with AT-3 and MSC were injected every day, from the third until the seventeenth after intervention, with 50mg/Kg intraperitoneal Irigenin dissolved in DMSO. Primary tumors were

resected once they reached 0.4cm. For resection surgery, mice were anesthetized as described above.

Post-resection, mice were maintained alive an extra two months to allow the growth of metastasis and then sacrificed to quantify tumor lung metastatic foci. Metastases were counted in hematoxylin and eosin stained slides of formalin fixed paraffin embedded lungs.

5. DATA TREATMENT

5.1. Human tumor database information

Fibronectin RNA expression and splicing data were obtained from TSVdb and SNAIL1 protein and RNA data was obtained from cBioPortal for the same cohort of patients. Characteristics of each patient were also downloaded from cBioPortal database.

Only full length fibronectin isoforms including or excluding the exon 33 were taken into account to calculate the percentage of isoforms including the EDA. For each studied tumor type, tumors were independently analyzed in two groups according with their reported tumor stage: stage I and II or stage III and IV. The number of patients with available data for each group and tumor type (ranging from 69 to 590) is detailed in Figure 17. Tumors were further classified by their SNAIL1 protein levels (high and low) and the percentage of EDA inclusion (high and low). Only 5-10% of the patients were considered as high SNAIL1 expression. EDA inclusion rate of at least 80% was set

as high EDA ratio. For statistical analysis, the high/low percentages of EDA inclusion in high versus low SNAIL1 tumors were compared.

5.2. RNA-seq analysis

Total RNA was extracted from cultured cells with GenElute Mammalian Total RNA Miniprep kit (Sigma). Samples were paired-end sequenced in CRG Sequencing Unit until reaching 80M reads/sample. RNA-seq data was analyzed for splicing using two different softwares, reaching comparable results. The SANJUAN software designed by P. Papasaikas was run with a threshold of 0.15 delta Percentage Spliced In (ΔPSI) (https://github.com/ppapasaikas/SANJUAN). Data processing was carried out by Dr. Elena Martín, from Dr. Juan Valcárcel's lab (CRG, Barcelona, Spain). The SUPPA software designed by Dr. Eduardo Eyras' lab was run with a threshold of 0.1 ΔPSI (https://github.com/comprna/SUPPA). Data processing was carried out by Dr. Juan Luis Trincado, from Dr. Eduardo Eyras' lab (GRIB, Barcelona, Spain).

5.3. Statistical analysis

All the results shown were representative from at least three independent experiments. Data are represented as mean ± SEM. When appropriate, statistical analyses were conducted using GraphPad Prism software (GraphPad, La Jolla, CA, USA) and data were analyzed for significance using Unpaired T-Test and Chi-squared test. P values < 0.05 are symbolized with one asterisk, $p < 0.01$ with two asterisks and $p < 0.001$ with three asterisks.

BIBLIOGRAPHY

1. Siegel, R. L., Miller, K. D. & Jemal, A. Cancer statistics, 2020. *CA. Cancer J. Clin.* **70**, 7–30 (2020).

2. Hanahan, D. & Weinberg, R. A. The Hallmarks of Cancer. *Cell* **100**, 57–70 (2000).

3. Hanahan, D. & Weinberg, R. A. Hallmarks of cancer: The next generation. *Cell* **144**, 646–674 (2011).

4. Hanahan, D. Hallmarks of Cancer: New Dimensions. *Cancer Discov.* **12**, 31–46 (2022).

5. Mehlen, P. & Puisieux, A. Metastasis: A question of life or death. *Nat. Rev. Cancer* **6**, 449–458 (2006).

6. Chaffer, C. L. & Weinberg, R. A. A perspective on cancer cell metastasis. *Science (80-.).* **331**, 1559–1564 (2011).

7. Bissell, M. J. & Hines, W. C. Why don't we get more cancer? A proposed role of the microenvironment in restraining cancer progression. *Nat. Med.* **17**, 320–329 (2011).

8. Kalluri, R. The biology and function of fibroblasts in cancer. *Nat. Rev. Cancer* **16**, 582–598 (2016).

9. Balkwill, F. & Mantovani, A. Inflammation and cancer: Back to Virchow? *Lancet* **357**, 539–545 (2001).

10. Virchow, R. *Die cellularpathologie in ihrer Begruendung auf Physiologische und Gewebelehre*. (1858).

11. Duvall, M. *Atlas d'Embyologie*. (1879).

12. Erdogan, B. & Webb, D. J. Cancer-associated fibroblasts modulate growth factor signaling and extracellular matrix remodeling to regulate tumor metastasis. *Biochem. Soc. Trans.* **45**, 229–236 (2017).

13. Kis, K., Liu, X. & Hagood, J. S. Myofibroblast differentiation and survival in fibrotic disease. *Expert Rev. Mol. Med.* **13**, e27 (2011).

14. Koliaraki, V., Pallangyo, C. K., Greten, F. R. & Kollias, G. Mesenchymal Cells in Colon Cancer. *Gastroenterology* **152**, 964–979 (2017).

15. Lau, L. F. CCN1/CYR61: the very model of a modern matricellular protein. *Cell. Mol. Life Sci.* **68**, 3149–3163 (2011).

16. Flier, J. S., Underhill, L. H. & Dvorak, H. F. Tumors: Wounds That Do Not Heal. *N. Engl. J. Med.* **315**, 1650–1659 (1986).

17. Dvorak, H. F. Tumors: Wounds That Do Not Heal--Redux. *Cancer*

Immunol. Res. **3**, 1–11 (2015).

18. Murray, P. J. Macrophage Polarization. *Annu. Rev. Physiol.* **79**, 541–566 (2017).

19. Amatangelo, M. D., Bassi, D. E., Klein-Szanto, A. J. P. & Cukierman, E. Stroma-derived three-dimensional matrices are necessary and sufficient to promote desmoplastic differentiation of normal fibroblasts. *Am. J. Pathol.* **167**, 475–488 (2005).

20. Guinney, J. *et al.* The consensus molecular subtypes of colorectal cancer. *Nat. Med.* **21**, 1350–1356 (2015).

21. Calon, A. *et al.* Stromal gene expression defines poor-prognosis subtypes in colorectal cancer. *Nat. Genet.* **47**, 320–329 (2015).

22. Francí, C. *et al.* Snail1 protein in the stroma as a new putative prognosis marker for colon tumours. *PLoS One* **4**, 1–7 (2009).

23. Butcher, D. T., Alliston, T. & Weaver, V. M. A tense situation: forcing tumour progression. *Nat. Rev. Cancer* **9**, 108–122 (2009).

24. Winkler, J., Abisoye-Ogunniyan, A., Metcalf, K. J. & Werb, Z. Concepts of extracellular matrix remodelling in tumour progression and metastasis. *Nat. Commun.* **11**, 1–19 (2020).

25. Özdemir, B. C. *et al.* Depletion of Carcinoma-Associated Fibroblasts and Fibrosis Induces Immunosuppression and Accelerates Pancreas Cancer with Reduced Survival. *Cancer Cell* **25**, 719–734 (2014).

26. Orozco, C. A. *et al.* Targeting galectin-1 inhibits pancreatic cancer progression by modulating tumor–stroma crosstalk. *Proc. Natl. Acad. Sci. U. S. A.* **115**, E3769–E3778 (2018).

27. Lu, P., Weaver, V. M. & Werb, Z. The extracellular matrix: A dynamic niche in cancer progression. *J. Cell Biol.* **196**, 395–406 (2012).

28. Cox, T. R. & Erler, J. T. Remodeling and homeostasis of the extracellular matrix: implications for fibrotic diseases and cancer. *Dis. Model. Mech.* **4**, 165–178 (2011).

29. Gaggioli, C. *et al.* Fibroblast-led collective invasion of carcinoma cells with differing roles for RhoGTPases in leading and following cells. *Nat. Cell Biol.* **9**, 1392–1400 (2007).

30. Jang, M. *et al.* Targeting extracellular matrix glycation to attenuate fibroblast activation. *Acta Biomater.* **141**, 255–263 (2022).

31. Caliari, S. R. *et al.* Stiffening hydrogels for investigating the dynamics

of hepatic stellate cell mechanotransduction during myofibroblast activation. *Sci. Rep.* **6**, 21387 (2016).

32. Singh, P., Carraher, C. & Schwarzbauer, J. E. Assembly of Fibronectin Extracellular Matrix. *Annu. Rev. Cell Dev. Biol.* **26**, 397–419 (2010).

33. Guan, J. L., Trevithick, J. E. & Hynes, R. O. Retroviral expression of alternatively spliced forms of rat fibronectin. *J. Cell Biol.* **110**, 833–847 (1990).

34. Spada, S., Tocci, A., Di Modugno, F. & Nisticò, P. Fibronectin as a multiregulatory molecule crucial in tumor matrisome: from structural and functional features to clinical practice in oncology. *J. Exp. Clin. Cancer Res.* **40**, 102 (2021).

35. Lee, S. H. & Dominguez, R. Regulation of actin cytoskeleton dynamics in cells. *Mol. Cells* **29**, 311–325 (2010).

36. Zent, J. & Guo, L.-W. Signaling Mechanisms of Myofibroblastic Activation: Outside-in and Inside-Out. *Cell. Physiol. Biochem.* **49**, 848–868 (2018).

37. Shinde, A. V., Humeres, C. & Frangogiannis, N. G. The role of α-smooth muscle actin in fibroblast-mediated matrix contraction and remodeling. *Biochim. Biophys. Acta - Mol. Basis Dis.* **1863**, 298–309 (2017).

38. Khatau, S. B. *et al.* A perinuclear actin cap regulates nuclear shape. *Proc. Natl. Acad. Sci.* **106**, 19017–19022 (2009).

39. Wang, J., Zohar, R. & McCulloch, C. A. Multiple roles of α-smooth muscle actin in mechanotransduction. *Exp. Cell Res.* **312**, 205–214 (2006).

40. Conklin, M. W. *et al.* Aligned collagen is a prognostic signature for survival in human breast carcinoma. *Am. J. Pathol.* **178**, 1221–1232 (2011).

41. Han, W. *et al.* Oriented collagen fibers direct tumor cell intravasation. *Proc. Natl. Acad. Sci.* **113**, 11208–11213 (2016).

42. Castelló-Cros, R., Khan, D. R., Simons, J., Valianou, M. & Cukierman, E. Staged stromal extracellular 3D matrices differentially regulate breast cancer cell responses through PI3K and beta1-integrins. *BMC Cancer* **9**, 1–19 (2009).

43. Nieto, M. A. The snail superfamily of zinc-finger transcription factors. *Nat. Rev. Mol. Cell Biol.* **3**, 155–166 (2002).

44. Grau, Y., Carteret, C. & Simpson, P. Mutations and chromosomal rearrangements affecting the expression of snail, a gene involved in embryonic patterning in Drosophila melanogaster. *Genetics* **108**, 347–360 (1984).

45. Labonne, C. & Bronner-Fraser, M. Snail-related transcriptional repressors are required in Xenopus for both the induction of the neural crest and its subsequent migration. *Dev. Biol.* **221**, 195–205 (2000).

46. Carver, E. A., Jiang, R., Lan, Y., Oram, K. F. & Gridley, T. The Mouse Snail Gene Encodes a Key Regulator of the Epithelial-Mesenchymal Transition. *Mol. Cell. Biol.* **21**, 8184–8188 (2001).

47. Peinado, H., Ballestar, E., Esteller, M. & Cano, A. Snail mediates E-cadherin repression by the recruitment of the Sin3A/histone deacetylase 1 (HDAC1)/HDAC2 complex. *Mol. Cell. Biol.* **24**, 306–19 (2004).

48. Herranz, N. *et al.* Polycomb Complex 2 Is Required for E-cadherin Repression by the Snail1 Transcription Factor . *Mol. Cell. Biol.* **28**, 4772–4781 (2008).

49. Hou, Z. *et al.* The LIM Protein AJUBA Recruits Protein Arginine Methyltransferase 5 To Mediate SNAIL-Dependent Transcriptional Repression. *Mol. Cell. Biol.* **28**, 3198–3207 (2008).

50. Ikenouchi, J., Matsuda, M., Furuse, M. & Tsukita, S. Regulation of tight junctions during the epithelium-mesenchyme transition:direct repression of the gene expression of claudins/occludin by Snail. *J. Cell Sci.* **116**, 1959–1967 (2003).

51. Kalluri, R. & Weinberg, R. A. The basics of epithelial-mesenchymal transition. *J. Clin. Invest.* **119**, 1420–1428 (2009).

52. Wang, Y., Shi, J., Chai, K., Ying, X. & Zhou, B. P. The Role of Snail in EMT and Tumorigenesis. *Curr. Cancer Drug Targets* **13**, 963–972 (2013).

53. Stanisavljevic, J., Porta-de-la-Riva, M., Batlle, R., de Herreros, A. G. & Baulida, J. The p65 subunit of NF-κB and PARP1 assist Snail1 in activating fibronectin transcription. *J. Cell Sci.* **124**, 4161–4171 (2011).

54. Wu, W.-S. *et al.* Snail collaborates with EGR-1 and SP-1 to directly activate transcription of MMP 9 and ZEB1. *Sci. Rep.* **7**, 17753 (2017).

55. Hwang, W. *et al.* SNAIL Regulates Interleukin-8 Expression, Stem Cell–Like Activity, and Tumorigenicity of Human Colorectal Carcinoma

Cells. *Gastroenterology* **141**, 279-291.e5 (2011).

56. Rembold, M. *et al.* A conserved role for Snail as a potentiator of active transcription. *Genes Dev.* **28**, 167–181 (2014).

57. Rowe, R. G. *et al.* Mesenchymal cells reactivate Snail1 expression to drive three-dimensional invasion programs. *J. Cell Biol.* **184**, 399–408 (2009).

58. Batlle, R. *et al.* Snail1 controls TGF-β responsiveness and differentiation of mesenchymal stem cells. *Oncogene* **32**, 3381–3389 (2013).

59. Sou, P. W., Delic, N. C., Halliday, G. M. & Lyons, J. G. Snail transcription factors in keratinocytes: Enough to make your skin crawl. *Int. J. Biochem. Cell Biol.* **42**, 1940–1944 (2010).

60. López-Novoa, J. M. & Nieto, M. A. Inflammation and EMT: an alliance towards organ fibrosis and cancer progression. *EMBO Mol. Med.* **1**, 303–314 (2009).

61. Stanisavljevic, J. *et al.* Snail1-expressing fibroblasts in the tumor microenvironment display mechanical properties that support metastasis. *Cancer Res.* **75**, 284–295 (2015).

62. Manetti, M. *et al.* Endothelial-to-mesenchymal transition contributes to endothelial dysfunction and dermal fibrosis in systemic sclerosis. *Ann. Rheum. Dis.* **76**, 924–934 (2017).

63. Biswas, H. & Longmore, G. D. Action of SNAIL1 in Cardiac Myofibroblasts Is Important for Cardiac Fibrosis following Hypoxic Injury. *PLoS One* **11**, e0162636 (2016).

64. Scarpa, M. *et al.* Snail1 transcription factor is a critical mediator of hepatic stellate cell activation following hepatic injury. *Am. J. Physiol. Liver Physiol.* **300**, G316–G326 (2011).

65. Alba-Castellón, L. *et al.* Snail1-dependent activation of cancer-associated fibroblast controls epithelial tumor cell invasion and metastasis. *Cancer Res.* **76**, 6205–6217 (2016).

66. Ghosh, S. & Garcia-Blanco, M. A. Coupled in vitro synthesis and splicing of RNA polymerase II transcripts. *RNA* **6**, 1325–1334 (2000).

67. Pan, Q., Shai, O., Lee, L. J., Frey, B. J. & Blencowe, B. J. Deep surveying of alternative splicing complexity in the human transcriptome by high-throughput sequencing. *Nat. Genet.* **40**, 1413–1415 (2008).

68. Dvinge, H. & Bradley, R. K. Widespread intron retention diversifies most cancer transcriptomes. *Genome Med.* **7**, 45 (2015).

69. Cartegni, L., Chew, S. L. & Krainer, A. R. Listening to silence and understanding nonsense: exonic mutations that affect splicing. *Nat. Rev. Genet.* **3**, 285–298 (2002).

70. Krämer, A. The structure and function of proteins involved in mammalian pre-mRNA splicing. *Annu. Rev. Biochem.* **65**, 367–409 (1996).

71. Wilkinson, M. E., Charenton, C. & Nagai, K. RNA Splicing by the Spliceosome. *Annu. Rev. Biochem.* **89**, 359–388 (2020).

72. Koren, E., Lev-Maor, G. & Ast, G. The emergence of alternative 3′ and 5′ splice site exons from constitutive exons. *PLoS Comput. Biol.* **3**, 0895–0908 (2007).

73. Roca, X., Sachidanandam, R. & Krainer, A. R. Determinants of the inherent strength of human 5′ splice sites. *RNA* **11**, 683–698 (2005).

74. Lee, Y. & Rio, D. C. Mechanisms and Regulation of Alternative Pre-mRNA Splicing. *Annu. Rev. Biochem.* **84**, 291–323 (2015).

75. Wang, Y. *et al.* Mechanism of alternative splicing and its regulation. *Biomed. Reports* **3**, 152–158 (2015).

76. Shepard, P. J. & Hertel, K. J. The SR protein family. *Genome Biol.* **10**, 242 (2009).

77. Blenclowe, B. J. Exonic splicing enhancers: mechanism of action, diversity and role in human genetic diseases. *Trends Biochem. Sci.* **0004**, 106–110 (2000).

78. Schaal, T. D. & Maniatis, T. Multiple Distinct Splicing Enhancers in the Protein-Coding Sequences of a Constitutively Spliced Pre-mRNA. *Mol. Cell. Biol.* **19**, 261–273 (1999).

79. Kahles, A. *et al.* Comprehensive Analysis of Alternative Splicing Across Tumors from 8,705 Patients. *Cancer Cell* **34**, 211-224.e6 (2018).

80. Singh, B., Trincado, J. L., Tatlow, P. J., Piccolo, S. R. & Eyras, E. Genome sequencing and RNA-motif analysis reveal novel damaging noncoding mutations in human tumors. *Mol. Cancer Res.* **16**, 1112–1124 (2018).

81. Popp, M. W. & Maquat, L. E. Nonsense-mediated mRNA Decay and Cancer. *Curr. Opin. Genet. Dev.* **48**, 44–50 (2018).

82. Ladomery, M. Aberrant Alternative Splicing Is Another Hallmark of

Cancer. *Int. J. Cell Biol.* **2013**, 1–6 (2013).

83. Bonnal, S. C., López-Oreja, I. & Valcárcel, J. Roles and mechanisms of alternative splicing in cancer — implications for care. *Nat. Rev. Clin. Oncol.* **17**, 457–474 (2020).

84. Dvinge, H. *et al.* RNA splicing factors as oncoproteins and tumor suppressors. *Nat Rev Cancer* **16**, 413–430 (2016).

85. Anczuków, O. *et al.* SRSF1-Regulated Alternative Splicing in Breast Cancer. *Mol. Cell* **60**, 105–117 (2015).

86. Anczuków, O. *et al.* The splicing factor SRSF1 regulates apoptosis and proliferation to promote mammary epithelial cell transformation. *Nat. Struct. Mol. Biol.* **19**, 220–228 (2012).

87. Martinez-Montiel, N., Rosas-Murrieta, N. H., Ruiz, M. A., Monjaraz-Guzman, E. & Martinez-Contreras, R. Alternative splicing as a target for cancer treatment. *Int. J. Mol. Sci.* **19**, 1–28 (2018).

88. Sheikh, O. & Yokota, T. Pharmacology and toxicology of eteplirsen and SRP-5051 for DMD exon 51 skipping: an update. *Arch. Toxicol.* **96**, 1–9 (2022).

89. Lin, J. C. Therapeutic applications of targeted alternative splicing to cancer treatment. *Int. J. Mol. Sci.* **19**, 75 (2018).

90. White, E. S. & Muro, A. F. Fibronectin splice variants: Understanding their multiple roles in health and disease using engineered mouse models. *IUBMB Life* **63**, 538–546 (2011).

91. Pankov, R. & Yamada, K. M. Fibronectin at a glance. *J. Cell Sci.* **115**, 3861–3863 (2002).

92. Schwarzbauer, J. E., Tamkun, J. W., Lemischka, I. R. & Hynes, R. O. Three different fibronectin mRNAs arise by alternative splicing within the coding region. *Cell* **35**, 421–431 (1983).

93. Efthymiou, G. *et al.* Shaping Up the Tumor Microenvironment With Cellular Fibronectin. *Front. Oncol.* **10**, (2020).

94. Ffrench-Constant, C. Alternative Splicing of Fibronectin—Many Different Proteins but Few Different Functions. *Exp. Cell Res.* **221**, 261–271 (1995).

95. Muro, A. F. *et al.* Regulated splicing of the fibronectin EDA exon is essential for proper skin wound healing and normal lifespan. *J. Cell Biol.* **162**, 149–160 (2003).

96. McKeown-Longo, P. J. & Higgins, P. J. Hyaluronan, Transforming Growth Factor β, and Extra Domain A-Fibronectin: A Fibrotic Triad. *Adv. Wound Care* **10**, 137–152 (2021).

97. Rossnagl, S. *et al.* EDA-Fibronectin Originating from Osteoblasts Inhibits the Immune Response against Cancer. *PLOS Biol.* **14**, e1002562 (2016).

98. Borsi, L., Castellani, P., Allemanni, G., Neri, D. & Zardi, L. Preparation of Phage Antibodies to the ED-A Domain of Human Fibronectin. *Exp. Cell Res.* **240**, 244–251 (1998).

99. Kumra, H. & Reinhardt, D. P. Fibronectin-targeted drug delivery in cancer. *Adv. Drug Deliv. Rev.* **97**, 101–110 (2016).

100. Vibe-Pedersen, K., Kornblihtt, A. R. & Baralle, F. E. Expression of a human alpha-globin/fibronectin gene hybrid generates two mRNAs by alternative splicing. *EMBO J.* **3**, 2511–2516 (1984).

101. Mardon, H. J., Sebastio, G. & Baralle, F. E. A role for exon sequences in alternative splicing of the human fibronection gene. *Nucleic Acids Res.* **15**, 7725–7733 (1987).

102. Caputi, M. *et al.* A novel bipartite splicing enhancer modulates the differential processing of the human fibronectin EDA exon. *Nucleic Acids Res.* **22**, 1018–1022 (1994).

103. Muro, A. F., Iaconcig, A. & Baralle, F. E. Regulation of the fibronectin EDA exon alternative splicing. Cooperative role of the exonic enhancer element and the 5′ splicing site. *FEBS Lett.* **437**, 137–141 (1998).

104. Buratti, E. *et al.* RNA Folding Affects the Recruitment of SR Proteins by Mouse and Human Polypurinic Enhancer Elements in the Fibronectin EDA Exon. *Mol. Cell. Biol.* **24**, 1387–1400 (2004).

105. Cramer, P. *et al.* Coupling of Transcription with Alternative Splicing: RNA Pol II Promoters Modulate SF2/ASF and 9G8 Effects on an Exonic Splicing Enhancer. *Mol. Cell* **4**, 251–258 (1999).

106. Tacke, R. & Manley, J. L. The human splicing factors ASF/SF2 and SC35 possess distinct, functionally significant RNA binding specificities. *EMBO J.* **14**, 3540–51 (1995).

107. Lopez-Mejia, I. C. *et al.* Tissue-specific and SRSF1-dependent splicing of fibronectin, a matrix protein that controls host cell invasion. *Mol. Biol. Cell* **24**, 3164–3176 (2013).

108. Cramer, P., Pesce, C. G., Baralle, F. E. & Kornblihtt, A. R. Functional association between promoter structure and transcript alternative splicing. *Proc. Natl. Acad. Sci.* **94**, 11456–11460 (1997).

109. Manabe, R., Ohe, N., Maeda, T., Fukuda, T. & Sekiguchi, K. Modulation of Cell-adhesive Activity of Fibronectin by the Alternatively Spliced EDA Segment. *J. Cell Biol.* **139**, 295–307 (1997).

110. Liao, Y., Gotwals, P. J., Koteliansky, V. E., Sheppard, D. & Van De Water, L. The EIIIA Segment of Fibronectin Is a Ligand for Integrins α9β1 and α4β1 Providing a Novel Mechanism for Regulating Cell Adhesion by Alternative Splicing. *J. Biol. Chem.* **277**, 14467–14474 (2002).

111. Okamura, Y. *et al.* The Extra Domain A of Fibronectin Activates Toll-like Receptor 4. *J. Biol. Chem.* **276**, 10229–10233 (2001).

112. Amin, A. *et al.* Lung cancer cell-derived EDA-containing fibronectin induces an inflammatory response from monocytes and promotes metastatic tumor microenvironment. *J. Cell. Biochem.* **122**, 562–576 (2021).

113. Doddapattar, P. *et al.* Fibronectin Splicing Variants Containing Extra Domain A Promote Atherosclerosis in Mice Through Toll-Like Receptor 4. *Arterioscler. Thromb. Vasc. Biol.* **35**, 2391–2400 (2015).

114. Bhattacharyya, S., Midwood, K. S., Yin, H. & Varga, J. Toll-Like Receptor-4 Signaling Drives Persistent Fibroblast Activation and Prevents Fibrosis Resolution in Scleroderma. *Adv. Wound Care* **6**, 356–369 (2017).

115. Bhattacharyya, S. & Varga, J. Endogenous ligands of TLR4 promote unresolving tissue fibrosis: Implications for systemic sclerosis and its targeted therapy. *Immunol. Lett.* **195**, 9–17 (2018).

116. Serini, G. *et al.* The Fibronectin Domain ED-A Is Crucial for Myofibroblastic Phenotype Induction by Transforming Growth Factor-β1. *J. Cell Biol.* **142**, 873–881 (1998).

117. Shinde, A. V *et al.* The α4β1 integrin and the EDA domain of fibronectin regulate a profibrotic phenotype in dermal fibroblasts. *Matrix Biol.* **41**, 26–35 (2015).

118. Manabe, R., Ohe, N. & Sekiguchi, K. Alternatively Spliced EDA Segment Regulates Fibronectin-dependent Cell Cycle Progression and Mitogenic Signal Transduction. *J. Biol. Chem.* **274**, 5919–5924 (1999).

119. Sottile, J. & Hocking, D. C. Fibronectin Polymerization Regulates the

Composition and Stability of Extracellular Matrix Fibrils and Cell-Matrix Adhesions. *Mol. Biol. Cell* **13**, 3546–3559 (2002).

120. Efthymiou, G. *et al.* Fibronectin Extra Domains tune cellular responses and confer topographically distinct features to fibril networks. *J. Cell Sci.* **134**, (2021).

121. Klingberg, F. *et al.* The fibronectin ED-A domain enhances recruitment of latent TGF-β-binding protein-1 to the fibroblast matrix. *J. Cell Sci.* **131**, 1–12 (2018).

122. Li, C. X. *et al.* MicroRNA-21 preserves the fibrotic mechanical memory of mesenchymal stem cells. *Nat. Mater.* **16**, 379–389 (2017).

123. Kelsh, R. M., McKeown-Longo, P. J. & Clark, R. A. F. EDA Fibronectin in Keloids Create a Vicious Cycle of Fibrotic Tumor Formation. *J. Invest. Dermatol.* **135**, 1714–1718 (2015).

124. Zhang, L. *et al.* Design and Evaluation of a Polypeptide that Mimics the Integrin Binding Site for EDA Fibronectin to Block Profibrotic Cell Activity. *Int. J. Mol. Sci.* **22**, 1575 (2021).

125. Balza, E., Borsi, L., Allemanni, G. & Zardi, L. Transforming growth factor β regulates the levels of different fibronectin isoforms in normal human cultured fibroblasts. *FEBS Lett.* **228**, 42–44 (1988).

126. White, E. S. *et al.* Control of fibroblast fibronectin expression and alternative splicing via the PI3K/Akt/mTOR pathway. *Exp. Cell Res.* **316**, 2644–2653 (2010).

127. Batlle, E. *et al.* The transcription factor Snail is a repressor of E-cadherin gene expression in epithelial tumour cells. *Nat. Cell Biol.* **2**, 84–89 (2000).

128. Lambies, G. *et al.* TGFβ-Activated USP27X Deubiquitinase Regulates Cell Migration and Chemoresistance via Stabilization of Snail1. *Cancer Res.* **79**, 33–46 (2019).

129. Kornblihtt, A. R. *et al.* Alternative splicing: a pivotal step between eukaryotic transcription and translation. *Nat. Rev. Mol. Cell Biol.* **14**, 153–165 (2013).

130. Xu, Y., Zhao, W., Olson, S. D., Prabhakara, K. S. & Zhou, X. Alternative splicing links histone modifications to stem cell fate decision. *Genome Biol.* **19**, 133 (2018).

131. Franco-Barraza, J., Beacham, D. A., Amatangelo, M. D. & Cukierman, E. Preparation of Extracellular Matrices Produced by Cultured and

Primary Fibroblasts. *Curr. Protoc. Cell Biol.* **71**, 10.9.1–10.9.34 (2016).

132. Wershof, E. *et al.* A FIJI macro for quantifying pattern in extracellular matrix. *Life Sci. Alliance* **4**, e202000880 (2021).

133. Malara, A. *et al.* EDA fibronectin–TLR4 axis sustains megakaryocyte expansion and inflammation in bone marrow fibrosis. *J. Exp. Med.* **216**, 587–604 (2019).

134. Khan, M. M. *et al.* Alternatively-Spliced Extra Domain A of Fibronectin Promotes Acute Inflammation and Brain Injury After Cerebral Ischemia in Mice. *Stroke* **43**, 1376–1382 (2012).

135. Amin, A. *et al.* Irigenin, a novel lead from Western Himalayan chemiome inhibits Fibronectin-Extra Domain A induced metastasis in Lung cancer cells. *Sci. Rep.* **6**, 37151 (2016).

136. Walser, T. C. *et al.* Silencing the Snail-Dependent RNA Splice Regulator ESRP1 Drives Malignant Transformation of Human Pulmonary Epithelial Cells. *Cancer Res.* **78**, 1986–1999 (2018).

137. Craene, B. De & Berx, G. Regulatory networks defining EMT during cancer initiation and progression. *Nat. Rev. Cancer* **13**, 97–110 (2013).

138. Reinke, L. M., Xu, Y. & Cheng, C. Snail Represses the Splicing Regulator Epithelial Splicing Regulatory Protein 1 to Promote Epithelial-Mesenchymal Transition. *J. Biol. Chem.* **287**, 36435–36442 (2012).

139. Baulida, J., Díaz, V. M. & García de Herreros, A. Snail1: A Transcriptional Factor Controlled at Multiple Levels. *J. Clin. Med.* **8**, 757 (2019).

140. Invrea, F. *et al.* Patient-derived xenografts (PDXs) as model systems for human cancer. *Curr. Opin. Biotechnol.* **63**, 151–156 (2020).

141. Chao, C. *et al.* Patient-derived Xenografts from Colorectal Carcinoma: A Temporal and Hierarchical Study of Murine Stromal Cell Replacement. *Anticancer Res.* **37**, 3405–3412 (2017).

142. Delitto, D. *et al.* Patient-Derived Xenograft Models for Pancreatic Adenocarcinoma Demonstrate Retention of Tumor Morphology through Incorporation of Murine Stromal Elements. *Am. J. Pathol.* **185**, 1297–1303 (2015).

143. Blomme, A. *et al.* Murine stroma adopts a human-like metabolic phenotype in the PDX model of colorectal cancer and liver metastases. *Oncogene* **37**, 1237–1250 (2018).

144. Wang, X. *et al.* Breast tumors educate the proteome of stromal tissue in an individualized but coordinated manner. *Sci. Signal.* **10**, (2017).

145. Bussard, K. M., Mutkus, L., Stumpf, K., Gomez-Manzano, C. & Marini, F. C. Tumor-associated stromal cells as key contributors to the tumor microenvironment. *Breast Cancer Res.* **18**, 84 (2016).

146. Eiro, N. *et al.* Breast Cancer Tumor Stroma: Cellular Components, Phenotypic Heterogeneity, Intercellular Communication, Prognostic Implications and Therapeutic Opportunities. *Cancers (Basel).* **11**, 664 (2019).

147. Kramer, C. J. H. *et al.* The prognostic value of tumour–stroma ratio in primary breast cancer with special attention to triple-negative tumours: a review. *Breast Cancer Res. Treat.* **173**, 55–64 (2019).

148. Velez, D. O. *et al.* 3D collagen architecture induces a conserved migratory and transcriptional response linked to vasculogenic mimicry. *Nat. Commun.* **8**, 1651 (2017).

149. Ray, A. & Provenzano, P. P. Aligned forces: Origins and mechanisms of cancer dissemination guided by extracellular matrix architecture. *Curr. Opin. Cell Biol.* **72**, 63–71 (2021).

150. Hu, C., Zhao, Y., Wang, X. & Zhu, T. Intratumoral Fibrosis in Facilitating Renal Cancer Aggressiveness: Underlying Mechanisms and Promising Targets. *Front. Cell Dev. Biol.* **9**, 651620 (2021).

151. van der Horst, G., Bos, L. & van der Pluijm, G. Epithelial Plasticity, Cancer Stem Cells, and the Tumor-Supportive Stroma in Bladder Carcinoma. *Mol. Cancer Res.* **10**, 995–1009 (2012).

152. Zhou, L., Yang, K., Andl, T., Wickett, R. R. & Zhang, Y. Perspective of Targeting Cancer-Associated Fibroblasts in Melanoma. *J. Cancer* **6**, 717–726 (2015).

153. Rybak, J.-N., Roesli, C., Kaspar, M., Villa, A. & Neri, D. The Extra-domain A of Fibronectin Is a Vascular Marker of Solid Tumors and Metastases. *Cancer Res.* **67**, 10948–10957 (2007).

154. Colak, S. & ten Dijke, P. Targeting TGF-β Signaling in Cancer. *Trends in Cancer* **3**, 56–71 (2017).

155. Ou, J. *et al.* Fibronectin extra domain A (EDA) sustains CD133+/CD44+ subpopulation of colorectal cancer cells. *Stem Cell Res.* **11**, 820–833 (2013).

156. Francí, C. *et al.* Expression of Snail protein in tumor-stroma interface.

Oncogene **25**, 5134–5144 (2006).

157. Sahai, E. *et al.* A framework for advancing our understanding of cancer-associated fibroblasts. *Nat. Rev. Cancer* **20**, 174–186 (2020).

158. Font, J. & Mackay, J. P. Beyond DNA: Zinc Finger Domains as RNA-Binding Modules. in *Engineered Zinc Finger Proteins* 479–491 (2010).

159. Hall, T. M. T. Multiple modes of RNA recognition by zinc finger proteins. *Curr. Opin. Struct. Biol.* **15**, 367–373 (2005).

160. Sapra, A. K. *et al.* Splicing Factor ChIP and ChRIP: Detection of Splicing and Splicing Factors at Genes by Chromatin Immunoprecipitation. in *Alternative pre-mRNA Splicing: Theory and Protocols* 417–427 (2012).

161. Sala, L. *et al.* Abrogation of myofibroblast activities in metastasis and fibrosis by methyltransferase inhibition. *Int. J. Cancer* **145**, 3064–3077 (2019).

162. Luco, R. F., Allo, M., Schor, I. E., Kornblihtt, A. R. & Misteli, T. Epigenetics in Alternative Pre-mRNA Splicing. *Cell* **144**, 16–26 (2011).

163. Zhang, L. *et al.* Cross-talk between PRMT1-mediated methylation and ubiquitylation on RBM15 controls RNA splicing. *Elife* **4**, (2015).

164. Ohkura, N., Takahashi, M., Yaguchi, H., Nagamura, Y. & Tsukada, T. Coactivator-associated Arginine Methyltransferase 1, CARM1, Affects Pre-mRNA Splicing in an Isoform-specific Manner. *J. Biol. Chem.* **280**, 28927–28935 (2005).

165. Sinha, R. *et al.* Arginine Methylation Controls the Subcellular Localization and Functions of the Oncoprotein Splicing Factor SF2/ASF. *Mol. Cell. Biol.* **30**, 2762–2774 (2010).

166. Cheng, D., Côté, J., Shaaban, S. & Bedford, M. T. The Arginine Methyltransferase CARM1 Regulates the Coupling of Transcription and mRNA Processing. *Mol. Cell* **25**, 71–83 (2007).

167. Hamey, J. J. & Wilkins, M. R. Methylation of Elongation Factor 1A: Where, Who, and Why? *Trends Biochem. Sci.* **43**, 211–223 (2018).

168. Kornblihtt, A. R., De la Mata, M., Fededa, J. P., Muñoz, M. J. & Nogués, G. Multiple links between transcription and splicing. *RNA* **10**, 1489–1498 (2004).

169. Lev Maor, G., Yearim, A. & Ast, G. The alternative role of DNA methylation in splicing regulation. *Trends Genet.* **31**, 274–280 (2015).

170. Losino, N. *et al.* EDA-Containing Fibronectin Increases Proliferation of

Embryonic Stem Cells. *PLoS One* **8**, e80681 (2013).

171. Riching, K. M. *et al.* 3D Collagen Alignment Limits Protrusions to Enhance Breast Cancer Cell Persistence. *Biophys. J.* **107**, 2546–2558 (2014).

172. Cheung, K. J. & Ewald, A. J. A collective route to metastasis: Seeding by tumor cell clusters. *Science (80-.).* **352**, 167–169 (2016).

173. Lintz, M., Muñoz, A. & Reinhart-King, C. A. The Mechanics of Single Cell and Collective Migration of Tumor Cells. *J. Biomech. Eng.* **139**, (2017).

174. Liu, L. *et al.* Minimization of thermodynamic costs in cancer cell invasion. *Proc. Natl. Acad. Sci.* **110**, 1686–1691 (2013).

175. Pastushenko, I. & Blanpain, C. EMT Transition States during Tumor Progression and Metastasis. *Trends Cell Biol.* **29**, 212–226 (2019).

176. Wei, S. C. *et al.* Matrix stiffness drives epithelial–mesenchymal transition and tumour metastasis through a TWIST1–G3BP2 mechanotransduction pathway. *Nat. Cell Biol.* **17**, 678–688 (2015).

177. Saad, S., Gottlieb, D. J., Bradstock, K. F., Overall, C. M. & Bendall, L. J. Cancer cell-associated fibronectin induces release of matrix metalloproteinase-2 from normal fibroblasts. *Cancer Res.* **62**, 283–9 (2002).

178. Mak, M., Spill, F., Kamm, R. D. & Zaman, M. H. Single-Cell Migration in Complex Microenvironments: Mechanics and Signaling Dynamics. *J. Biomech. Eng.* **138**, 210041–210048 (2016).

179. Wolf, K. *et al.* Physical limits of cell migration: Control by ECM space and nuclear deformation and tuning by proteolysis and traction force. *J. Cell Biol.* **201**, 1069–1084 (2013).

180. Wyckoff, J. B., Pinner, S. E., Gschmeissner, S., Condeelis, J. S. & Sahai, E. ROCK- and Myosin-Dependent Matrix Deformation Enables Protease-Independent Tumor-Cell Invasion In Vivo. *Curr. Biol.* **16**, 1515–1523 (2006).

181. Doss, B. L. *et al.* Cell response to substrate rigidity is regulated by active and passive cytoskeletal stress. *Proc. Natl. Acad. Sci.* **117**, 12817–12825 (2020).

182. Kim, D. & Wirtz, D. Focal adhesion size uniquely predicts cell migration. *FASEB J.* **27**, 1351–1361 (2013).

183. Maziveyi, M. & Alahari, S. K. Cell matrix adhesions in cancer: The proteins that form the glue. *Oncotarget* **8**, 48471–48487 (2017).

184. Goffin, J. M. *et al.* Focal adhesion size controls tension-dependent recruitment of α-smooth muscle actin to stress fibers. *J. Cell Biol.* **172**, 259–268 (2006).

185. Hoffman, L. M. *et al.* Mechanical stress triggers nuclear remodeling and the formation of transmembrane actin nuclear lines with associated nuclear pore complexes. *Mol. Biol. Cell* **31**, 1774–1787 (2020).

186. D'Urso, M. & Kurniawan, N. A. Mechanical and Physical Regulation of Fibroblast–Myofibroblast Transition: From Cellular Mechanoresponse to Tissue Pathology. *Front. Bioeng. Biotechnol.* **8**, (2020).

187. Brenot, A., Knolhoff, B. L., DeNardo, D. G. & Longmore, G. D. SNAIL1 action in tumor cells influences macrophage polarization and metastasis in breast cancer through altered GM-CSF secretion. *Oncogenesis* **7**, 32 (2018).

188. Dhuri, K. *et al.* Antisense Oligonucleotides: An Emerging Area in Drug Discovery and Development. *J. Clin. Med.* **9**, 2004 (2020).

189. Bhattacharyya, S. *et al.* Pharmacological Inhibition of Toll-Like Receptor-4 Signaling by TAK242 Prevents and Induces Regression of Experimental Organ Fibrosis. *Front. Immunol.* **9**, 2434 (2018).

190. Lefebvre, J. S. *et al.* Extra domain A of fibronectin primes leukotriene biosynthesis and stimulates neutrophil migration through activation of Toll-like receptor 4. *Arthritis Rheum.* **63**, 1527–1533 (2011).

191. Rajak, S. *et al.* Cellular Fibronectin Containing Extra Domain A Causes Insulin Resistance via Toll-like Receptor 4. *Sci. Rep.* **10**, 9102 (2020).

192. Hernandez, H., Medina-Ortiz, W. E., Luan, T., Clark, A. F. & McDowell, C. M. Crosstalk Between Transforming Growth Factor Beta-2 and Toll-Like Receptor 4 in the Trabecular Meshwork. *Investig. Opthalmology Vis. Sci.* **58**, 1811 (2017).

193. Kwon, A. *et al.* Extra domain A-containing fibronectin expression in Spin90 -deficient fibroblasts mediates cancer-stroma interaction and promotes breast cancer progression. *J. Cell. Physiol.* **235**, 4494–4507 (2020).

194. Castelló-Cros, R. & Cukierman, E. Stromagenesis During Tumorigenesis: Characterization of Tumor-associated Fibroblasts and Stroma-derived 3D Matrices. in *Extracellular matrix protocols* 275–

305 (2009).

195. Weischenfeldt, J. & Porse, B. Bone Marrow-Derived Macrophages (BMM): Isolation and Applications. *Cold Spring Harb. Protoc.* **2008**, pdb.prot5080 (2008).

196. Püspöki, Z., Storath, M., Sage, D. & Unser, M. Transforms and Operators for Directional Bioimage Analysis: A Survey. in *Focus on Bio-Image Informatics* 69–93 (2016).

197. Otero, J., Navajas, D. & Alcaraz, J. Characterization of the elastic properties of extracellular matrix models by atomic force microscopy. in *Cell-derived matrices Part A* 59–83 (2020).

198. Villanueva, E. *et al.* Efficient recovery of the RNA-bound proteome and protein-bound transcriptome using phase separation (OOPS). *Nat. Protoc.* **15**, 2568–2588 (2020).